



National Library
of Canada

Acquisitions and
Bibliographic Services Branch

395 Wellington Street
Ottawa, Ontario
K1A 0N4

Bibliothèque nationale
du Canada

Direction des acquisitions et
des services bibliographiques

395, rue Wellington
Ottawa (Ontario)
K1A 0N4

Your file - Votre référence

Our file - Notre référence

NOTICE

The quality of this microform is heavily dependent upon the quality of the original thesis submitted for microfilming. Every effort has been made to ensure the highest quality of reproduction possible.

If pages are missing, contact the university which granted the degree.

Some pages may have indistinct print especially if the original pages were typed with a poor typewriter ribbon or if the university sent us an inferior photocopy.

Reproduction in full or in part of this microform is governed by the Canadian Copyright Act, R.S.C. 1970, c. C-30, and subsequent amendments.

AVIS

La qualité de cette microforme dépend grandement de la qualité de la thèse soumise au microfilmage. Nous avons tout fait pour assurer une qualité supérieure de reproduction.

S'il manque des pages, veuillez communiquer avec l'université qui a conféré le grade.

La qualité d'impression de certaines pages peut laisser à désirer, surtout si les pages originales ont été dactylographiées à l'aide d'un ruban usé ou si l'université nous a fait parvenir une photocopie de qualité inférieure.

La reproduction, même partielle, de cette microforme est soumise à la Loi canadienne sur le droit d'auteur, SRC 1970, c. C-30, et ses amendements subséquents.

Canada

THE UNIVERSITY OF ALBERTA

**ANALYSIS OF CONDITIONAL SYMMETRIC INSTABILITY
IN CENTRAL ALBERTA**

BY

NACIM AKTARY



A thesis submitted to the Faculty of Graduate Studies and
Research in partial fulfilment of the requirements for the
degree of **DOCTOR OF PHILOSOPHY**

IN

METEOROLOGY

DEPARTMENT OF GEOGRAPHY

METEOROLOGY DIVISION

EDMONTON, ALBERTA

FALL, 1993



National Library
of Canada

Acquisitions and
Bibliographic Services Branch

395 Wellington Street
Ottawa, Ontario
K1A 0N4

Bibliothèque nationale
du Canada

Direction des acquisitions et
des services bibliographiques

395, rue Wellington
Ottawa (Ontario)
K1A 0N4

Your file *Votre référence*

Our file *Notre référence*

The author has granted an irrevocable non-exclusive licence allowing the National Library of Canada to reproduce, loan, distribute or sell copies of his/her thesis by any means and in any form or format, making this thesis available to interested persons.

L'auteur a accordé une licence irrévocable et non exclusive permettant à la Bibliothèque nationale du Canada de reproduire, prêter, distribuer ou vendre des copies de sa thèse de quelque manière et sous quelque forme que ce soit pour mettre des exemplaires de cette thèse à la disposition des personnes intéressées.

The author retains ownership of the copyright in his/her thesis. Neither the thesis nor substantial extracts from it may be printed or otherwise reproduced without his/her permission.

L'auteur conserve la propriété du droit d'auteur qui protège sa thèse. Ni la thèse ni des extraits substantiels de celle-ci ne doivent être imprimés ou autrement reproduits sans son autorisation.

ISBN 0-315-88348-0

Canada

THE UNIVERSITY OF ALBERTA

RELEASE FORM

NAME OF AUTHOR: **Nacim AKTARY**


TITLE OF THESIS: **Analysis of Conditional Symmetric Instability
in Central Alberta**

DEGREE: **Doctor of Philosophy**

YEAR THIS DEGREE GRANTED: **Fall 1993**

Permission is hereby granted to the University of Alberta Library to reproduce single copies of this thesis and to lend or sell such copies for private, scholarly or scientific research purposes only.

The author reserves all other publication and other rights in association with the copyright in the thesis, and except as hereinbefore provided neither the thesis nor any substantial portion thereof may be printed or otherwise reproduced in any material form whatever without the author's prior written permission.

......

#23, 3210 119 Avenue

Edmonton, Alberta

Canada, T5W-4V6

24 August 1993

UNIVERSITY OF ALBERTA
FACULTY OF GRADUATE STUDIES AND RESEARCH

The undersigned certify that they have read, and recommend to the Faculty of Graduate Studies and Research, for acceptance, a thesis entitled: ANALYSIS OF CONDITIONAL SYMMETRIC INSTABILITY IN CENTRAL ALBERTA, submitted by NACIM AKTARY in partial fulfilment of the requirements for the degree of DOCTOR OF PHILOSOPHY in METEOROLOGY.

G W Reuter

G. W. Reuter, Supervisor

G S Strong

G. S. Strong, External Examiner

F E Hicks

F. E. Hicks

E P Lozowski

E. P. Lozowski

R B Charlton

R. B. Charlton

J D Wilson

J. D. Wilson

Date 24 August 1993

Dedication

To my 3-year-old little Sara,
with daddy's love and affection.

Abstract

Operational sounding data are analyzed to assess the occurrence of conditional symmetric instability (CSI) in the airflow over central Alberta. The observational data consist of 1460 soundings released from Stony Plain, covering the two year period 1990 to 1991. The snowstorm of 4 and 5 October 1990 was investigated in more detail, including an analysis of synoptic maps and radar reflectivity imageries. This thesis proposes a new index for the potential of long-lasting rain events, based on the presence of a deep moist layer that is conditional symmetrically unstable. The major findings were:

(a) Snow bands can be formed over central Alberta by the release of conditional symmetric instability, even when the synoptic forcing is very weak.

(b) More than 20% of all the soundings sampled in 1990 and 1991 were convectively stable, yet had the potential for conditional symmetric instability. However, a strong seasonal dependence was evident: During the three winter months, about 40% of all soundings had conditional symmetrically unstable layers, while only 2% of the summer soundings were conditional symmetrically unstable. The values for both spring and fall were about 20%.

(c) About 15% of the total precipitation falling at Stony Plain was associated with soundings that were convectively stable, yet conditional symmetrically unstable. During the

winter period more than half of the snow was associated with conditional symmetrically unstable situations.

(d) A generalized Slantwise Showalter Index, the SSI, was found to be useful for identifying some cases of significant rainfall events during 1990.

Acknowledgments

I would like to present my sincere thanks and appreciation to Dr. G. W. Reuter, my supervisor, for his advice and counsel necessary for the preparation of this thesis. Dr. Reuter was always helpful to me and his valuable guidance and continuous support are gratefully acknowledged.

My heart-felt thanks are going to Dr. E. R. Reinelt who helped me overcome the difficulties I faced when I started. Although Dr. Reinelt is no longer residing in Edmonton, he has a special place in my memory.

I wish to express my thanks and gratitude to Dr. G. S. Strong, my External Examiner, and to Dr. F. E. Hicks for being present at my thesis oral defense. I am grateful to Drs. E. P. Lozowski, R. B. Charlton and J. D. Wilson for their kindness during my period of study at the University of Alberta and for their presence at my oral defense examination.

The help and friendly attitude of Mr. Terry Thompson, Ms. Laura Smith and others are very much appreciated.

Financial support for this research was provided by the Natural Sciences and Engineering Research Council and the Atmospheric Environment Service of Canada.

Table of Contents

| | |
|---------|--|
| Chapter | |
| 1. | Introduction 1 |
| 1.1 | Research topic 1 |
| 1.2 | Instabilities in atmospheric flows 2 |
| 1.3 | Review of observational studies of slantwise convection 8 |
| 1.4 | Review of Alberta precipitation 10 |
| 1.5 | Statement of the research problems 14 |
| | References 17 |
| 2. | Theory of conditional symmetric instability 23 |
| 2.1 | Basic criterion for CSI 23 |
| | (a) Horizontal tube displacement 26 |
| | (b) Vertical tube displacement 26 |
| | (c) Slantwise tube displacement 27 |
| 2.2 | Moist Richardson number criterion for CSI 28 |
| 2.3 | Equivalent potential vorticity criterion for CSI 30 |
| 2.4 | Assessing CSI from sounding data 31 |
| 2.5 | Limitations of CSI theory 34 |
| | References 36 |
| 3. | Band formation in an Alberta snowstorm 37 |

| | | |
|-------|--|----|
| 3.1 | Introduction | 37 |
| 3.2 | Observational data and method of analysis | 40 |
| 3.2.1 | Radar data | 40 |
| 3.2.2 | Surface and sounding data | 40 |
| 3.2.3 | Assessment of CSI from single sounding data | 41 |
| 3.2.4 | Computation of absolute vorticity | 44 |
| 3.3 | Results | 44 |
| 3.3.1 | Synoptic overview | 44 |
| 3.3.2 | Formation of a baroclinic zone | 47 |
| 3.3.3 | Sounding data | 49 |
| 3.3.4 | Distribution of snowfall | 51 |
| 3.3.5 | Assessment of CSI | 55 |
| 3.4 | Discussion | 57 |
| | References | 59 |
| 4. | Convective and symmetric instabilities and their effects on precipitation: A climatological analysis for central Alberta | 63 |
| 4.1 | Introduction | 63 |
| 4.1.1 | Convection in Alberta | 63 |
| 4.1.2 | Slantwise instability in Alberta | 64 |
| 4.1.3 | Statement of the problem | 66 |
| 4.2 | Observational data set | 67 |
| 4.3 | Method of assessment of CI and CSI | 69 |
| 4.3.1 | Assessing convective instability, CI | 69 |

| | |
|--|---------|
| 4.3.2 Assessing conditional symmetric instability, CSI | 71 |
| 4.4 Results for the frequency of occurrence of CI and CSI | 76 |
| 4.5 Precipitation due to CI and CSI | 80 |
| 4.6 Discussion and conclusion | 85 |
| References | 90 |
| 5. Relationship between slantwise instability, vertical shear and precipitation: Results for central Alberta | 95 |
| 5.1 Introduction | 95 |
| 5.2 Vertical shear and slantwise instability relationship | 97 |
| 5.3 Vertical distribution of symmetrically unstable layers | 99 |
| 5.4 On the possible use of the moist Richardson number in predicting the amount of precipitation | 103 |
| 5.5 Conclusions and discussion | 106 |
| 6. A slantwise Showalter index based on conditional symmetric instability: Results for central Alberta | 110 |
| 6.1 Introduction | 110 |

| | | |
|-----|--|-----|
| 6.2 | Slantwise Showalter Index | 114 |
| 6.3 | Error analysis | 119 |
| 6.4 | Database and method of analysis | 121 |
| 6.5 | Results | 124 |
| 6.6 | Discussion and conclusion | 133 |
| | References | 137 |
| 7. | Summary, conclusions and recommendations | 141 |
| 7.1 | Summary and conclusions | 141 |
| 7.2 | Recommendations for further research | 144 |

List of Tables

Chapter 3

| | |
|--|----|
| Table 1. Stability analysis for CSI for different layers of the sounding data at 12 UTC 4 October and 00 UTC 5 October 1990..... | 56 |
|--|----|

Chapter 4

| | |
|---|----|
| Table 1. Precipitation amounts and number of days with precipitation for each month of 1990 and 1991, compared with climatological values..... | 69 |
| Table 2. Stability analysis for 0000 UTC 4 February 1990..... | 75 |
| Table 3. Comparison of the number of soundings per month that were identified as being unstable for CI, unstable for CSI and absolutely stable..... | 77 |
| Table 4. Number of soundings <u>with precipitation</u> per month identified as unstable for CI, unstable for CSI and absolutely stable..... | 82 |
| Table 5. Monthly accumulated precipitation amounts for CI, for CSI and for absolutely stable soundings..... | 82 |

Chapter 5

| | |
|--|----|
| Table 1. Comparison of the number of absolutely stable (AS) and conditionally slantwise unstable (CSI) layers for different ranges of $\partial v/\partial z$ in the 90-80 kPa layers..... | 99 |
|--|----|

| | |
|--|-----|
| Table 2. Vertical distribution of slantwise unstable layers for all soundings during January 1990 and January 1991 that had $1 > Ri_m > 0$ | 101 |
| Table 3. Vertical distribution of slantwise unstable layers for each month during 1990 and 1991..... | 102 |
| Table 4. The average moist Richardson number $\langle Ri_m \rangle$, the 12-hourly accumulated precipitation and the depth of the symmetrically unstable soundings..... | 105 |

Chapter 6

| | |
|---|-----|
| Table 1. Monthly precipitation accumulation and the number of days with precipitation for the "normal" year and 1990..... | 122 |
| Table 2. Monthly frequency of soundings (0000 and 1200 UTC) for each of $SI_{85} < 0$, $SI_{90} < 0$, $SSI_{85} < 0$ and $SSI_{90} < 0$ in 1990..... | 124 |
| Table 3. List of soundings with $RH_{85} \geq 60\%$ and either $SI_{85} < 0$ or $SSI_{85} < 0.9$ | 127 |
| Table 4. List of soundings with $RH_{90} \geq 60\%$ and either $SI_{90} < 0$ or $SSI_{90} < 0.9$ | 130 |
| Table 5. Number of observed events and number of cases correctly predicted by the conditions $\{SSI_{85} < 0$ and $RH_{85} \geq 60\%$ } and $\{SSI_{90} < 0$ and $RH_{90} \geq 60\%$ } for different ranges of 12-hourly accumulated precipitation.... | 132 |

List of Figures

Chapter 2

- Figure 1. Schematic x-z cross section, depicting surfaces of constant M (solid lines, $M_3 > M_2 > M_1$) and θ_e (dashed lines, $\theta_{e3} > \theta_{e2} > \theta_{e1}$) values..... 27

Chapter 3

- Figure 1. Maps showing surface isobars and 50 kPa height contours for western Canada at 00 UTC 4 October (top), 12 UTC 4 October (middle) and 00 UTC 5 October 1990 (bottom)..... 46
- Figure 2. 70 kPa (left) and 85 kPa (right) analysis at 00 UTC 4 October (top), 12 UTC 4 October (middle) and 00 UTC 5 October 1990 (bottom)..... 48
- Figure 3. Measurements from the Stony Plain (WSE) sounding at 00 UTC 4 October (a), 12 UTC 4 October (b) and 00 UTC 5 October 1990 (c)..... 50
- Figure 4. Isopleths of snowfalls (in cm) accumulated over the 24-hour period ending at 00 UTC 5 October 1990..... 52
- Figure 5. Radar CAPPIs at one-hour time intervals from 19 UTC 4 to 2 UTC 5 October 1990..... 54

Chapter 4

- Figure 1. Number of soundings for each month in the period

| | |
|---|----|
| 1990-1991 that were convectively stable (CI), symmetrically unstable (SI) and absolutely stable (AS)..... | 79 |
| Figure 2. Number of soundings for each month in the period 1990-1991 with precipitation at Stony Plain within 12 hours..... | 83 |
| Figure 3. Relative contribution, to precipitation amounts from soundings that were convectively unstable (CI), symmetrically unstable (SI) and absolutely stable (AS)..... | 84 |
| Figure 4. Pie diagrams showing the seasonal variations of the importance of convective instability, slantwise instability and absolute stability..... | 86 |

Chapter 1

Introduction

1.1 Research topic

This thesis addresses some important issues regarding the role of Conditional Symmetric Instability (CSI) in producing and organizing precipitation in weather systems over Alberta. During the last few years, CSI has been a "hot" subject area in mesoscale meteorology both from an observational and a modelling perspective. At the Fifth Conference on Mesoscale Processes held at Atlanta (American Meteorological Society 1993) more than 15 scientific papers were devoted to Slantwise Convection arising from CSI. For the last ten years, about 10 research papers on CSI had appeared annually in the scientific journals. Ample attention is devoted to slantwise convection in recent meteorology textbooks; e.g. Mesoscale Meteorology and Forecasting (Ray 1986), A Short Course in Cloud Physics (Rogers and Yau 1989), Cloud and Storm Dynamics (Cotton and Anthes 1989), Storms (Cotton 1990), Extratropical Cyclones (Newton and Holopainen 1990).

With so much effort devoted toward the theme of CSI, what can be added? In particular, what is the new contribution of the present thesis? Before a precise statement of the thesis problem is given, all the relevant concepts and the pertinent literature will be reviewed in order to provide the necessary background for this work. The major atmospheric instability

categories will be reviewed in Section 1.2 to introduce the concept of symmetric instability. Section 1.3 will present a summary of the research literature on observational studies of slantwise convection. Section 1.4 will provide a discussion of Alberta weather systems and recent research for this region to complete the needed background. The research problem of this thesis will be formulated in Section 1.5.

1.2 Instabilities in atmospheric flows

The concepts of stability and instability are of fundamental importance in atmospheric dynamics. Suppose one can identify two initial states of the atmosphere that differ only slightly from each other. The flow will be regarded as unstable if the two states diverge in their evolution, so that the difference between them becomes large after a finite time lapse. Because the initial state is imperfectly known, the evolution of an unstable flow pattern is very difficult (if not impossible) to predict. Clearly, the degree of stability is closely related to the degree of predictability of the flow evolution. A stable flow will vary in space and time in an orderly manner directly determined by its initial conditions. A flow that is barely unstable will generally contain a very well defined train of disturbances with a specific wavelength that is partially determined by the character of the mean flow (Ray 1986). When the degree of instability increases, other disturbances of different wavelengths and scales will appear

together with the main disturbances, and a spectrum of peaks will show multiple peaks. Eventually, as instability increases further, the flow reaches the "turbulence state" in which the motions are extremely chaotic.

One of the important instabilities in the atmosphere is **baroclinic instability**, which occurs at the typical time scale of 2-5 days and a horizontal spatial scale of 500-2000 km. It arises when a strongly baroclinic flow (i.e. with significant horizontal temperature gradient) is slightly disturbed by a wavy perturbation. It accounts for widespread vertical motion of the order of a few cm s^{-1} that may lead to precipitation systems on the synoptic scale. Cyclogenesis is a manifestation of baroclinic instability in extratropical regions.

On the much smaller micro-scale, **conditional instability** (e.g. Rogers and Yau 1989, p. 32) occurs in the atmosphere to produce cumulus convection with localized updrafts of several ms^{-1} . Cumulus clouds have dimensions of the order of one kilometre and can form and decay in about 20 minutes. It is often convenient to examine Conditional Instability in terms of parcel theory. The basic assumption of this approach is that a "parcel" constitutes of a fixed amount of air (enclosed by a material surface) that remains in hydrostatic balance with its immediate environment. When a parcel of saturated air is displaced upward, its temperature will decrease according to the pseudo-adiabatic rate. If the ambient lapse rate is larger than the pseudo-adiabatic lapse rate, the displaced

parcel will be warmer than its surroundings and will be accelerated in the direction of the parcel's displacement.

Another type of instability, which is closely related to conditional instability, is **convective instability** (CI) that can arise when a layer of moist air of finite depth is lifted vertically (Rogers and Yau 1989 p. 35). A layer of air that is conditionally unstable needs not be convectively unstable; nor is a convectively unstable layer necessarily conditionally unstable. Convective instability becomes important primarily for an atmospheric layer that is very moist and is capped by dry air aloft. When this column of air is lifted the moist air will become saturated and will follow the pseudo-adiabatic lapse rate, while the dry air continues with the dry adiabatic lapse rate. A necessary criterion for convective instability is that the equivalent potential temperature (or the wet-bulb potential temperature) decreases with height.

Another type of instability is **inertial instability**. As a fluid motion is settled by a stable buoyancy gradient in the vertical, it is similarly stabilized while in rotation around a vertical axis. This is because the pressure field that develops in geostrophic equilibrium will return back a horizontally displaced air parcel to its original position, as does the hydrostatic pressure field in the case of conditional instability, when the ambient temperature lapse rate is less than pseudo-adiabatic. Consider a west to east oriented tube of air, capable of moving laterally through a zone having a

north-south pressure gradient. As the tube of air conserves its absolute angular momentum, any northward displacement will result in an increase in the tube's zonal velocity, whereas a southward displacement will result in a decrease in its zonal velocity. The amount of the change in the zonal velocity is given by the displacement distance multiplied by the local Coriolis parameter. If the environmental geostrophic pressure gradient does not increase northward, then the air tube will have a supergeostrophic velocity and tend to return southward. Thus, a flow with a mean northward wind shear, algebraically smaller than the Coriolis parameter, is stable to horizontal displacements. If the horizontal shear exceeds the Coriolis parameter, a northward initial displacement will accelerate the tube farther toward the north. The necessary condition for inertial instability can be generalized to two dimensions by the requirement that

$$f < -\left[\frac{\partial v}{\partial x} - \frac{\partial u}{\partial y}\right] = -\zeta, \quad (1)$$

where u is the zonal velocity, v is the meridional velocity, f is the Coriolis parameter and ζ is the vertical component of relative vorticity. In other words, (1) simply means that inertial instability exists when the absolute vorticity of the flow is negative. In the free atmosphere the conditions for inertial instability are very seldom met, mainly because the flow is close to its state of geostrophic balance. However, for the ocean currents, inertial instability is a prevailing

mechanism for creating unstable flow patterns.

Yet, another type of atmospheric instability is **Symmetric Instability**. On the cumulus scale (or micro-scale) the effects of buoyancy are important and on the synoptic scale the earth rotation is the dominant feature. For intermediate scale (i.e. mesoscale) phenomena, the effects of both buoyancy and earth rotation are important. In the case of a hydrostatically and geostrophically balanced mean air flow, having a vertical (and possibly horizontal) shear, both effects can act together so that their combined effect can lead to a new kind of buoyant-inertial instability. Initially, this new kind of instability was studied in relation to the general structure of planetary atmospheres and arose from symmetric meridional perturbations on a baroclinic circular vortex. In this context, its motion fields are zonally symmetric and, thus, the buoyant-inertial instability was termed "Symmetric Instability" to contrast with the azimuthally modulated classic baroclinic instability. Dry symmetric instability was investigated by Eliassen (1962), Stone (1966), Ooyama (1966) and Hoskins (1974).

As will be seen in Chapter 2, a necessary condition for a geostrophically balanced flow to become unstable for a small slantwise displacement is given by

$$(N^2/S^2) < [f/(f+\zeta)] \quad (2)$$

where N is the Brunt-Väisälä frequency and S is the vertical shear. The acceleration rate associated with the symmetric instability is of the order of f^2H , where H is the horizontal

component of the slanted displacement. Thus, this instability will predict rather gently accelerated motions along tilted surfaces, with slopes similar to those of frontal surfaces (i.e. surfaces of constant density) and with time scales of the order of f^{-1} (i.e. a few hours). Symmetric instability is indeed a mesoscale instability.

Inequality (2), required for symmetric instability, holds very seldom in the atmosphere, suggesting that dry symmetric instability is extremely rare. The potential importance of symmetric instability became apparent only upon recognition by Bennetts and Hoskins (1979) that the destabilizing effects of condensation could be applied to symmetric instability and this led to the concept of **conditional** symmetric instability, CSI. As with conditional (buoyant) instability, the effects of latent heat greatly complicate the stability problem and the presence of sufficient moisture amounts becomes a key element to assess the potential for the CSI release. The latent heat set free during the release of CSI causes the flow to develop a series of sloped two-dimensional mesoscale rolls whose axes are aligned with the mean geostrophic windshear direction. The slopes of these rolls, along the vertical, are close to the slopes of the environmental density surfaces. The air's ascending motion will cause adiabatic expansion which will result in cooling and formation of cloud by condensation of water vapour. Once the cloud becomes thick enough, precipitation is formed (usually by the Bergeron-Findeisen

process). The precipitation field resulting from CSI tends to be organized in parallel bands, oriented in the direction of the vertical wind shear vector. The horizontal scale of these bands ranges from 25 to 500 km (Emanuel 1979). Observational studies of slantwise convection often rely on weather radars. Weather radar displays of CAPPI (at 1 or 2 km above the ground) are convenient for determining the degree of organization in precipitation fields. Specially, strong precipitation bands due to slantwise convection appear on a CAPPI as bands of high reflectivity values aligned in the direction of thermal windshear (e.g. Seltzer et al. 1985).

1.3 Review of observational studies of slantwise convection

Emanuel (1983b) made a detailed study of the Oklahoma snowstorm of 2-3 December 1982. His analysis indicated that the observed precipitation bands occurred in a baroclinic flow that was conditionally unstable for moist symmetric instability. Sanders and Bosart (1985) analyzed the snowstorm of 11-12 February 1983 which produced a heavy snowband across the northeastern United States, extending from North Carolina to New England. Their analysis revealed a region of CSI at about 40 kPa, between Pittsburgh and Wallops Island. Although the snow band was attributed to frontogenetical forcing, CSI was thought to be responsible for pulse-like eruptions of cloud tops. Seltzer et al. (1985) analyzed 15 cases of banded and non-banded precipitation far removed from surface frontal

zones. In the cases where banded precipitation was observed, some regions of the atmosphere were symmetrically unstable. Wolfsberg et al. (1986) investigated the mechanisms of band formation for the 11 December 1982 New England snowstorm and found that the presence of CSI can explain many of the observed features of the bands such as their alignment and slope. Gyakum (1987) studied the storm of the evening of 9 December 1982 during which unpredicted snow, freezing rain and sleet began in northern Illinois. The atmospheric structure revealed that the presence of CSI may have caused the rapid onset of this precipitation over Illinois. Cases of banded overrunning precipitation associated with CSI, in the southern plains of the United States during the winter of 1981-82, were studied by Byrd (1989). He was able to conclude that symmetric instability is a very important forcing mechanism for many overrunning banded precipitation events. Reuter and Yau (1990) studied seven precipitation bands, which were observed during the Canadian Atlantic Storm Project (CASP), to assess the importance of slantwise instability. Most of these cases had weak slantwise instability or slantwise neutrality, suggesting that CSI is likely ubiquitous for Atlantic Canada during the winter months. Snook (1992) used data from a wind-profiler and radar to "forecast" precipitation bands arising from slantwise convection in an operational setting. The conclusion was that, identification of CSI in the atmosphere could improve the forecasting of the location and the timing of the mesoscale

precipitation events. Emanuel (1988) analyzed soundings made by aircraft over North Carolina and New England, and showed that the air in the warm sector of winter cyclones was stable for vertical convection but close to conditional slantwise neutrality. High-resolution dropsonde data indicated that CSI did occur in the warm sectors of rapidly developing cyclones over the ocean (Reuter and Yau 1993).

Most of the research regarding CSI has been conducted for the coastal regions of United States and eastern Canada, and no case study has been made for a continental land surface like the Canadian Prairies. One exception is the study of Reuter and Nguyen (1993) dealing with a summertime lee-cyclogenesis system that developed on 17-18 July 1986 over Alberta. They documented that the middle troposphere had the potential for CSI. However, because the lower troposphere was found to be unstable for (upright) cumulus convection, it was impossible to determine the exact role of CSI on the rain production in that system.

1.4 Review of Alberta precipitation

In North America the Rocky Mountains range constitutes an impressive north-south mountain barrier extending some 2500 km from northern Canada to southern Texas. This mountain barrier strongly affects the regional weather and precipitation. The orographic effects are very strongly felt in the province of Alberta, Canada. The provincial boundaries extend from 49°N to

60°N and from 110°W to 120°W with the southwestern border with British Columbia (south of 54°N) along the Continental Divide. During the winter, lee cyclogenesis is common and is generally associated with an upper shortwave trough that drifts eastward over the Rocky Mountains (Chung et al. 1976). In the summer, the topography causes differential slope heating which gives rise to convergence, triggering convective outbreaks (Smith and Yau 1987). The annual amount of total precipitation for Alberta is fairly low, ranging from about 300 mm per year in the southeast to 400-450 mm in northern areas, except for the foothills regions where annual accumulations reach 550-600 mm (Stamp 1988). Sunshine in Alberta ranges from 1900 hours per year in the north to 2300 in the south. The mean temperature for January ranges from -8 °C in the south to -24 °C in the north and for July from 20 °C to 16 °C, respectively.

Central Alberta is a region of severe convection during the summer months. Climatological statistics show that the area is affected by hail on an average of 61 days each summer (Wojtiw 1975), and between 10 and 20 tornadoes are reported annually (Newark 1984). These storms can result in extensive damage, as in the case of the severe hailstorm that swept over Calgary on 7 September 1991. The total cost to the insurance companies was over \$400 million, mainly due to the claims for repairing damaged cars and roofs. The most disastrous event was the Edmonton tornado of 31 July 1987, which left 27 people dead and 300 injured and also caused \$250 million of property

damage (Bullas and Wallace 1988). These cases underscore the need for an improved forecasting of severe storms.

Almost all of Alberta's farmlands have experienced hail damage at one time or another. But the heaviest and most consistent hailfalls usually occur within the "Alberta hail belt". This area consists of a land strip, some 100-130 km wide and about 400 km long. The "belt" stretches in a NNW-SSE direction, from Edmonton to Lethbridge, including Calgary. Hail occurs in the belt on an average of 61 days a year, between 15 May and 15 September, reaching its peak in July. Weather radars, located at Penhold, (52.2°N, 113.8°N, 904 m ASL) have been used by the Alberta Research Council since 1957 to study severe storms in central Alberta (Gibson and Kochtubajda 1991). The main purpose of the studies was to collect information about the mechanisms of the hailstorms and hailstone formation and growth and evaluate the effectiveness of weather modification techniques. The Alberta Hail Project indeed yielded much scientific information about various aspects of hail storms including the following:

- formation of hail (Longley and Thompson 1965),
- multicell hailstorms (Chisholm and Renick 1972),
- growth of individual hail stones (English 1973),
- forecasting of hailstorms (Renick and Maxwell 1977),
- distribution of hailstone sizes (Cheng and English 1983),
- supercell hailstorms (Krauss and Marwitz 1984),
- water budget of hailstorms (Rogers and Sakellariou 1986),

- role of topography for hailstorms (Smith and Yau 1987),
- hailstorm feeder clouds (Cheng and Rogers 1988),
- mesoscale upper air analysis (Strong 1989),
- hail identification using polarization radar (Al-Jumily et al. 1991)
- causes of severe convection (Smith and Yau 1993a,b).

The Rocky Mountains range "drains" a significant amount of moisture when westerly flows descend on the lee side (e.g. Reinelt 1970). Concern about lack of sufficient irrigation water for better crop yields prompted the farmers of southern Alberta to resort to the potential of rain enhancement using glaciogenic cloud seeding. The cloud seeding operations were carried out during the summer from 1956 to 1968 by dispersing silver iodide (AgI) particles from ground generators and from aircrafts. After an eight year suspension, private cloud seeding operations were performed again in the summer of 1977. At the farmers request, the Alberta Department of Agriculture supported cloud seeding operations in southern Alberta from 1980 to 1983. A statistical analysis showed that the claims of enhanced rainfalls due to cloud seeding (rather than natural variability) were not well founded (Aktary 1985). To address the problem of water shortage for irrigation, a large new dam is being build on the Oldman river near Pincher Creek, Alberta to provide sufficient water to Lethbridge and the adjacent areas in southern Alberta.

The rain enhancement attempts and the new dam building project show the importance of precipitation on the economy of Alberta. Thus, it is desirable to have a full knowledge of the atmospheric processes that contribute toward the production of precipitation in Alberta weather systems.

1.5 Statement of the research problems

This thesis investigates the presence of conditional symmetric instability (CSI) for the region around Stony Plain, in central Alberta (located near Edmonton). This work fulfils the needs to clarify the role of slantwise convection in the continental weather systems that develop on the lee side of the Rocky Mountains. The specific issues investigated in this thesis can be stated in terms of four related problems:

Problem 1: Presence of "pure" slantwise convection.

Does CSI occur in central Alberta weather systems without the presence of (vertical) convective instability or surface fronts? And if so, does this "pure" slantwise convection cause precipitation bands to form?

Problem 2: Frequency of slantwise convection.

What is the frequency of occurrence of CSI in central Alberta? How does this vary with the seasons throughout the year? What fraction of the observed monthly precipitation arises from slantwise convection?

Problem 3: Slantwise convection and precipitation.

Where in the atmosphere (in the vertical) does CSI occur more often? Is the degree of slantwise instability related to the amount of observed precipitation? Does the magnitude of the vertical wind shear provide an indication of the slantwise stability properties of the flow?

Problem 4: Forecasting of the precipitation potential with a slantwise instability index.

What is a good parameter or index that can quantify the amount of CSI in the atmosphere and be easily computed from sounding data? How sensitive is such a slantwise instability index to inaccuracies in observed sounding data? How useful is this index to forecast the potential of significant mesoscale precipitation events? Is it justified to use such a slantwise instability index operationally?

The approach taken in this thesis is to analyze observed data sampled by radiosonde and rain gauges at Stony Plain. The analysis covers the period from 1 January 1990 to 31 December 1991; i.e. two complete calendar years. For the weather events of 4-5 October 1990, remotely sensed satellite and radar data were also examined. To investigate the occurrence of slantwise instability, the upper air data were analyzed using the single sounding method that was pioneered by Emanuel (1983a,b) and Seltzer et al. (1985).

Chapter 2 gives the necessary mathematical background to develop this "single sounding method" from first principles; this chapter includes no original or new material and can be skipped by the readers who are familiar with the parcel theory of CSI. Chapters 3 to 6 deal with the above four problems and each one focuses on one problem only. These four chapters form the bulk of the thesis and each one will present some original contribution. They are written in "paper" format; i.e. each one has its own introduction, method of analysis, results and conclusion and, thus, can be read independently. Chapter 3, Chapter 4 and Chapter 6 have been submitted for publication to Contributions to Atmospheric Physics, Monthly Weather Review and Atmosphere-Ocean, respectively. Chapter 6 has been accepted, while the two other manuscripts are still presently under review. The final chapter of the thesis will synthesise the findings and make some suggestions for further research in the future.

The "paper" format thesis abides by certain conventions. Each chapter has its own list of references. Also, the numbers assigned to tables, figures and equations refer to the current chapter and not to previous ones. A minor disadvantage of the "paper" format is that there is some overlap in the material, such as duplication of some key equations and references. The advantage, however, is that the thesis text remains concise and focused as required for journal publications.

References

- Admirat, P., G. G. Goyer, L. Wojtiw, E. A. Carte, D. Roos and E. P. Lozowski, 1985: A comparative study of hail in Switzerland, Canada and South Africa. *J. of Climatol.*, 5, 35-51.
- Aktary, N., 1985: Evaluation of ground generator cloud seeding in southern Alberta (1977-1983). M.Sc. thesis, Department of Geography, University of Alberta, Edmonton, 166 pp.
- Al-Jumily, K. J., R. B. Charlton and R. G. Humphries, 1991: Identification of rain and hail with circular polarization radar. *J. Appl. Meteor.*, 30, 1075-1087.
- Bennetts, D. A., and B. J. Hoskins, 1979: Conditional symmetric instability a possible explanation for frontal rainbands. *Quart. J. Roy. Meteor. Soc.*, 105, 945-962.
- Bullas, J. M., and A. F. Wallace, 1988: The Edmonton tornado, July 31, 1987. Preprints, 15th Conf. on Severe Local Storms, Baltimore, Amer. Meteor. Soc., 437-443.
- Byrd, G. P., 1989: A composite analysis of winter season overrunning precipitation bands over the southern plains of the United States. *J. Atmos. Sc.*, 46, 1119-1132.
- Cheng, L., and M. English, 1983: A relationship between hailstone concentration and size. *J. Atmos. Sc.*, 40, 204-213.
- _____, _____, and R. Wong, 1985: Hailstone size distributions and their relationship to storm thermodynamics. *J. Clim. Appl. Meteor.*, 37, 812-826.

- ____, and D. C. Rogers, 1988: Hailfalls and hailstorm feeder clouds - An Alberta case study. J. Atmos. Sc., 45, 3533-3545.
- Chisholm, A. J. and J. H. Renick 1972: Supercell and multicell Alberta hailstorms. Abstracts, Intern. Conf. on Cloud Physics. London, England, 67-68.
- ____, 1973: Alberta hailstorms, Part I: Radar case studies and airflow models. Meteor. Monogr., 36, Amer. Meteor. Soc., Boston, 1-36.
- Chung, Y. S., K. D. Hage and E. R. Reinelt, 1976: On lee cyclogenesis and airflow in the Canadian Rocky Mountains and the East Asian Mountains. Mon. Wea. Rev., 104, 879-891.
- Cotton, W. R., 1990: Storms. *ASTeR Press, Fort Collins, Colorado, 158 pp.
- ____, and R. A. Anthes, 1989: Storm and cloud dynamics. Academic press, San Diego, Cal., 883 pp.
- Eliassen, A., 1962: On the vertical circulation in frontal zones. Geophys. Publ., Bjerknes Memorial Vol., 147-160.
- Emanuel, K. A., 1979: Inertial instability and mesoscale convective systems. Part I: Linear theory of inertial instability in rotating viscous fluids. J. Atmos. Sci., 36, 2425-2449.
- ____, 1983a: The Lagrangian parcel dynamics of moist symmetric instability. J. Atmos. Sc., 40, 2368-2376.
- ____, 1983b: On assessing local conditional symmetric

- instability from atmospheric soundings. Mon. Wea. Rev., 111, 2016-2033.
- _____, 1988: Observational evidence of slantwise convective adjustment. Mon. wea. rev., 116, 1805-1816.
- English, M., 1973: Growth of large hail in the storm. Alberta hailstorms, Part II, Meteor. Monogr., 36, 37-98.
- Gibson, C., and B. Kochtubajda, 1991: Overview of weather clutter research at the Alberta Research Council. 48th (NATO) AGARD-EPP, Symposium, CP-501, Ottawa, 19 1-10.
- Gyakum, J. R., 1987: Evolution of a surprise snowfall in the United States Midwest. Mon. Wea. Rev., 115, 2322-2345.
- Hoskins, B. J., 1974: The role of potential vorticity in symmetric stability and instability. Quart. J. Roy. Meteor. Soc., 100, 480-482.
- Krauss, T. W., and J. D. Marwitz, 1984: Precipitation processes within an Alberta supercell hailstorm. J. Atmos. Sci., 41, 1025-1034.
- Longley, R. W., and C. E. Thompson 1965: A study of the causes of hail. J. Appl. Meteor., 4, 69-84.
- Newark, M. J., 1984: Canadian tornadoes, 1950-1979. Atmos.-Ocean, 22, 343-353.
- Newton, C. and E.O. Holopainen, 1990: Extratropical cyclones. Amer. Meteor. Soc., Boston, 262.
- Ooyama, K., 1966: On the stability of the baroclinic circular vortex: A sufficient criterion for instability. J. Atmos. Sci., 23, 43-53.

- Ray, 1986: Mesoscale meteorology and forecasting. Amer. Meteor. Soc., Boston, 723.
- Reinelt, E. R., 1970: On the role of orography in the precipitation regime of Alberta. The Albertan Geographer, 6, 45-58.
- Renick, J. H., and J. B. Maxwell, 1977: Forecasting hailfall in Alberta. Meteor. Monogr., 38, Amer. Meteor. Soc., Boston, 145-151.
- Reuter, G. W., and M. K. Yau, 1990: Observation of slantwise convective instability in winter cyclones. Mon. Wea. Rev., 118, 447-458.
- ____, and _____, 1993: Assessment of slantwise convection in ERICA cyclones. Mon. Wea. Rev., 121, 375- 386.
- ____, and C. D. Nguyen, 1994: Organization of cloud and precipitation in an Alberta storm. Atmospheric Research (in press).
- Rogers, R. R., and N. K. Sakellariou, 1986: Precipitation production in three Alberta thunderstorms. Atmos. -Ocean, 24, 145-168.
- ____, and M. K. Yau, 1989: A short course in cloud physics. Pergamon Press, Oxford, 293 pp.
- Sanders, F., and L. F. Bosart, 1985: Mesoscale structure in the megalopolitan snowstorm of 11-12 February 1983. Part I: Frontogenetical forcing and symmetric instability. J. Atmos. Sc., 42, 1050-1061.
- Seltzer, M. A., R. E. Passarelli and K. A. Emanuel, 1985: The

- possible role of symmetric instability in the formation of precipitation bands. *J. Atmos. Sci.*, 42, 2207-2219.
- Smith, S. B. and M. K. Yau, 1937: The mesoscale effect of topography on the genesis of Alberta hailstorms. *Beitr. Phys. Atmosph.*, 60, 371-392.
- ____, and ____ , 1993a: The causes of severe convective outbreaks in Alberta. Part I: A comparison of a severe outbreak with two non-severe events. *Mon. Wea. Rev.*, 121, 1099-1125.
- ____, and ____ , 1993b: The causes of severe convective outbreaks in Alberta. Part II: Conceptual model and statistical analysis. *Mon. Wea. Rev.*, 121, 1126-1133.
- Snook, J. S., 1992: Current techniques for real-time evaluation of conditional symmetric instability. *Wea. and Forecasting*, 7, 430-439.
- Stamp, R. M., 1988: Alberta. *Canadian Encyclopedia*, 2nd Ed., Hurtig Publ., Edmonton, p 51.
- Stone, P. H., 1966: On non-geostrophic baroclinic instability. *J. Atmos. Sci.*, 23, 390-400.
- Strong, G. S., 1989: LIMEX-85: Processing of data sets from an Alberta mesoscale upper air experiment. *Clim., Bul.*, 23, 98-118.
- Wojtiw, L., 1975: Climatology of hailstorms in Alberta. *NHRE Symposium/Workshop on hail*, Estes Park, NCAR, Boulder, Colorado, Preprint 1, Sec. 11, c.1. 14 pp.
- Wolfsberg, D. G., K. A. Emanuel and R. E. Passarelli, 1986:

Band formation of a New England winter storm. Mon. Wea.
Rev., 114, 1552-1569.

Chapter 2

Theory of Conditional Symmetric Instability

2.1 Basic criterion for CSI

To explain the basic theory of conditional symmetric instability it is instructive to consider first a very simple flow arrangement. The following is assumed:

- (a) The flow is two-dimensional in a single vertical plane.
- (b) The flow is in hydrostatic and geostrophic balance.
- (c) There is a horizontal temperature (and density) gradient in the cross-flow direction; i.e. the flow is baroclinic.
- (d) The air is saturated with respect to water vapour.
- (e) The air equivalent potential temperature, θ_e , increases with height; i.e. the flow is convectively stable.

For this configuration, a Cartesian coordinate system (x, y, z) can be placed so that the z -axis points vertically upwards, the y -axis points in the direction of the flow motion and the x -axis is normal to the flow, pointing toward the warmer air. Under these conditions, since $(\partial p / \partial y) = 0$, the pressure gradient force in the y direction is zero and $u = 0$. Since the saturated flow is in geostrophic balance the vertical wind shear, $\partial v / \partial z$, can be found from the horizontal gradient of equivalent potential temperature, θ_e , using the (saturated) thermal wind balance (e.g. Durran and Klemp 1982; Emanuel 1983a)

$$\frac{\partial v}{\partial z} = \frac{g}{f} \frac{\Gamma_m}{\Gamma_d} \frac{1}{\theta_e} \frac{\partial \theta_e}{\partial x}, \quad (1)$$

where g is the gravitational acceleration, f is the Coriolis parameter, Γ_m is the saturated adiabatic lapse rate, and Γ_d is the dry adiabatic lapse rate. Since the positive x -axis points toward the warmer air, the thermal shear $\partial v / \partial z$ is positive in this case.

Consider now a tube of saturated air that has an infinite length in the y direction. Let us displace the air tube from its initial position. If all the air thermodynamic processes are adiabatic (thermal radiation and frictional heating are negligible), θ_e of the air tube remains the same; i.e. θ_e is a conservative variable (e.g. Holton 1979, p 331):

$$\frac{d\theta_e}{dt} = \frac{d}{dt} \left\{ \theta \exp \left(\frac{Lw_s}{C_p T} \right) \right\} = 0. \quad (2)$$

In (2), T is the temperature ($^{\circ}\text{K}$) at the lifting condensation level, L is the latent heat of vaporisation of water, w_s is the actual mixing ratio, C_p is the specific heat of dry air at constant pressure. Another variable that is conserved during the tube displacement is the so-called absolute angular momentum, M (e.g. Emanuel 1983)

$$M \equiv v + f x, \quad (3)$$

where x denotes the distance of the tube from the origin. The derivation of why M is indeed conservative is based on the

geostrophic balance:

$$\frac{dM}{dt} = \frac{d(v+fx)}{dt} = \frac{dv}{dt} + f u = -\frac{1}{\rho} \frac{\partial p}{\partial y} = 0. \quad (4)$$

Any displacement of the tube in the x-z plane is governed by the conservation of its M and θ_e . In order to detect the presence of CSI, the tube's M and θ_e values must be compared with those of the environment. Specifically, the components of the tube's acceleration are given by (e.g. Sanders and Bosart 1985):

$$\frac{du}{dt} = f (M_P - M_E) = f M', \quad (5)$$

and

$$\frac{dw}{dt} = g \frac{\theta_P - \theta_E}{\theta_E} \approx g \frac{\theta_{eP} - \theta_{eE}}{\theta_{eE}} = g \frac{\theta'_e}{\theta_{eE}}, \quad (6)$$

where, subscripts P and E refer to the tube and environment, respectively. The prime denotes the difference between the air tube value and the environment value of each variable. Thus, the horizontal and vertical accelerations are proportional to $M_P - M_E$ and $\theta_{eP} - \theta_{eE}$, respectively.

Consider now the simple situation where the surfaces of constant M and constant θ_e are planar as shown on Figure 1. To examine this particular flow field we consider the movement of three tubes: in the horizontal (tube A), vertical (tube B) and slantwise (tube C) directions.

(a) Horizontal tube displacement

The tube of air is initially at point A. It is displaced horizontally to a new position A1 (Figure 1). During this displacement, the tube conserves its original values of the absolute angular momentum $M=M_A$ and the equivalent potential temperature $\theta_e=\theta_{eA}$. At A1 the ambient air has $M=M_{A1}$ and $\theta_{e1}=\theta_{eA1}$. Since $M_A > M_{A1}$, $M' > 0$ yielding a positive horizontal acceleration du/dt (i.e. directed toward the right). As a result, the tube will be accelerated back to its original position A. After "overshooting" through point A, the tube will reach A2. Here, however, the tube's M value is less than that of the ambient air; $M_A < M_{A2}$, and hence $du/dt < 0$. Again the parcel is moved back to its original position. Clearly, a horizontal displacement of the tube will result in horizontal oscillations of the tube around its position of origin A.

(b) Vertical tube displacement

Now, consider a vertically upward displacement of a tube from point B to point B1. At its initial position B, the tube has $M=M_B$ and $\theta_e=\theta_{eB}$ and it will conserve both these quantities. When the tube is displaced vertically to B1, the ambient air has $M=M_{B1}$ and $\theta_e=\theta_{eB1}$. Clearly, the excess equivalent potential temperature of the tube $\theta_e'=\theta_{eB}-\theta_{eB1} < 0$; this causes a negative vertical acceleration, $dw/dt < 0$. Thus a vertical displacement of a tube of air results in a vertical oscillation, indicating stable conditions.

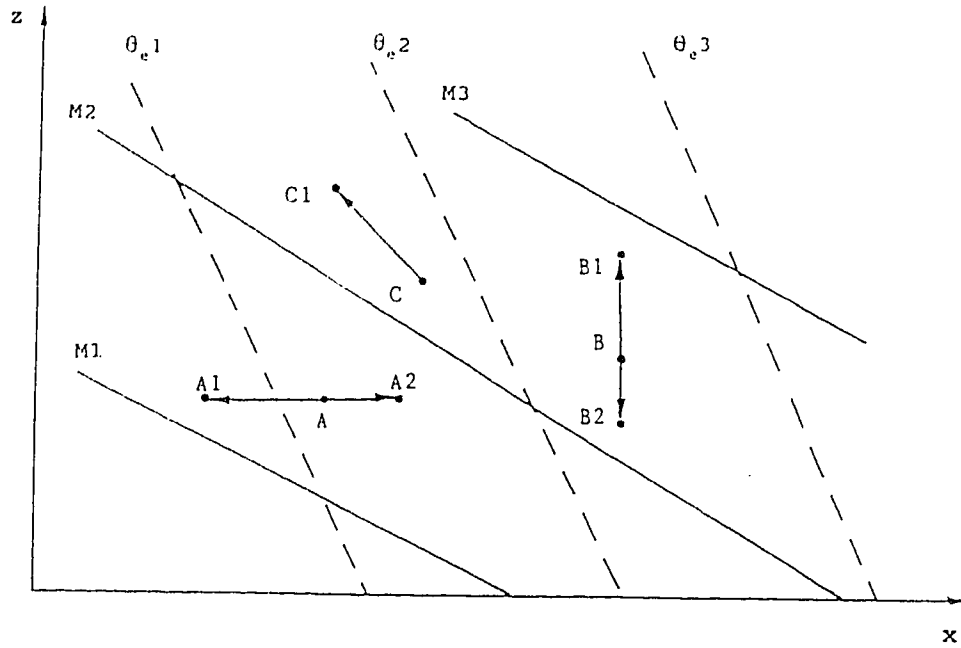


Figure 1. Schematic x-z cross-section, depicting surfaces of constant M (solid lines, $M3 > M2 > M1$) and θ_e (dashed lines, $\theta_{e3} > \theta_{e2} > \theta_{e1}$) values. A horizontal, a vertical and a slantwise displacement of an air tube are shown at A, B and C, respectively.

(c) Slantwise tube displacement

Consider a tube originally at C (with $M=M_C$ and $\theta_e=\theta_{ec}$). The air tube is displaced in a slantwise ascent with a slope intermediate between the slopes of the environmental M and θ_e surfaces. At point C1, the tube's M value M_C is smaller than that of the ambient air M_{C1} . Thus $M' < 0$, causing $du/dt < 0$. In the vertical, however, $\theta_e' = \theta_{ec} - \theta_{ec1} > 0$ causing an upward acceleration

of the tube, $dw/dt > 0$. From the orientation of the surfaces of constant M and θ_e values (Figure 1), it follows that M' and θ_e' will always have the same signs as the x and z components of the displacement at $C1$, respectively. Therefore, the tube will tend to accelerate further in its slantwise ascent, along the line from C to $C1$ and beyond. Thus, the tube's small slantwise displacement has generated an accelerated motion in the same direction, showing the instability of the flow pattern. This instability is **Slantwise Convective Instability or Conditional Symmetrical Instability (CSI)**. The main conclusion to be drawn is the following: CSI requires the slope of the M surface to be shallower than the slope of the θ_e surface. Simply put, CSI will be present whenever, on the cross-section, the ratio of the slope of the M isopleth to the slope of the θ_e isopleth is less than 1.

2.2 Moist Richardson number criterion for CSI

Detecting the presence of CSI along the flow by means of a cross-section (similar to Figure 1) is complicated. In fact, for a single atmospheric sounding the use of a cross-section is impossible and a more practical way of detection is needed. An easy way of solving the problem is to derive, for the above **ratio**, a mathematical expression involving measured or derived quantities. The numerical value of the ratio will indicate the presence or absence of conditional symmetric instability in an atmospheric layer.

Referring to Figure 1, when a tube is displaced along a surface of constant M , an increment δx in the horizontal is accompanied with an increment δz in the vertical. Because the parcel conserves its M , the total differential dM is zero:

$$dM = (\partial M / \partial x) \delta x + (\partial M / \partial z) \delta z = 0, \quad (7)$$

where $\partial M / \partial x$ and $\partial M / \partial z$ are partial rates of change of M with x and z , respectively. From (7), the slope of the M surface is $(\delta z / \delta x)_M$, given by

$$(\delta z / \delta x)_M = - \frac{\partial M / \partial x}{\partial M / \partial z}, \quad (8)$$

where subscript M indicates that the motion is along a line of constant M value. Differentiating (3) with respect to x and z , and substituting these expressions in (8), gives

$$(\delta z / \delta x)_M = - \frac{f + (\partial v / \partial x)}{\partial v / \partial z}. \quad (9)$$

Note that the ratio's numerator is the vertical component of the absolute vorticity $\eta = f + (\partial v / \partial x)$, as by assumption, there is no variation of v in the y direction.

Similarly, the slope of a constant θ_e surface is given by

$$(\delta z / \delta x)_{\theta_e} = - \frac{\partial \theta_e / \partial x}{\partial \theta_e / \partial z}. \quad (10)$$

The horizontal gradient $\partial \theta_e / \partial x$ can be found from the vertical windshear relationship (1) and substituted into (10) to obtain

$$(\delta z / \delta x)_{\theta_e} = - \frac{f}{g} \frac{\Gamma_d}{\Gamma_m} \theta_e \frac{\partial v / \partial z}{\partial \theta_e / \partial z}. \quad (11)$$

The ratio of the slope of the constant M surface to the slope of the constant θ_e surface is given by

$$\frac{(\delta z / \delta x)_M}{(\delta z / \delta x)_{\theta_e}} = \frac{f + (\partial v / \partial x)}{f} \frac{\Gamma_m}{\Gamma_d} \frac{g}{\theta_e} \frac{(\partial \theta_e / \partial z)}{(\partial v / \partial z)^2} \equiv Ri_m \quad (12)$$

This ratio is called the **moist Richardson number (Ri_m)**. First, it is to be noted that Ri_m is always positive, unless $\partial \theta_e / \partial z < 0$; but $\partial \theta_e / \partial z < 0$ indicates (vertical) convective instability (CI). When $0 < Ri_m < 1$, a slantwise displacement can result in unstable conditions for saturated slantwise convection. In short, for a layer of moist air the stability criteria are:

- $Ri_m < 0 \quad \Rightarrow \quad$ potential for CI,
- $Ri_m = 0 \quad \Rightarrow \quad$ convective neutrality,
- $1 > Ri_m > 0 \quad \Rightarrow \quad$ potential for CSI,
- $Ri_m = 1 \quad \Rightarrow \quad$ slantwise neutrality and
- $Ri_m > 1 \quad \Rightarrow \quad$ absolute stability.

2.3 Equivalent potential vorticity criterion for CSI

For dynamical studies it is more convenient to express the CSI instability criterion in terms of absolute vorticity. Consider again the flow structure in which the slope of the surface of constant M is shallower than that of θ_e (Figure 1). When an air tube is moved along its constant θ_e surface in the

positive x direction, it will experience a gradual decrease of the ambient air M values, i.e.,

$$(\partial M / \partial x)_{\theta_e} < 0. \quad (13)$$

Differentiating (3) with respect to x and substituting into (13) gives

$$\eta_{\theta_e} = [(\partial v / \partial x) + f]_{\theta_e} < 0. \quad (14)$$

According to (14), there is a potential for CSI when the vertical component of the absolute vorticity decreases along a surface of constant θ_e value. Alternatively, it can be shown that when the equivalent potential vorticity, q_e , is negative ($q_e < 0$), the two-dimensional saturated flow is unstable for moist slantwise convection (e.g. Bennetts and Hoskins 1979). In a Cartesian co-ordinate system q_e is defined by

$$q_e = f \frac{g}{\theta_e} \left[\left(f + \frac{\partial v}{\partial x} \right) \frac{\partial \theta_e}{\partial z} - \frac{\partial \theta_e}{\partial x} \frac{\partial v}{\partial z} \right]. \quad (15)$$

2.4 Assessing CSI from sounding data

Several techniques have been developed to determine the presence of CSI, using sounding data (Emanuel 1983b). One of the techniques involves the construction of x-z cross-sections portraying both the M and θ_e fields. The x-axis is chosen to be perpendicular to the direction of the major geostrophic windshear; i.e. the x-axis is parallel to the maximum thermal gradient. The position of the radiosonde stations have to be

projected onto the x-axis and at these sites M and θ_e values are computed, along the vertical, from radiosonde measurement data. Horizontal interpolation is used to complete the cross-sections. The potential for slantwise convection can then be assessed by comparing the slopes of constant M and θ_e lines (e.g. Reuter and Yau 1990) or by constructing thermodynamic soundings along a selected constant M surface (e.g. Reuter and Yau 1993). Both of these methods require a dense (mesoscale) network of simultaneous sounding measurement, otherwise the uncertainties associated with the horizontal interpolation of data, between adjacent soundings, become problematic.

In western Canada the network of operational upper air stations is far from dense because the distance between two adjacent sounding sites is typically 750 km. Since slantwise convection occurs on a smaller scale, the CSI assessment must be based on data from a single sounding, supported by synoptic scale flow charts for the standard pressure levels. The moist Richardson number criterion for CSI can be used with data from a single sounding (e.g. Seltzer et al. 1985). Any atmospheric layer for which the Ri_m value is between 0 and 1 is subject to a potential for moist slantwise overturning. More detail about this technique will be given in the next chapter.

Emanuel (1983b) developed a technique to assess CSI that allows one to obtain a sounding along a constant M surface. This technique uses regular radiosonde temperature, humidity and wind data and the vertical distribution of the large-scale

absolute vorticity. The latter can be approximated from the operational vorticity charts. Atmospheric thermodynamic data, along a constant M surface, can be analyzed on thermodynamic diagrams such as a tephigram. The analysis allows one to find the slantwise convective condensation level, slantwise level of free convection and slantwise level of zero buoyancy.

This technique is founded on the concept of Slantwise Convective Available Potential Energy (SCAPE), the slantwise counterpart of CAPE of cumulus convection, expressed as:

$$SCAPE = \int_1^2 \left[g \frac{T_P - T_E}{T_E} + \frac{1}{2} \frac{f}{\eta} \frac{d[(v - v_1)^2]}{dz} \right] dz, \quad (16)$$

where g is the gravitational acceleration, T_P and T_E are the parcel and the environment absolute temperature, respectively, f is the Coriolis parameter, η is the absolute vorticity of the flow, z is height, $v = v(z)$ is the ambient wind speed and v_1 is the parcel's v at z_1 . The first term in (16) depicts the standard positive area on a tephigram and represents the potential energy due to vertical acceleration. The second term is the contribution, to potential energy, from centrifugal forces due to horizontal accelerations. If g and T_E within the layer are constant, (16) can be rewritten as

$$SCAPE = \frac{g}{T_E} \int_1^2 \left[\Delta T + \frac{1}{2} \frac{T_E}{g} \frac{f}{\eta} \frac{d(\Delta v)^2}{dz} \right] dz, \quad (17)$$

where $\Delta T = T_P - T_E$ and $\Delta v = v - v_1$. The second term in brackets is equivalent to a "temperature adjustment" ΔT ($^{\circ}\text{K}$), to be added

to the lifted temperature of the parcel at the top of the layer under analysis. In a simple manner, the adjustment term ΔT is approximated by

$$\Delta T = \frac{1}{2} \frac{f}{\eta} \frac{T}{g} \frac{(\Delta v)^2}{\Delta z} \quad (18)$$

where T is the layer mean absolute temperature, Δv is the thermal wind speed and Δz is the thickness of the layer. If a parcel is lifted adiabatically from a lower level to a higher level where its new temperature is T_p , the adjustment ΔT must be added to T_p to find T_{ps} , the slantwise temperature of the lifted parcel. Then, CSI can be assessed on a layer by layer basis by comparing T_{ps} to the temperature of the environment at the top of the layer.

2.5 Limitations of CSI theory

When the theory of CSI is applied to the real atmosphere, some caution is needed to assure that the basic assumptions are indeed satisfied. First, the theory requires that the wind be unidirectional in the layer under analysis for slantwise convection. Furthermore the flow must satisfy the thermal wind balance and this may not always be the case. Particularly, the surface boundary layer is not suited for CSI assessment. Note that the thermal wind balance is a less stringent requirement than that of geostrophic balance, as the vertically averaged non-geostrophic wind has no effect.

When the air is moist but unsaturated, CSI can only be

released after the whole air mass has been lifted to reach and maintain saturation. Clearly, this is not generally the case, and this indicates that the analysis of moist but unsaturated air can only point to the potential for instability. The CSI theory neglects the effects of mixing and pressure deviations. There may be observed cases where these effects may be significant. And as in all stability analysis, the results are dependent on the accuracy and resolution of the measurements.

References

- Bennetts, D. A., and B. J. Hoskins, 1979: Conditional symmetric instability a possible explanation for frontal rainbands. *Quart. J. Roy. Meteor. Soc.*, 105, 945-962.
- Durran, D. R., and J.B. Klemp, 1982: On the effects of moisture on the Brunt- Väisälä frequency. *J. Atmos. Sc.*, 39, 2152- 2158.
- Emanuel, K. A., 1983a: The Lagrangian parcel dynamics of moist symmetric instability. *J. Atmos. Sc.*, 40, 2368-2376.
- _____, 1983b: On assessing local conditional symmetric instability from atmospheric soundings. *Mon. Wea. Rev.*, 111, 2016-2033.
- Holton, J. R., 1979: An introduction to dynamic meteorology. Sec. Edition, Academic Press, New York, 391 pp.
- Reuter, G. W. and M. K. Yau, 1990: Observations of slantwise convective instability in winter cyclones. *Mon. Wea. Rev.*, 118, 447-458.
- _____, and _____, 1993: Assessment of slantwise convection in ERICA cyclones. *Mon. Wea. Rev.*, 121, 375-386.
- Sanders, F., and L. F. Bosart, 1985: Mesoscale structure in the megalopolitan snowstorm of 11-12 February 1983. Part I: Frontogenetical forcing and symmetric instability. *J. Atmos. Sc.*, 42, 1050-1061.
- Seltzer, M. A., R. E. Passarelli, and K.A. Emanuel, 1985: The possible role of symmetric instability in the formation of precipitation bands. *J. Atmos. Sci.*, 42, 2207-2219.

Chapter 3

Band formation in an Alberta snowstorm

3.1 Introduction

Forecasting heavy snow events over central Alberta is challenging for every forecaster. The Rocky Mountains and the adjacent foothills constitute a complicated topography that influences the timing and distribution of heavy snow in this region (Reinelt 1970). The major NW-SE mountain barrier often provides for lee cyclogenesis (Chung et al. 1976) that may cause major snowstorms. Unlike the attention given to severe summertime convection in Alberta (Chisholm 1973; Rogers and Sakellariou 1986; Al-Jumily et al. 1991; Smith and Yau 1987; 1993), little attention has been given to Alberta snow events. In fact, not a single case study of Alberta snow storms could be found in the literature.

In this chapter the synoptic and mesoscale events that led to the heavy snowstorm of 4 and 5 October 1990 will be investigated. Radar measurements indicated that in the area of analysis, the heavy snow in this storm fell predominantly from a single narrow band oriented in the direction of the upper-level flow. This is not uncommon, since mid-latitude cyclones often exhibit precipitation bands at the mesoscale (Hobbs 1978). A number of theories have been developed to explain the existence of these bands. The theories include

differential temperature advection (Browning et al. 1973), Ekman layer instability (Lilly 1966), gravity wave ducting (Lindzen and Tung 1976), seeder-feeder processes (Rutledge and Hobbs 1983), frontogenesis (Sanders 1955) and conditional symmetric instability (Bennetts and Hoskins 1979; Emanuel 1979; 1983a,b).

At the very outset it should be stressed that here, the aim is not to determine the relative importance of all these different mechanisms in causing snowbands over this region. Rather, the aim is simply to identify the role of conditional symmetric instability, CSI, on band formations. The special interest of this study in CSI, for the prairies snowstorms, is motivated by the fact that most case studies of slantwise convection have been conducted for the east coast of North America: Carolinas (Emanuel 1988), Massachusetts (Sanders and Bosart 1986), New England (Wolfsberg et al. 1986), Nova Scotia (Donaldson and Stewart 1989; Reuter and Yau 1990). During the winter the east coast regions have strong baroclinicity (large temperature gradient) that provides favourable conditions for the onset of slantwise convection. It is not clear whether CSI plays a similar role in organizing precipitation patterns in continental snowstorms occurring over the prairies. In the literature, the only suggestion of slantwise convection in prairie storms is the recent case study of the Alberta heavy rainstorm of 17-18 July 1986 (Reuter and Nguyen 1993). The analysis showed that the heavy precipitation was associated

with linear bands and that the middle troposphere had the potential for slantwise convection. The lower troposphere, however, was unstable for vertical cumulus convection; thus it was difficult to determine how much CSI really contributed toward the rain formation in that particular event.

This chapter proposes to document the occurrence of CSI during the 4-5 October 1990 snowstorm over central Alberta. The data consisted of reflectivity measurements collected by C-band radar, and upper air balloon soundings. These data, in combination with upper air charts and surface synoptic maps, will be used to focus on the role of CSI as a possible forcing mechanism for a persistent band of heavy snow.

The novelty of this stability analysis using data from a single sounding site is that, contrary to previous studies by some other investigators, it includes the contribution of the vertical large-scale vorticity which affects the CSI property of a layer. The flow vorticity values were estimated by the Laplacian of geopotential heights, using the finite-difference approximation at different pressure levels. Previous studies (e.g. Parsons and Hobbs 1983; Seltzer et al. 1985; Donaldson and Stewart 1989; Reuter and Yau 1990; Reuter and Nguyen 1993) were all based on the assumption that the absolute vorticity, η , can be approximated by the planetary vorticity, f , at the local latitude. Simply put, $\eta = f + (\partial u / \partial y + \partial v / \partial x) \approx f$, where u and v are the x-component and the y-component, respectively, of the real wind.

3.2 Observational data and methods of analysis

3.2.1 Radar data

The radar data, used in this study, were collected as part of a field experiment conducted by the Alberta Research Council (ARC) to test the accuracy of radar-derived rainfall measurements (Kochtubajda et al. 1990). The CWSR-81 type ARC radar is located in Penhold (52.2°N, 113.8°W) near Red Deer, at 904 m of elevation. It operates at a wavelength of 5 cm and transmits a peak power of 250 kW with a pulse repetition frequency of 250 Hz. The antenna consists of a parabolic reflector which concentrates the power into a narrow cone with a beam-width of 1.1° and its gain factor is 43 dB. The antenna performs a volume scan, rotating at close to 3 rpm with an upper elevation limit of 20°. After the standard range effects correction, the data for different elevation angles were synthesized to obtain Constant Altitude Plan Position Indicator (CAPPI) scans at 1.5 km above ground.

3.2.2 Surface and sounding data

The other data sets used in this analysis are rather standard. Operational sounding balloons were released from Stony Plain (53.5°N, 114.1°W, 766 m ASL) at 00 and 12 UTC on a daily basis. Digital data of pressure, temperature, height, relative humidity, wind speed and direction, recorded during balloon soundings were obtained from the 'upper air archive' of AES (Atmospheric Environment Service of Canada). Surface

analysis maps and upper air contour charts were obtained from the Canadian Meteorological Centre (CMC) and NOAA, National Meteorological Centre (NMC) of the U.S.A. Precipitation data were taken from the AES Monthly Record.

3.2.3 Assessment of CSI from single sounding data

The potential for slantwise convection can be evaluated by computing the moist Richardson number, Ri_m , using upper air sounding data. The Ri_m computation starts with choosing the primary direction of the thermal shear; this direction is perpendicular to that of the strongest temperature gradient. Once this direction is determined, the observed wind vector is decomposed into its two orthogonal components u (cross-shear component) and v (along-shear component). Specifically, when the major thermal shear blows from an angle α (degrees from north), the along-band component v is computed by

$$v = V \cos(\alpha - \beta), \quad (1)$$

where V denotes the speed of the observed wind vector blowing from an angle β (degrees from north). The moist Richardson number is given by (e.g. Seltzer et al. 1985):

$$Ri_m = \frac{\eta}{f} \frac{\Gamma_m}{\Gamma_d} \frac{g}{\theta_e} \frac{(\partial \theta_e / \partial z)}{(\partial v / \partial z)^2}, \quad (2)$$

where η is the flow's absolute vorticity, f is the Coriolis parameter, θ_e is the equivalent potential temperature, g is the gravitational acceleration, z is the height and Γ_m and Γ_d

are the saturated and dry adiabatic lapse rates, respectively. For saturated air CSI exists when:

$$1 > Ri_m > 0. \quad (3)$$

Emanuel (1979) showed that the horizontal scale for slantwise unstable motion ranges from about 50 to 500 km, and that it has a time scale of a few hours. As there are often small fluctuations in thermodynamic and wind parameters, particularly during stormy conditions, it makes little sense to compute Ri_m for very thin layers.

Analyzing thin layers will certainly miss the mesoscale stratification of the atmosphere which really determines the slantwise stability properties. With this in mind it seemed reasonable to subdivide the atmosphere beneath the tropopause into a few layers, each being about 1000 m thick. As the sounding data were available at the standard pressure levels it was convenient to simply work with the following layers: 90-85 kPa, 85-80 kPa, 80-70 kPa, 70-60 kPa, 60-50 kPa, 50-40 kPa and 40-35 kPa.

Some details regarding the computation of the quantities used in (2) are given below. At any given pressure level, the equivalent potential temperature θ_e was computed by Bolton's (1980) expression:

$$\theta_e = \theta \exp \left[\left(\frac{3376.0}{T_{lcl}} - 2.54 \right) w (1.0 + 0.81w) \right], \quad (4)$$

where θ is the potential temperature in °K, T_{lcl} is the lifting

condensation level temperature in °K and w is the mixing ratio of the air, in kg/kg. For use in (4), θ and w are given by:

$$\theta = T \left[\frac{100}{P} \right]^{0.2854 (1.0 - 0.28w)}, \quad (5)$$

$$w = 0.622 \left[\frac{e}{p - e} \right], \quad (6)$$

where T is the absolute air temperature, p and e are the total air pressure and water vapour partial pressure, respectively. The formulae for computing e and T_{lcl} are (Bolton 1980):

$$e = 0.6112 \exp \left[\frac{17.67 t}{t + 243.5} \right], \quad (7)$$

$$T_{lcl} = \left[\frac{1}{T_d - 56} + \frac{\ln(T/T_d)}{800} \right]^{-1} + 56, \quad (8)$$

where t is the air temperature in °C, and T_d is the dewpoint temperature in °K. T_d is calculated by the following formula where $B = 5.42 \times 10^3$ and RH is the relative humidity measured by the radiosonde (see Rogers and Yau 1989, p. 14)

$$T_d = \frac{B}{(B/T) - \ln(RH/100)}. \quad (9)$$

The ratio Γ_m/Γ_d was computed by the expression (e.g. see Iribarne and Godson 1981, p. 182):

$$\frac{\Gamma_m}{\Gamma_d} = \frac{1 + (Lw/R_d T)}{1 + 0.622 (L^2 w / C_{pd} R_d T^2)}, \quad (10)$$

where L is the specific latent heat of vaporisation, R_d is the specific gas constant for dry air and C_{pd} is the specific heat

capacity of dry air at constant pressure.

3.2.4 Computation of absolute vorticity

The absolute vorticity of the flow, $\eta = f + (\partial u / \partial y + \partial v / \partial x)$, on a surface of constant pressure p can be approximated quite accurately by the geostrophic absolute vorticity:

$$\eta \approx \eta_g = f + \frac{g}{f} \left[\frac{\partial^2 z}{\partial x^2} + \frac{\partial^2 z}{\partial y^2} \right] = f + \frac{g}{f} \nabla^2 z, \quad (11)$$

where z denotes the height of the pressure surface p and ∇^2 is the two-dimensional Laplacian. The Laplacian at point (x, y) was replaced with its standard finite-difference approximation

$$\nabla^2 z \approx \frac{z(x+d, y) + z(x-d, y) + z(x, y+d) + z(x, y-d) - 4z(x, y)}{d^2} \quad (12)$$

where d is one half of the grid spacing. For the computation of η , d was taken to be 333 km (3° latitude) and the Coriolis parameter $f = 11.7 \times 10^{-5} \text{ s}^{-1}$ (for latitude 53.5°N). The CMC upper air maps at 85, 70 and 50 kPa constant pressure surfaces were used to evaluate η . As η values are also contoured on the 50 kPa height/vorticity map, the accuracy of approximations (11) and (12) proved to be satisfactory. Linear interpolation was used for obtaining a vertical profile of η .

3.3 Results

3.3.1 Synoptic overview

A weak 50 kPa height ridge with its axis lying over

British Columbia was the conspicuous feature at 00 UTC 4 October, as shown on Figure 1. The NVA (negative vorticity advection) associated with this ridge resulted in subsidence warming causing clear sky conditions over central Alberta. To the east, at the Manitoba-Saskatchewan border, the 50 kPa wind field showed a closed circulation which had dominated the Alberta weather on the previous day. In response to the upper ridge, the MSL pressure field at 00 UTC 4 October has formed a col-pattern (e.g. Pettersen 1956, p 38) indicating rather calm wind conditions over Alberta. The surface low centre associated with the closed upper-low was analyzed at Trout Lake, Ontario, outside the displayed map area.

In the next 12 hours, the upper ridge had become more curved, while moving slowly toward the east. The PVA region (the major synoptic forcing for ascending motion) was still far west of Alberta, with its axis aligned over the Pacific coast. At the surface, the col pattern had followed suit and traversed eastward. Also, a closed surface low (with centre value of 99.6 kPa) was formed over western British Columbia, with a trough extending southeastward. Satellite imagery confirmed surface reports that British Columbia, as well as western Alberta had extensive cloud cover at that stage.

By 00 UTC 5 October, the 50 kPa ridge axis shifted over Alberta, with a shortwave trough moving behind. The surface low was carried along, with its centre located at Revelstoke (YRV), just west of the continental divide. Except for a few

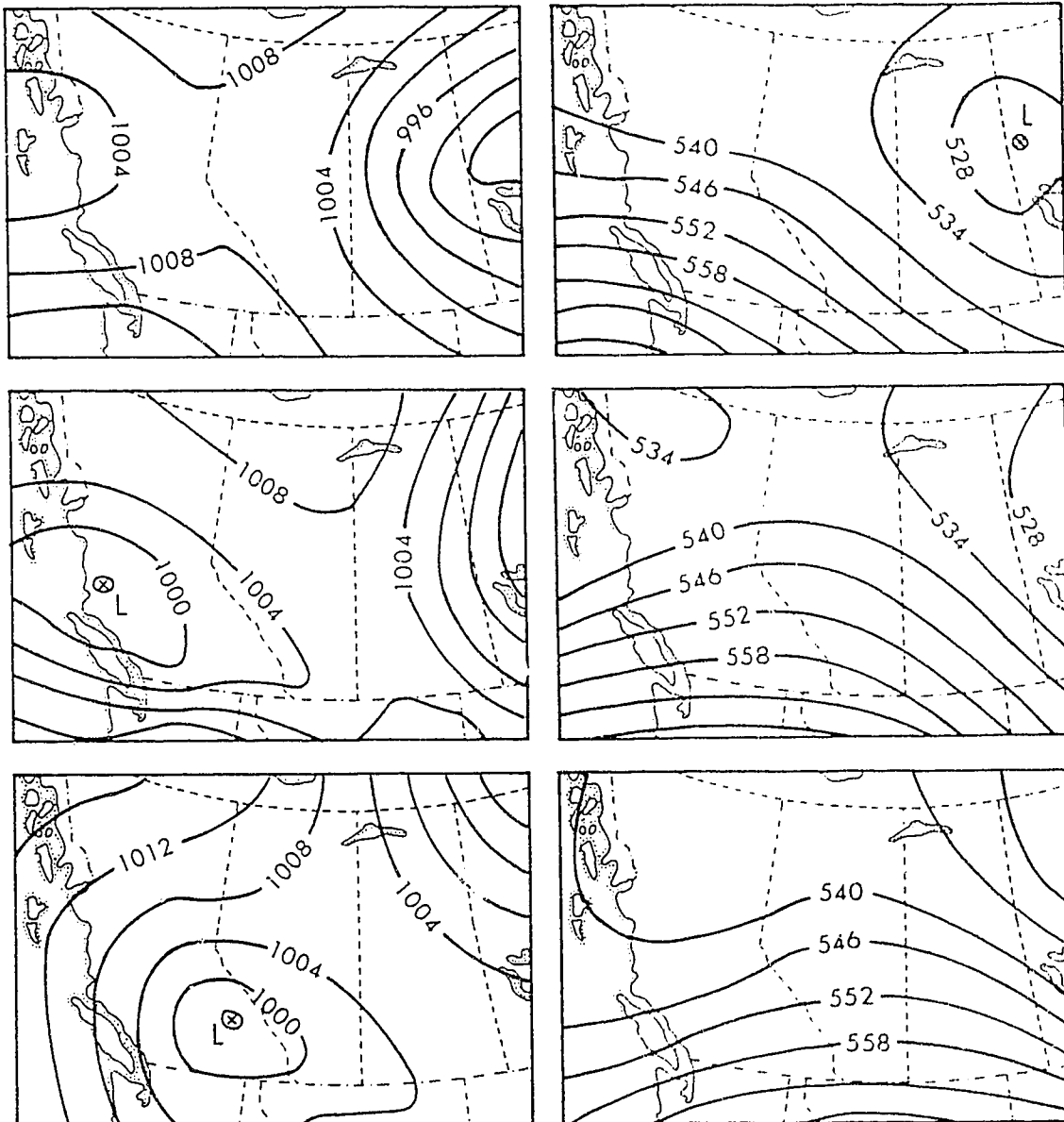


Figure 1. Maps showing surface isobars (in mb) and 50 kPa height contours (in decameter) for western Canada at 00 UTC 4 October (top), 12 UTC 4 October (middle) and 00 UTC 5 October 1990 (bottom).

stations in the north, all Alberta surface stations reported cloud and snow. In the boundary layer the synoptic flow is from the east, which probably induces some topographic lifting in the foothills of the Rocky Mountains. Some clouds may have been caused by these upslope conditions (Reinelt 1970).

3.3.2 Formation of a baroclinic zone

The isobars' hyperbolic pattern, corresponding to a col in the surface pressure field, was indicative of significant deformation in the low-level flow at 00 UTC and 12 UTC 4 October. As theory suggests, a persistent zone of 'stretching deformation' would intensify a pre-existent baroclinic zone, i.e. cold air advection and warm air advection would tend to strengthen the horizontal temperature gradient. The surface maps, however, indicated that the surface temperature field was largely controlled by the slopes in the topography and variable snow cover, providing complex spatial patterns of surface albedos and associated surface temperature values. With such small-scale variations it is not easy to recognize a coherent and organized large-scale pattern in the thermal field. However, the isotherms pattern at 85 kPa level, valid at 00 UTC 4 October (Figure 2), indicated a weak north-south temperature gradient ($\approx 1^\circ\text{C}/100\text{ km}$). By 12 UTC, baroclinicity had become stronger ($\approx 2.5^\circ\text{C}/100\text{ km}$) with the gradient vector pointing towards the south-southeast. The intensification

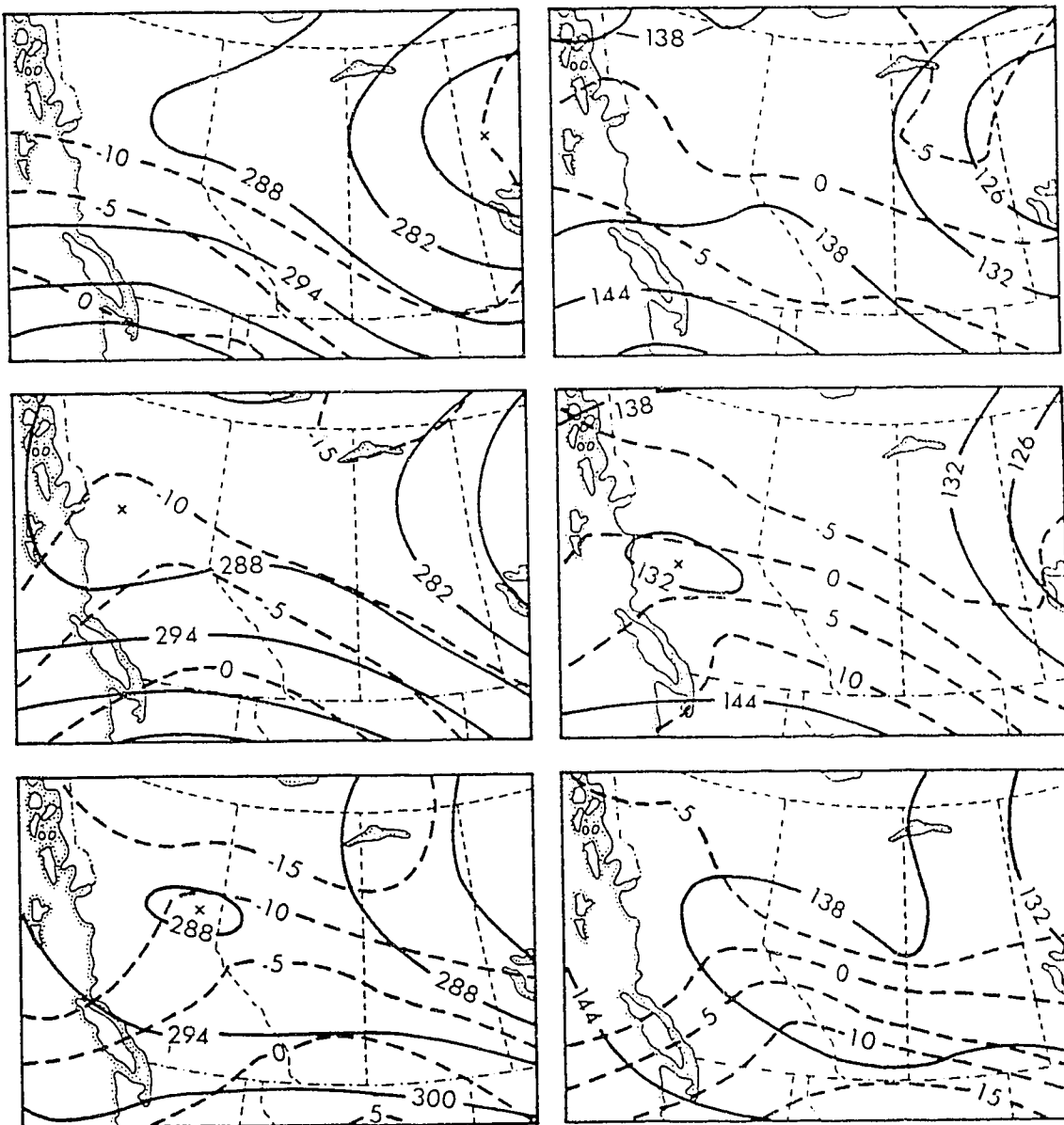


Figure 2. 70 kPa (left) and 85 kPa (right) analysis at 00 UTC 4 October (top), 12 UTC 4 October (middle) and 00 UTC 5 October 1990 (bottom). Solid contours indicate the height (in decameters) of the constant pressure surface and dashed lines indicate isotherms (in °C).

continued during the next twelve hours and the temperature gradient reached close to $4^{\circ}\text{C}/100\text{ km}$ at the 85 kPa level. A similar trend was apparent at 70 kPa (Figure 2), where the isotherms merged closer together during the 24-hour period. The windshear corresponding to this north-south baroclinic zone caused the strong zonal wind at the 50 kPa level. As will be shown later, the presence of this strong vertical shear was also instrumental in destabilizing the flow with respect to CSI.

3.3.3 Sounding data

Figure 3 shows the sounding data sampled at Stony Plain (WSE), the only upper air station in Alberta. At 00 UTC 4 October, the low-level air was mild, but with a significant dewpoint depression indicating fairly dry conditions. The 12 UTC sounding indicated cooler and moister conditions, and the wind blew from the west increasing strongly with height. At 00 UTC 5 October, the air was saturated from the surface up to 75 kPa. In the lowest levels, the wind was coming from the east or southeast. From 80 up to 70 kPa, however, strong veering occurred and the wind direction shifted to west. The zonal component of the vertical wind shear vector remained strong in the layer from 80 to 40 kPa.

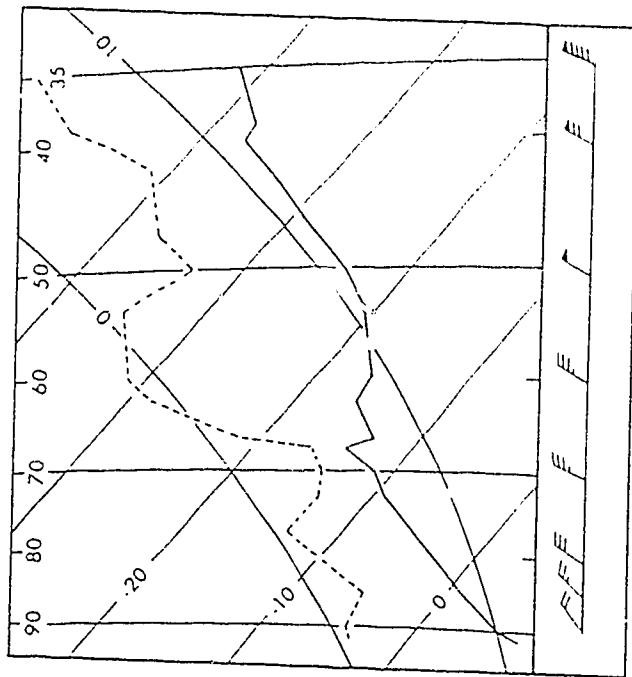


Fig. 3(a)

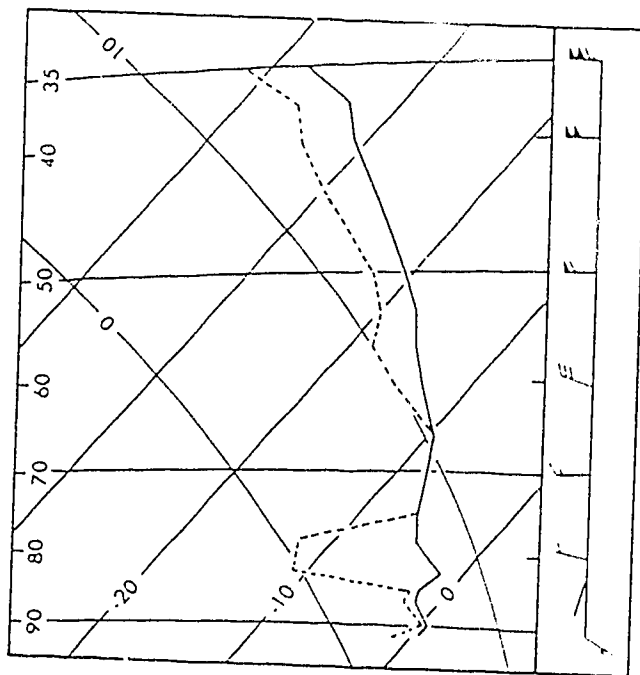


Fig. 3(b)

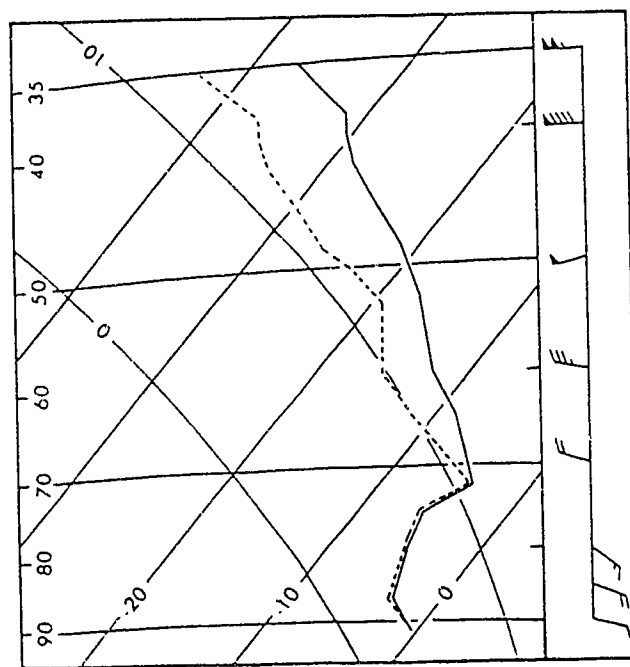


Fig. 3(c)

Figure 3. Measurements from the Stony Plain (WSE) sounding at 00 UTC 4 October (a), 12 UTC 4 October (b) and 00 UTC 5 October 1990 (c). Temperature (solid curve) and dew point (dashed curve) are plotted on a skewed tephigram. Horizontal lines are isobars (in mb). Straight lines skewed to the right are isotherms (in °C). Lines curving to the left are pseudo-adiabats. The panel on the right depicts the observed wind speed and wind direction at 90, 85, 80, 70, 60, 50, 40 and 35 kPa using the conventional station model. Each full barb indicates 10 knots, and a solid flag 50 knots.

3.3.4. Distribution of snowfall

Synoptic surface reports, as well as satellite imagery indicated the presence of a cloud cover over southern and central Alberta from 12 UTC 4 October to 00 UTC 5 October. All the precipitation falling east of the Canadian Rockies fell as snow or wet snow. Large snow amounts fell in the area of analysis between Edmonton and Red Deer. The observed depth of 'new' snow, accumulated from 00 UTC 4 to 00 UTC 5 October 1990

was analyzed and is depicted in Figure 4. A large snowfall of 34 cm, accumulated over 24 hours, was reported at Blindman and several other stations also reported large snow accumulations (Dakota 32 cm, Stony Plain 18 cm). These snowfalls were rather large compared to the typical snow episodes of the Alberta fall season. The temporal and spatial distributions of the

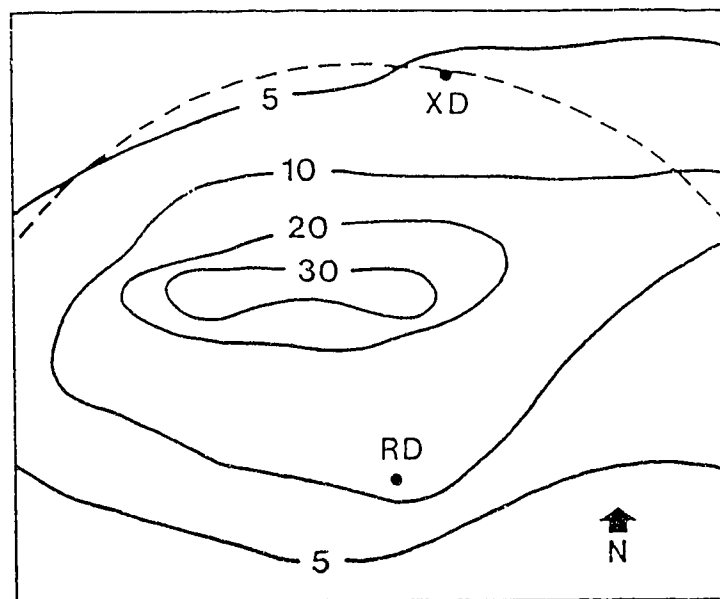


Figure 4. Isopleths of snowfalls (in cm) accumulated over the 24-hour period ending at 00 UTC 5 October 1990. The geography of the region is indicated by the Red Deer (RD) and Edmonton (XD) stations. The semi-circle indicates the northern half of the 120 km range ring, centred at the radar site, near Red Deer.

instantaneous snowfall rates could be sampled using the ARC C-band radar located at Penhold, near Red Deer. Figure 5 shows the hourly evolution of the radar reflectivity field Z (dBz) at 1.5 km above the ground. For interpreting Z values, the empirical Z - R relationship (see Rogers and Yau 1989, p. 191)

$$Z = 2000 R^2, \quad (13)$$

was used, where Z is given in units of mm^6/m^3 , and R denotes the precipitation rate in mm per hour of liquid water (when snow is melted). Since the density of dry snow is about one tenth of that of the liquid water, the symbol R in (13) can alternatively be interpreted as the snowfall rate in cm per hour. With these assumptions, snowfall rates of 0.1, 0.5 and 1 cm/h will correspond to reflectivity values of 13, 27 and 33 dBz, respectively ($\text{dBz} = 10 \cdot \log Z$).

At 19 UTC on 4 October, the CAPPI indicated extensive shield of snowfall (≈ 0.2 cm/h) north of Red Deer. The snow field was interspersed with a few intense cells (≈ 0.5 cm/h) that were roughly aligned in a west-to-east banded pattern. Within the 6 hours that followed, precipitation areas extended further towards the east, and the banded structure of intense snowfall became more organized. From 22 UTC 4 October to 1 UTC 5 October, the highest reflectivity values were concentrated in a narrow band about 10-20 km wide. This persistent band was oriented in a west to east direction, and this was also the direction of the thermal windshear for both 85 and 70 kPa at 00 UTC 5 October 1990.

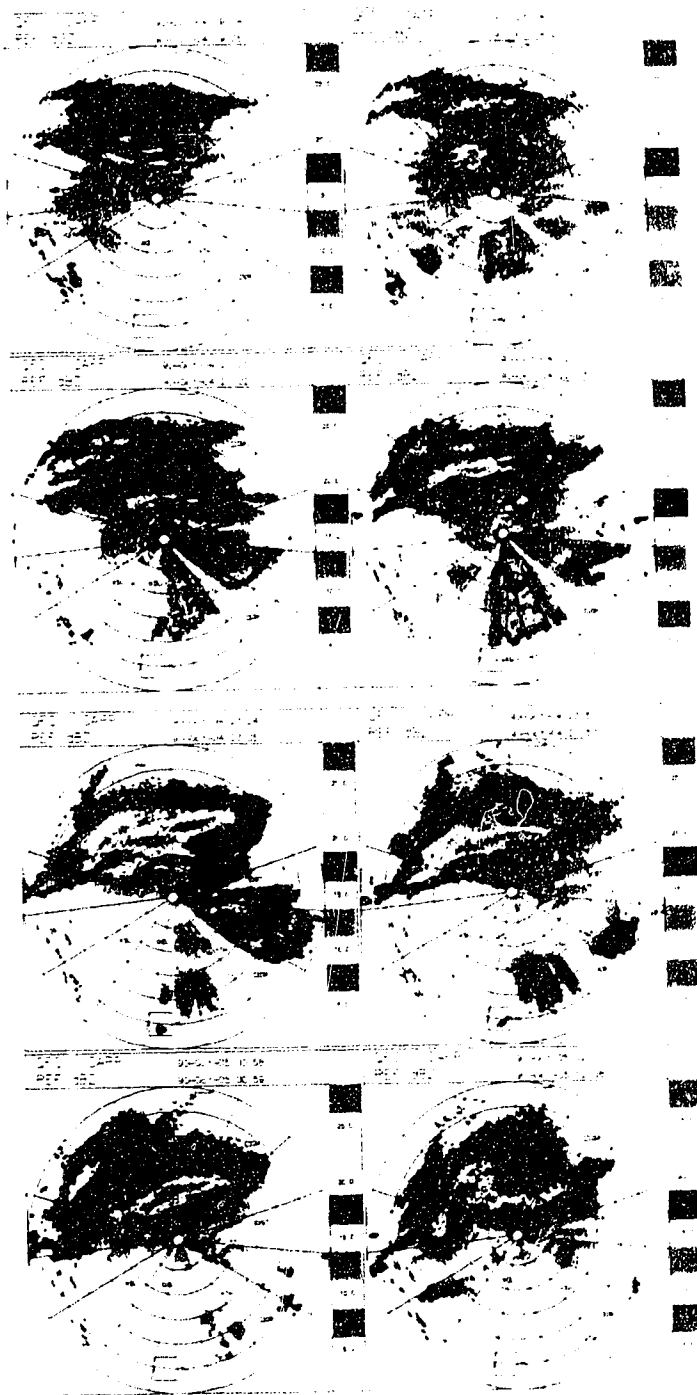


Figure 5. Radar CAPPIs at one-hour time intervals from 19 UTC 4 to 2 UTC 5 October 1990. Range marks are spaced 20 km apart. The radar reflectivity fields at constant altitude of 1.5 km is displayed by different colours. The colour scheme is linear in dBZ, changing every 5 dB as indicated on the right.

3.3.5 Assessment of CSI

The organization of the precipitation field needs to be explained, because the synoptic-scale ascent associated with the developing baroclinic zone cannot account for the observed band of heavy snowfall. Since both the snowband and the strong thermal shear were pointing in the same direction (towards the east) the assessment of the presence of conditional symmetric instability as a possible snow-producing mechanism seemed very logical.

The relevant soundings were those from 12 UTC 4 and 00 UTC 5 October. In both cases the thermal shear direction was chosen to be $\beta=270^\circ$, in agreement with the mid-tropospheric wind observations, the synoptic charts and the CAPPI display of the snowband. Table 1 shows the stability analysis for the sounding of 12 UTC 4 October; the sounding analysis indicated the following:

(1) The air mass was convectively unstable (θ_e decreased with height) in the 90-80 kPa layer. However, the inversion above this layer likely provided a firm lid on the shallow cumulus convection that might be spawned.

(2) The synoptic flow above the 80 kPa level had a cyclonic relative vorticity (positive value) so that the ratio $\eta/f > 1$. For this reason, neglecting this factor will provide a bias toward instability by underestimating the effective value of the Richardson number by about 20%.

(3) The combination of strong vertical shear and weak static stability causes CSI for the layer between 60 and 35 kPa. Once this layer becomes saturated (by ascending motion), slantwise overturning will be triggered. The radar data suggested that this might indeed have happened at about 20 UTC.

Table 1 Stability analysis for CSI for different layers of the sounding data at 12 UTC 4 October and 00 UTC 5 October 1990. Listed are the relative humidity, the lapse rate of equivalent potential temperature ($\partial\theta_e/\partial z$), the along-band component of the wind shear ($\partial v/\partial z$), the ratio of absolute to planetary vorticities (η/f) and the moist Richardson number. CU, SU, and S denote convectively unstable, moist symmetrically unstable and stable, respectively.

WSE, 12 UTC 4 October 1990

| Layer kPa | RH % | $\partial\theta_e/\partial z$ °K/km | $\partial v/\partial z$ m/s/km | η/f | Ri _m | Stability analysis |
|--------------|---------|--|-----------------------------------|----------|-----------------|-----------------------|
| 90 - 85 | 96 | -0.2 | 4.0 | 1.0 | -0.2 | CU |
| 85 - 80 | 74 | -3.9 | 3.5 | 1.0 | -7.2 | CU |
| 80 - 70 | 77 | 9.1 | 4.9 | 1.0 | 8.7 | S |
| 70 - 60 | 94 | 3.3 | 5.1 | 1.1 | 2.9 | S |
| 60 - 50 | 86 | 3.9 | 13.1 | 1.2 | 0.7 | SU |
| 50 - 40 | 80 | 2.8 | 11.7 | 1.2 | 0.6 | SU |
| 40 - 35 | 72 | 2.0 | 8.6 | 1.2 | 0.9 | SU |

WSE, 00 UTC 5 October 1990

| Layer kPa | RH % | $\partial\theta_e/\partial z$ °K/km | $\partial v/\partial z$ m/s/km | η/f | Ri _m | Stability analysis |
|--------------|---------|--|-----------------------------------|----------|-----------------|-----------------------|
| 90 - 85 | 100 | 1.5 | 1.5 | 1.2 | 17.2 | S |
| 85 - 80 | 99 | 7.4 | 10.5 | 1.2 | 1.8 | S |
| 80 - 70 | 97 | 11.4 | 2.3 | 1.2 | 59.5 | S |
| 70 - 60 | 86 | 0.2 | 6.4 | 1.3 | 0.1 | SU |
| 60 - 50 | 74 | 3.6 | 10.1 | 1.2 | 0.9 | SU |
| 50 - 40 | 67 | 2.5 | 9.2 | 1.2 | 0.8 | SU |
| 40 - 35 | 58 | 2.4 | 6.9 | 1.2 | 3.1 | S |

Table 1 also lists the stability analysis for the 00 UTC 5 October sounding, which was about the same time when the radar data revealed the presence of the strongest echoes. Now the air was found to be stable for vertical cumulus convection throughout the entire troposphere. On the other hand, however, the atmosphere was symmetrically unstable in the deep 70 to 40 kPa layer. The conditional symmetric instability was mainly due to the strong shear associated with the baroclinic zone.

3.4 Discussion

Despite the rather frequent occurrence of snowstorms on the Canadian prairies, no documentation regarding an Alberta snowstorm could be found in the research literature. This is rather surprising, for so much research has been reported on summertime convection. The present chapter "breaks the ice" by documenting the 4-5 October 1990 snowstorm, that dumped up to 30 cm in central Alberta. A synoptic analysis showed that the system had little large-scale forcing for ascending air motion and, nevertheless, developed strong mesoscale snowfalls. Radar data revealed that the precipitation field was banded in the direction of the thermal shear vector. Using a single sounding analysis, it was deduced that the snow band was, very likely, related to the presence of CSI in the high shear regime. The stability analysis included the factor η/f which was omitted in previous such studies which used a similar single sounding analysis method.

In the past, most observations of CSI were made in the warm sector of winter cyclones developing in the coastal or marine regions. This study showed that CSI can also occur in the Canadian Prairies and without cyclogenesis. A study by Reuter and Nguyen (1993) also identified the presence of CSI (in addition to convective instability) in a July rainstorm that caused extensive river flooding. It is not clear from these two studies, however, whether CSI occurs often or seldom in the prairies. A "climatological" study, based on a few years of data, seems to be necessary to clarify whether CSI plays a major role in prairie precipitation systems and to what extent it has seasonal characteristics.

References

- Al-Jumily, K. J., R. B. Charlton and R. G. Humphries, 1991:
Identification of rain and hail with circular
polarization radar. *J. Appl. Meteor.*, 30, 1075-1087.
- Bennetts, D. A. and B. J. Hoskins, 1979: Conditional
symmetric instability a possible explanation for frontal
rainbands. *Quart. J. Roy. Meteor. Soc.*, 105, 945-962.
- Bolton, D., 1980: The computation of equivalent potential
temperature. *Mon. Wea. Rev.*, 108, 1046-1053.
- Browning, K. A., M. E. Hardman, T. W. Harrold and C. W.
Pardoe, 1973: The structure of rainbands within a mid-
latitude depression. *Quart. J. Roy. Meteor. Soc.*, 99,
215-231.
- Chisholm, A. J. 1973: Alberta hailstorms, Part I: Radar case
studies and airflow models. *Meteor. Monogr.*, No. 36,
Amer. Meteor. Soc., Boston, 1-36.
- Chung, Y. S., K. D. Hage and E. R. Reinelt, 1976: On lee
cyclogenesis and airflow in the Canadian Rocky Mountains
and the East Asian Mountains. *Mon. Wea. Rev.*, 104, 879-
891.
- Donaldson, N. R. and R. E. Stewart, 1989: On the
precipitation regions within two storms affecting the
Atlantic Canada. *Atmos. Ocean*, 27, 108-129.
- Emanuel, K. A., 1979: Inertial instability and mesoscale
convective systems. Part I: Linear theory of inertial
instability in rotating viscous fluids. *J. Atmos. Sci.*,

- 36, 2425-2449.
- ____, 1983a: The Lagrangian parcel dynamics of moist symmetric instability. *J. Atmos. Sci.*, 40, 2368-2376.
- ____, 1983b: On assessing local conditional symmetric instability from atmospheric soundings. *Mon. Wea. Rev.*, 111, 2016-2033.
- ____, 1988: Observational evidence of slantwise convective adjustment. *Mon. Wea. Rev.*, 116, 1805-1816.
- Hobbs, P. V., 1978: Organization and structure of clouds and precipitation on the mesoscale and microscale in cyclonic storms. *Rev. Geophys. Space Phys.*, 16, 741-755.
- Iribarne, J. V. and W. L. Godson, 1981: Atmospheric thermodynamics. Sec. Ed. D. Reidel Publishing Company, Dordrecht, Holland, 259 pp.
- Kochtubajda, B., D. Andres and G. Van Der Vinne, 1990: Towards real-time runoff forecasting in small rural Alberta basins. *Proc. 8th Conf. on Hydrometeorology*, Kananaskis Park, Alberta, 160-164.
- Lilly, D. K., 1966: On the instability of the Ekman boundary layer flow. *J. Atmos. Sci.*, 23, 4812-494.
- Lindzen, R. S. and K. K. Tung, 1976: Banded convective activity and ducted gravity waves. *Mon. Wea. Rev.*, 104, 1602-1617.
- Parsons D. B. and P. V. Hobbs, 1983: The mesoscale and microscale structure and organization of clouds and precipitation in mid-latitude cyclones: XI: Comparisons

- between observational and theoretical aspects of rainbands. *J. Atmos. Sci.*, 40, 2377-2397.
- Petterssen, S., 1956: Weather analysis and forecasting: I: Motion and motion systems. 2nd edition, McGraw Hill Publ., 428 pp.
- Reinelt, E. R., 1970: On the role of orography in the precipitation regime of Alberta. *The Albertan Geographer*, 6, 45-58.
- Reuter, G. W. and M. K. Yau, 1990: Observation of slantwise convective instability in winter cyclones. *Mon. Wea. Rev.*, 118, 447-458.
- ____ and C. D. Nguyen, 1993: Organization of cloud and precipitation in an Alberta storm. *Atmos. Ocean*, (submitted).
- Rogers, R. R. and N. K. Sakellariou, 1986: Precipitation production in three Alberta thunderstorms. *Atmos. Ocean*, 24, 145- 168.
- ____ and M. K. Yau, 1989: A short course in cloud physics. Third edition. Pergamon Press, Oxford, 293 pp.
- Rutledge, S. A. and P. V. Hobbs, 1983: The mesoscale and microscale structure and organization of clouds and precipitation in mid-latitude cyclones: VIII: A model for the seeder-feeder process in warm-frontal rainbands. *J. Atmos. Sci.*, 40, 1185-1206.
- Sanders, F., 1955: An investigation of the structure and dynamics of an intense surface frontal zone. *J. Meteor.*,

12, 542-552.

Sanders, F., 1986: Frontogenesis and symmetric instability in a major New England snowstorm. *Mon. Wea. Rev.*, 114, 1847-1862.

Sanders, F. and L. F. Bosart, 1985: Mesoscale structure in a megalopolitan snowstorm of 11-12 February 1983. Part I: Frontogenetical forcing and symmetric instability. *J. Atmos. Sci.*, 42, 1050-1061.

Seltzer, M. A., R. E. Passarelli and K. A. Emanuel, 1985: The possible role of symmetric instability in the formation of precipitation bands. *J. Atmos. Sci.*, 42, 2207-2219.

Smith, S. B. and M. K. Yau, 1987: The mesoscale effect of topography on the genesis of Alberta hailstorms. *Beitr. Phys. Atmosph.*, 60, 371-392.

____ and ____ 1993: The causes of severe convective outbreaks in Alberta: I: A comparison of a severe outbreak with two non-severe events. *Mon. Wea. Rev.*, 121, 1099-1125.

Wolfsberg, D. G., K. A. Emanuel and R. E. Passarelli, 1986: Band formation of a New England winter storm. *Mon. Wea. Rev.*, 114, 1552-1569.

Chapter 4
Convective and symmetric instabilities
and their effects on precipitation:
A climatological analysis for
central Alberta

Remark: This chapter has been submitted to Monthly Weather Review for publication.

4.1 Introduction

This chapter presents a climatological analysis of both convective and symmetric instabilities. In order to motivate this research and make a clear statement of the problem, the background is briefly reviewed first.

4.1.1 Convection in Alberta

Residents of central Alberta are familiar with severe summertime convective storm events. In fact, central Alberta, located on the lee side of the majestic Rocky Mountains, has the highest frequency of large hail (Admirat et al. 1985). Climatological statistics show that this region is affected by hail on an average of 61 days each summer (Wojtiw 1975). Organized multicell or supercell storms develop three to five times a summer, often with tornadoes (Smith and Yau 1987). Recent examples of violent storms include the "Edmonton tornado" of 31 July 1987 which left 27 people dead and 300

injured and the "Calgary hailstorm" of 7 September 1991 which caused \$400 million worth of insurance claims for damaged homes and cars.

Over the last three decades, several studies have been conducted to determine the processes that cause the severe convection and precipitation (Chisholm 1973; Krauss and Marwitz 1984; Smith and Yau 1987; Cheng and Rogers 1988; Al-Jumily et al. 1991). By comparing a severe convective outbreak with two non-severe events, Smith and Yau (1993) identified the importance of the right phasing between surface heating and the advance of a synoptic-scale trough. They were able to identify the "ingredients" necessary for severe convection in Alberta. One of these necessary conditions was the presence of strong convective instability (i.e. $\partial\theta_e/\partial z < 0$). Despite the significant efforts devoted to many aspects of Alberta storms, no research about the regional "climatology" of the occurrence of convectively unstable soundings has been carried out in the past.

4.1.2 Slantwise instability in Alberta

This section "shifts gears" and moves from summertime convection to midlatitude winter cyclones. Soundings sampled in extratropical cyclones indicate that the atmosphere is usually absolutely stable for cumulus convection. Still, heavy rain (or snow) is not uncommon in cyclones, and it often falls from long-lasting cloud bands. These cloud bands have rather

different characteristics depending on where they are located relative to the warm and cold surface fronts (Hobbs 1978). In the warm sector, precipitation bands usually occur as multiple rolls with their axes parallel to the direction of the thermal shear vector. Observations suggest that the warm sector bands are manifestations of slantwise convective roll circulations which result from the release of the Conditional Symmetric Instability, CSI (Bennetts and Hoskins 1979; Emanuel 1979; Parsons and Hobbs 1983; Wolfsberg et al. 1986; Gyakum 1987; Emanuel 1988; Reuter and Yau 1993). There is observational evidence also that slantwise instability occasionally occurs in the cold sector of extratropical cyclones (e.g. Bennetts and Ryder 1984; Reuter and Yau 1990) and in baroclinic regions that are far away from a surface cyclone (e.g. Emanuel 1983b; Wolfsberg et al. 1986).

During recent years, there has been a growing research interest in slantwise instability from a different viewpoint:

- (a) possible interaction of CSI with frontogenesis (Sanders and Bosart 1985; Thorpe and Emanuel 1985)
- (b) possible interaction of CSI with explosive cyclogenesis (Kuo and Low-Nam 1990; Hedley and Yau 1991)
- (c) effects of CSI on stratiform precipitation (Zhang and Cho 1992)
- (d) application of CSI to forecasting local precipitation (e.g. Shutts 1990; Snook 1992).

Little has been done, however, to address the question of the

"climatology" of CSI for a specific region. Wolfsberg et al. (1986) reported several occurrences of slantwise instability, associated with precipitation bands in New England during the winter months. It is likely that CSI is also common during the winter time in the southern plains of the United States (Byrd 1989). An analysis of the Canadian Atlantic Storm Program (CASP) data showed that conditional symmetric instability is likely to be ubiquitous in baroclinic zones such as Atlantic Canada during the winter months (Reuter and Yau 1990).

Symmetric instability has been identified in two case studies of Alberta storms. The cyclone of 18 July 1986 had long-lasting multiple rainbands and the airmass was unstable in the layers with strong shear (Reuter and Nguyen 1993). A similar picture emerged from the snow storm which affected central Alberta on 4 October 1990; heavy snow bands formed in sheared layers in which conditional symmetric instability was present (Aktary and Reuter 1993). Still, it is not yet clear whether the above two events were extraordinary or whether slantwise instability occurs frequently in Alberta.

4.1.3 Statement of the problem

This investigation attempts to determine the frequency of occurrences of both the convective instability (CI) and the conditional symmetric instability (CSI) in central Alberta, with the emphasis on the seasonal dependence. The issue of the role of these instabilities in precipitation production will

also be addressed. Specifically, the maximum amount of the observed precipitation, associated with the release of CI and the release of CSI will be determined. By comparing these values, the relative importance of CI versus CSI in producing precipitation becomes evident. Seasonal variations will also be examined.

At the outset, it should be stressed that the purpose of this chapter is not to quantify the intensity of CI and CSI (for example by comparing CAPE or SCAPE values). Thus, the "severity" of the observed storms will not be discussed. The focus here is purely on establishing the existence of unstable layers and how they are related to the precipitation amounts, accumulated during the twelve hours after the sounding.

The organization of this chapter is as follows: Section 4.2 describes the data set, followed by a description of the method of analysis in Section 4.3. Results on the seasonal variations in the occurrences of CI and CSI are reported in Section 4.4, while results related to precipitation amounts are given in Section 4.5. The final section will present and discuss the major conclusions.

4.2 Observational data set

The radiosonde data were collected by balloon soundings released from Stony Plain (WSE, 53.5°N, 114.1°W, 766 m ASL). This is the only upper air station in Alberta. Thermodynamic and wind measurements for 00 and 12 UTC were obtained from the

"upper air archive" data, as compiled by the Atmospheric Environment Service of Canada. In addition to the upper air data, the analysis also used the 12-hour accumulated amounts of precipitation measured twice a day at Stony Plain. The times of precipitation observation coincided closely with the times of the radiosonde launches.

To quantify the frequency of occurrence of CI and SCI, it would be best to use several years of observed data. More data, however, would require significantly more time as each sounding has to be examined subjectively. A two year data set was considered as a fair compromise between the accuracy of the findings and the amount of work involved. Therefore, the analysis covers the period from 1 January 1990 to 31 December 1991. From the total of 1460 soundings, 61 were discarded due to incomplete data. August 1991 was the month with the most incomplete soundings (6/62) and the average was about two per month. In this analysis no distinction was made between the morning and afternoon soundings. Anderson (1991) indicated that the difference between the temperature lapse rates of the morning soundings and afternoon soundings is insignificant except near the ground. Also by considering all the soundings together, without splitting in two, the data set remained larger.

The years 1990 and 1991 were normal in terms of yearly precipitation (Table 1). Even on a monthly basis there were few outliers: April 1990, July 1990, May 1991 and June 1991

were relatively wet, while September 1990, July 1991 and November 1991 were relatively dry.

Table 1. Precipitation amounts and number of days with precipitation for each month of 1990 and 1991, compared with the 30-year climatological values.

| Years | Normal | | 1990 | | 1991 | |
|--------|--------------|--------------|--------------|--------------|--------------|--------------|
| Months | precip mm | # of days | precip mm | # of days | precip mm | # of days |
| Jan | 26.8 | 12 | 14.4 | 15 | 30.5 | 8 |
| Feb | 21.0 | 10 | 16.3 | 12 | 30.3 | 12 |
| Mar | 21.2 | 11 | 16.2 | 6 | 16.6 | 12 |
| Apr | 26.3 | 8 | 60.3 | 12 | 36.5 | 6 |
| May | 48.4 | 10 | 50.6 | 13 | 98.7 | 14 |
| Jun | 98.9 | 15 | 52.7 | 15 | 105.5 | 21 |
| Jul | 96.0 | 14 | 159.6 | 16 | 24.2 | 13 |
| Aug | 73.6 | 13 | 85.6 | 12 | 78.8 | 11 |
| Sep | 45.3 | 11 | 14.6 | 7 | 19.8 | 10 |
| Oct | 20.0 | 7 | 32.6 | 12 | 86.6 | 14 |
| Nov | 22.6 | 8 | 32.3 | 7 | 5.5 | 11 |
| Dec | 28.7 | 11 | 31.9 | 14 | 18.3 | 6 |
| Total | 528.8 | 130 | 567.1 | 141 | 551.3 | 138 |

4.3 Method of assessment of CI and CSI

4.3.1 Assessing convective instability, CI

A layer of moist air is convectively unstable when

$$(\partial\theta_e/\partial z) < 0 \quad (1)$$

where θ_e is the equivalent potential temperature and z denotes height. For moist, but unsaturated air, θ_e was computed from (Bolton 1980):

$$\theta_e = \theta \exp \left[\left(\frac{3376}{T_{lcl}} - 2.54 \right) w (1 + 0.81w) \right], \quad (2)$$

where θ is the potential temperature ($^{\circ}\text{K}$) of the moist air, given by

$$\theta = T \left[\frac{100}{p} \right]^{0.2854 (1 - 0.28w)}, \quad (3)$$

and T_{lcl} is the temperature ($^{\circ}\text{K}$) at the lifting condensation level, given in Bolton (1980)

$$T_{lcl} = \left[\frac{1}{T_d - 56} + \frac{\ln(T/T_d)}{800} \right]^{-1} + 56. \quad (4)$$

In the above, T is the temperature ($^{\circ}\text{K}$), p the air pressure (kPa) and w is the vapour mixing ratio (kg/kg). The latter is obtained by

$$w = 0.622 \left[\frac{e}{p - e} \right], \quad (5)$$

where the vapour pressure e (kPa) is:

$$e = 0.6112 \exp \left[\frac{17.67 t}{t + 243.5} \right], \quad (6)$$

with t being the air temperature, in $^{\circ}\text{C}$. The dewpoint T_d ($^{\circ}\text{K}$) was calculated with (see Rogers and Yau 1989, p. 14)

$$T_d = \frac{B}{(B/T) - \ln(RH/100)}. \quad (7)$$

where RH is the observed relative humidity and $B = 5420$ $^{\circ}\text{K}$ is

a constant.

When the temperature is subfreezing, it would be more accurate to include the ice phase in the thermodynamics by replacing the θ_e with the equivalent ice phase potential temperature. Even better, an ice-liquid water potential temperature (e.g. Tripoli and Cotton 1981) could be used to allow for mixed-phase conditions. However, this complication was not considered essential for this analysis because the sounding measurements did not have that degree of accuracy. It is clear that the use of ice phase thermodynamics would only marginally modify the stability analysis, because the latent heat of sublimation exceeds that of vaporization by only 13%.

4.3.2 Assessing conditional symmetric instability, CSI

Emanuel (1983) developed techniques for assessing the occurrence of conditional symmetric instability, using upper air sounding observations. The best approach is to make a cross-sectional analysis by projecting several soundings on a single vertical plane perpendicular to the geostrophic windshear. However, the spacing between adjacent soundings should not exceed one hundred kilometres otherwise horizontal interpolation can become problematic (Reuter and Yau 1993). A cross-sectional analysis is out of the question for western Canada where upper air stations are separated by an average distance of about 750 km. The alternative is to make single sounding analyses based on the vertical profile of the moist

Richardson number. This technique is explained in textbooks (e.g. Rogers and Yau 1989) and research papers (e.g. Seltzer et al. 1985; Donaldson and Stewart 1989). Thus, only a brief description is presented here.

Suppose that the flow is geostrophically balanced, with unidirectional shear. Let the x axis be perpendicular to the shear, and pointing toward the warmer air, while the y axis is in the direction of the flow. The moist Richardson number, Ri_m , is defined as:

$$Ri_m = \frac{f + \partial v_g / \partial x}{f} \frac{\Gamma_m}{\Gamma_d} \frac{g}{\theta_e} \frac{(\partial \theta_e / \partial z)}{(\partial v_g / \partial z)^2}, \quad (8)$$

where f is the Coriolis parameter, g is gravity, v_g is the geostrophic wind, and Γ_m and Γ_d are the saturated and the dry adiabatic lapse rates, respectively. The ratio of the moist to the dry adiabatic lapse rates is (e.g. Iribarne and Godson 1981 p. 182)

$$\frac{\Gamma_m}{\Gamma_d} = \frac{1 + (Lw/R_d T)}{1 + 0.622 (L^2 w / C_{pd} R_d T^2)}, \quad (9)$$

where L is the latent heat of vaporisation of water (Jkg^{-1}), and R_d and C_{pd} ($\text{Jkg}^{-1}\text{K}^{-1}$) are the specific gas constant for dry air and specific heat capacity of dry air at constant pressure, respectively. Bennetts and Hoskins (1979) showed that an infinitesimal small slantwise displacement will grow exponentially when Ri_m becomes less than 1.0 in a saturated flow. On the other hand, the initial slantwise displacement

decays exponentially when $Ri_m > 1$. Therefore the criteria for stabilities are the following:

$Ri_m < 0$: unstable for CI

$0 < Ri_m < 1$: stable for CI, but unstable for CSI

$Ri_m > 1$: absolutely stable for both CI and CSI.

Using (8) for computing the Ri_m values is problematic for single sounding data. First, there are no observations of v_g and without measurements of horizontal temperature gradient, v_g can not be calculated by using the thermal wind balance. Second, the rate of change of v_g with x is not known. Third, the geostrophic flow may not be unidirectional and may vary with height. To overcome these difficulties, the following standard method was used: the observed hodograph for each sounding was examined carefully to determine the direction of the "major shear" in the lower troposphere. Many soundings had rather unidirectional windshear, making the selection simple. There were, however, also cases with significant veering or backing. In such cases, the direction of the flow in the layer with high relative humidity (RH) and strong vertical wind shear was chosen. The high RH criterion was based on the fact that the release of CSI requires saturated air. Once the y -direction (i.e. major shear direction) is determined for a sounding, the wind's y -component, v , is found by projecting the observed wind V onto the y -axis:

$$v = V \cos(\alpha - \beta), \quad (10)$$

where α and β are the directions of V and v in degrees from the north, respectively. It was assumed that

$$\frac{(f + \partial v_g / \partial x)}{f (\partial v_g / \partial z)^2} \approx \frac{1}{(dv/dz)^2}, \quad (11)$$

for expression (11) will be satisfied when $\partial v_g / \partial z \approx dv/dz$ and $f + \partial v / \partial x \approx f$; this simplifies the Ri_m calculations to

$$Ri_m = \frac{\Gamma_m}{\Gamma_d} \frac{g}{\theta_e} \frac{(d\theta_e/dz)}{(dv/dz)^2}. \quad (12)$$

Seltzer et al. (1985) made 15 case studies and found that the ratio $[(f + dv/dx)]/f < 1.1$ and Byrd (1989) reported that in his analysis $[(f + dv/dx)]/f < 1.15$, with very few exceptions. In the free atmosphere the observed shear is usually a close approximation to its geostrophic value, and therefore the inaccuracy of (12) should be insignificant, provided the observed shear is larger than about $1 \text{ ms}^{-1}\text{km}^{-1}$. For smaller shear values expression (12) is less accurate, however, and in such cases the flow is absolutely stable, because $Ri_m \rightarrow \infty$ when $\partial v_g / \partial z \rightarrow 0$.

Eq (12) was used to compute Ri_m for the six separate layers: 90-85, 85-80, 80-70, 70-60, 60-50 and 50-40 kPa, for beneath 90 kPa the geostrophic balance becomes questionable. This is undoubtedly a coarse resolution for approximating vertical variations; however, the interest here is in the stratification characteristics of the "mesoscale" flow and not in the smaller-scale variations, which would be obtained when

using finer vertical resolution. A typical example of this stability analysis is shown in Table 2.

That particular sounding has three absolutely stable layers ($Ri_m > 1$), one convectively unstable layer ($Ri_m < 0$ or $\partial\theta_e/\partial z < 0$) and also two layers that are unstable for CSI ($0 < Ri_m < 1$). When considering the stability properties of the whole air mass, it was classified as convectively unstable because CI has a shorter time scale than CSI and would thus be released faster. To allow inter-comparisons of soundings with unstable conditions in different layers, it was useful to define the minimum Richardson number Ri_m^* which is simply the minimum value for the six layers. In the example shown in Table 2 $Ri_m^* = -19.4$.

Table 2. Stability analysis for 0000 UTC 4 February 1990.

| Layer (kPa) | $\partial\theta_e/\partial z$ ($^{\circ}/\text{km}$) | dv/dz ($\text{ms}^{-1}\text{km}^{-1}$) | Ri_m | Stability analysis |
|----------------|---|---|--------|-----------------------|
| 90-85 | 17.4 | 8.6 | 5.0 | absolute stable |
| 85-80 | 5.7 | 8.3 | 1.7 | absolute stable |
| 80-70 | -0.3 | 0.5 | -19.4 | convectively unstable |
| 70-60 | 0.8 | 5.6 | 0.6 | slantwise unstable |
| 60-50 | 4.3 | 14.3 | 0.6 | slantwise unstable |
| 50-40 | 1.7 | 2.7 | 6.6 | absolutely stable |

4.4 Results for the frequency of occurrence of CI and CSI

All twice-daily soundings between 1 January 1990 and 31 December 1991 were analyzed to determine the minimum moist Richardson number (Ri_m'). Then for each of the 24 months the number of cases associated with $Ri_m' < 0$, $0 \leq Ri_m' < 1$ and $Ri_m' \geq 1$ were counted. The three categories classified the soundings as being unstable for convective instability (CI), unstable for conditional symmetric instability (CSI) and absolutely stable (AS), respectively. The monthly number of soundings in each category during 1990 and 1991 is shown in Table 3.

During 1990, about two thirds of all soundings were convectively unstable (458 soundings out of a total of 704). Furthermore, the data indicated that the frequency of CI depends crucially on the season. During midsummer of 1990, almost all recorded soundings were convectively unstable, while during December, January and February 1990 only about a quarter of the soundings indicated convective instability. The frequency values found for 1991 agreed well with those found for 1990, both pointing toward an increase in the frequency of CI in the spring and a decrease during the fall. The combined 1990 and 1991 data set (Figure 1) underscored the seasonal dependence of CI.

Soundings that were convectively stable, but had at least one slantwise unstable layer occurred less frequently. During 1990 about 22% of the soundings corresponded to this category (157 cases out of 704). The value for 1991 was 19%. Again a

Table 3. Comparison of the number of soundings per months that were identified as being unstable for CI ($Ri_m^* < 0$), unstable for CSI ($0 < Ri_m^* < 1$) and absolute stable ($Ri_m^* > 1$).

| Years | 1990 | | | 1991 | | |
|--------|--------------|------------------|--------------|--------------|------------------|--------------|
| Months | CI | CSI | AS | CI | CSI | AS |
| | $Ri_m^* < 0$ | $0 < Ri_m^* < 1$ | $Ri_m^* > 1$ | $Ri_m^* < 0$ | $0 < Ri_m^* < 1$ | $Ri_m^* > 1$ |
| Jan | 16 | 26 | 16 | 10 | 22 | 28 |
| Feb | 14 | 23 | 16 | 28 | 19 | 7 |
| Mar | 33 | 20 | 8 | 32 | 13 | 16 |
| Apr | 42 | 9 | 6 | 46 | 8 | 5 |
| May | 59 | 2 | 0 | 54 | 4 | 4 |
| Jun | 57 | 1 | 0 | 56 | 0 | 0 |
| Jul | 59 | 1 | 0 | 58 | 1 | 0 |
| Aug | 58 | 3 | 0 | 55 | 0 | 0 |
| Sep | 53 | 4 | 0 | 53 | 2 | 0 |
| Oct | 35 | 22 | 2 | 34 | 13 | 13 |
| Nov | 22 | 20 | 16 | 26 | 17 | 12 |
| Dec | 10 | 26 | 25 | 17 | 25 | 16 |
| Total | 458 | 157 | 89 | 470 | 124 | 101 |

seasonal variation is evident. However, this time symmetric instability occurred most frequently during the winter, less often during the spring and fall and was almost entirely absent during the summer months. During mid-winter between 40 to 45% of the soundings were identified as being stable for cumulus convection but conditionally unstable for slantwise convection: 45% for Jan 90; 43% for Feb 90; 43% for Dec 90; 46% for Jan 91; 35% for Feb 91; and 43% Dec 91.

The similarity between the frequencies of CSI for the 6 different months was remarkable. The combined data set shown

in Figure 1 implies that CSI may be slightly more common in the fall than during the spring, but this requires more data for validation.

As far as absolutely stable soundings are concerned, the analysis showed that they were rather rare, and seasonally dependent. During the winter about 25% of the soundings were absolutely stable. The frequency of the absolutely stable soundings decreased in the spring, then essentially vanished during the summer, before picking up again in the fall.

Some of the soundings, while classified as convectively unstable, were actually of the "mixed-instability" type, in the sense that they contained both convectively unstable layers and slantwise unstable layers. The sounding of 00 UTC on 4 February 1990 (Table 2) is an example of such a "mixed-unstable" sounding. In this particular case, the 80-70 kPa layer indicated convective instability, while the 70-50 kPa layer was slantwise unstable. Clearly, for "mixed-unstable" cases, symmetric instability can occasionally be important once all the CAPE has been converted into kinetic energy. Examples of the release of both slantwise instability and cumulus convection have been given by Reuter and Yau (1993) and Reuter and Nguyen (1993). Based on these incidents, the frequency of "mixed-unstable" cases was also counted. The monthly frequency values for 1990 were 12, 7, 12, 20, 28, 20, 19, 26, 21, 20, 11 and 5, compared to 8, 15, 17, 20, 24, 20, 22, 24, 21, 23, 18 and 11 for the twelve months of 1991.

Typically about one quarter of the total number of soundings was of the "mixed-instability" type. The frequency value was the largest during the summer and smallest during the winter season, in good agreement with the frequency of occurrence of convective instability.

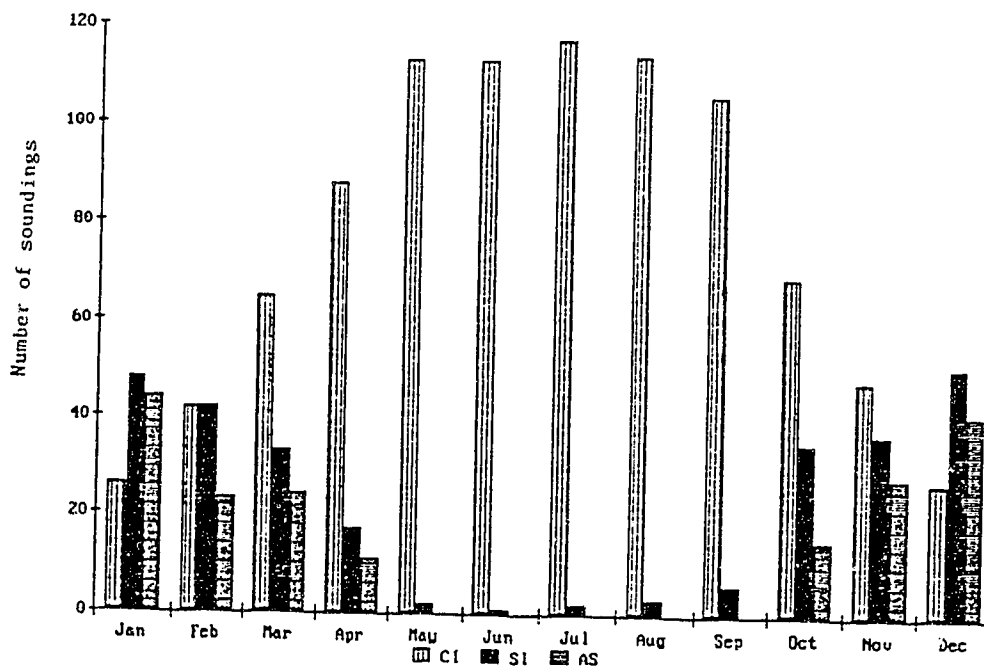


Fig. 1. Number of soundings for each month in the period 1990-1991 that were convectively stable (CI), symmetrically unstable (SI) and absolutely stable (AS).

4.5 Precipitation due to CI and CSI

When the CI (or CSI) is released the latent heat stored in the water vapour is converted into sensible heat, which generates buoyancy that produces upward motions. The storm updraft invigorates the condensation process that creates a positive feedback process until all of the CAPE (or SCAPE) is depleted. Once the convection passes above the freezing level, ice processes will become important and precipitation-size particles will be produced. Whether the precipitation reaches the ground as rain, snow or freezing rain, depends on the low level thermal structure and the nature of the hydrometeors.

In addition to CI and CSI, the air ascent can be caused by synoptic forcings like positive vorticity advection, warm air advection, frontogenetical forcing and by gravity waves, orographic lifting and others. It is very complex, if not impossible, to determine unambiguously the contribution of each forcing mechanism for a particular precipitation event. Nevertheless, some light about the importance of CI and CSI can be shed by comparing the following quantities:

NCI: Number of soundings per month associated with CI and precipitation within 12 hours at Stony Plain.

NCSI: Number of soundings per month associated with CSI and precipitation within 12 hours at Stony Plain.

NAS: Number of soundings per month with absolute stability and precipitation within 12 hours at Stony Plain.

PCI: Accumulated precipitation amount associated with NCI.

PCSI: Accumulated precipitation amount associated with NCSI.

PAS: Accumulated precipitation amount associated with NAS.

Table 4 and Table 5 list these values for each month in 1990 and 1991; Figure 2 and Figure 3 show the results when averaged for the two years. Two features immediately strike the eye: the strong dependence on the seasons, and the similarity between the results of 1990 and 1991. During the summer most of the rain was associated with convectively unstable soundings. During the months of June and July, PCI constituted 100% of the accumulated rain; while more than 80% of the accumulated rain resulted from convectively unstable soundings during the months of May, August, September and October. During the winter NCI became less, but still these rather few convectively unstable cases offered a substantial contribution towards the observed monthly precipitation amounts. Slantwise unstable cases were frequently associated with precipitation, particularly during the months of November and January, where about two thirds of the recorded snow fell within 12 hours of slantwise unstable soundings. In December, the soundings that were stable for CI and CSI provided the largest fraction of the observed snowfall. During the warm season, however, absolutely stable soundings had virtually no impact on the observed rainfall amounts.

Table 4. Number of soundings with precipitation per month identified as unstable for CI (NCI ; $Ri_m^* < 0$), unstable for CSI (NCSI ; $0 < Ri_m^* < 1$) and absolutely stable (NAS ; $Ri_m^* > 1$).

| Years | 1990 | | | 1991 | | |
|--------|---------------------|--------------------------|---------------------|---------------------|--------------------------|---------------------|
| Months | NCI $Ri_m^* < 0$ | NCSI $0 < Ri_m^* < 1$ | NAS $Ri_m^* > 1$ | NCI $Ri_m^* < 0$ | NCSI $0 < Ri_m^* < 1$ | NAS $Ri_m^* > 1$ |
| Jan | 6 | 9 | 9 | 5 | 7 | 5 |
| Feb | 2 | 8 | 7 | 12 | 5 | 2 |
| Mar | 6 | 3 | 3 | 6 | 4 | 7 |
| Apr | 11 | 6 | 3 | 8 | 1 | 0 |
| May | 19 | 1 | 0 | 20 | 2 | 4 |
| Jun | 26 | 0 | 0 | 33 | 0 | 0 |
| Jul | 22 | 0 | 0 | 22 | 1 | 0 |
| Aug | 19 | 1 | 0 | 12 | 0 | 0 |
| Sep | 10 | 0 | 0 | 15 | 0 | 0 |
| Oct | 12 | 7 | 0 | 12 | 6 | 7 |
| Nov | 7 | 8 | 8 | 11 | 6 | 7 |
| Dec | 2 | 9 | 15 | 4 | 8 | 3 |
| Total | 142 | 52 | 45 | 160 | 40 | 35 |

Table 5. Monthly accumulated precipitation amounts (in mm of equivalent liquid precipitation) recorded for soundings identified as unstable for CI (PCI ; $Ri_m^* < 0$), unstable for CSI (PCSI ; $0 < Ri_m^* < 1$) and absolutely stable (PAS ; $Ri_m^* > 1$).

| Years | 1990 | | | 1991 | | |
|--------|---------------------|--------------------------|---------------------|---------------------|--------------------------|---------------------|
| Months | PCI $Ri_m^* < 0$ | PCSI $0 < Ri_m^* < 1$ | PAS $Ri_m^* > 1$ | PCI $Ri_m^* < 0$ | PCSI $0 < Ri_m^* < 1$ | PAS $Ri_m^* > 1$ |
| Jan | 2.0 | 7.3 | 5.1 | 4.5 | 25.8 | 0.2 |
| Feb | 1.9 | 9.8 | 4.6 | 22.2 | 7.5 | 0.6 |
| Mar | 9.4 | 1.6 | 5.2 | 2.9 | 5.8 | 7.9 |
| Apr | 45.3 | 14.1 | 0.9 | 20.5 | 16.0 | 0.0 |
| May | 50.0 | 0.6 | 0.0 | 86.8 | 7.0 | 4.0 |
| Jun | 52.7 | 0.0 | 0.0 | 105.5 | 0.0 | 0.0 |
| Jul | 159.6 | 0.0 | 0.0 | 23.2 | 1.0 | 0.0 |
| Aug | 63.0 | 22.6 | 0.0 | 78.8 | 0.0 | 0.0 |
| Sep | 14.6 | 0.0 | 0.0 | 19.8 | 0.0 | 0.0 |
| Oct | 23.8 | 8.8 | 0.0 | 76.2 | 3.7 | 6.7 |
| Nov | 6.2 | 22.3 | 3.8 | 1.6 | 3.1 | 0.8 |
| Dec | 2.6 | 13.0 | 16.3 | Trace | 11.3 | 7.0 |
| Total | 431.1 | 100.1 | 35.9 | 442.0 | 82.1 | 27.2 |

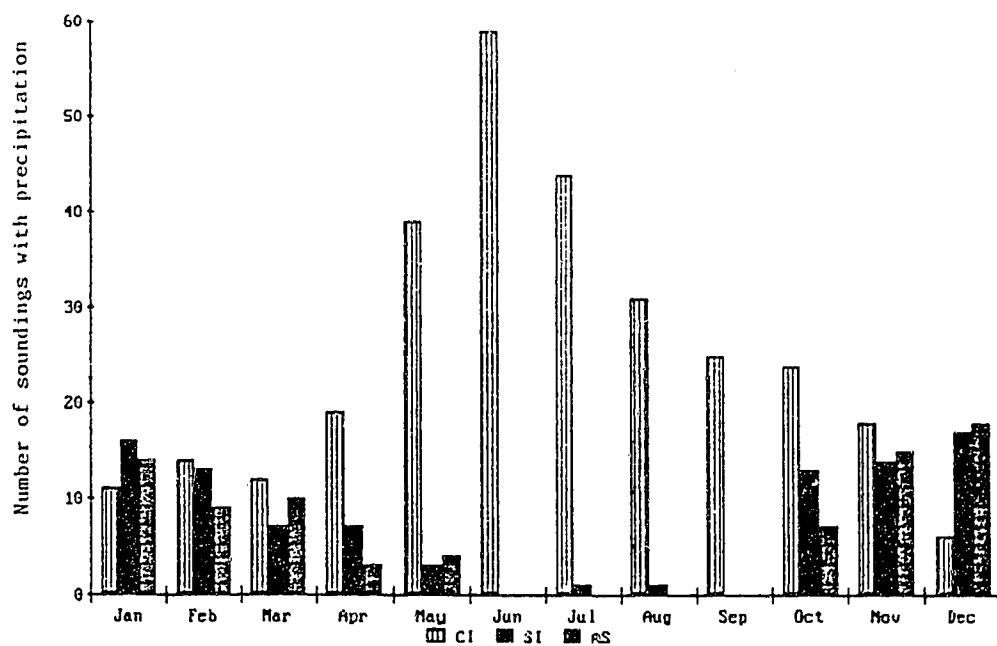


Fig. 2. Number of soundings for each month in the period 1990-1991 for which precipitation was recorded at Stony Plain within 12 hours. The soundings were subdivided into those with convective instability (CI), those with symmetric instability (SI) and those with absolute stability (AS).

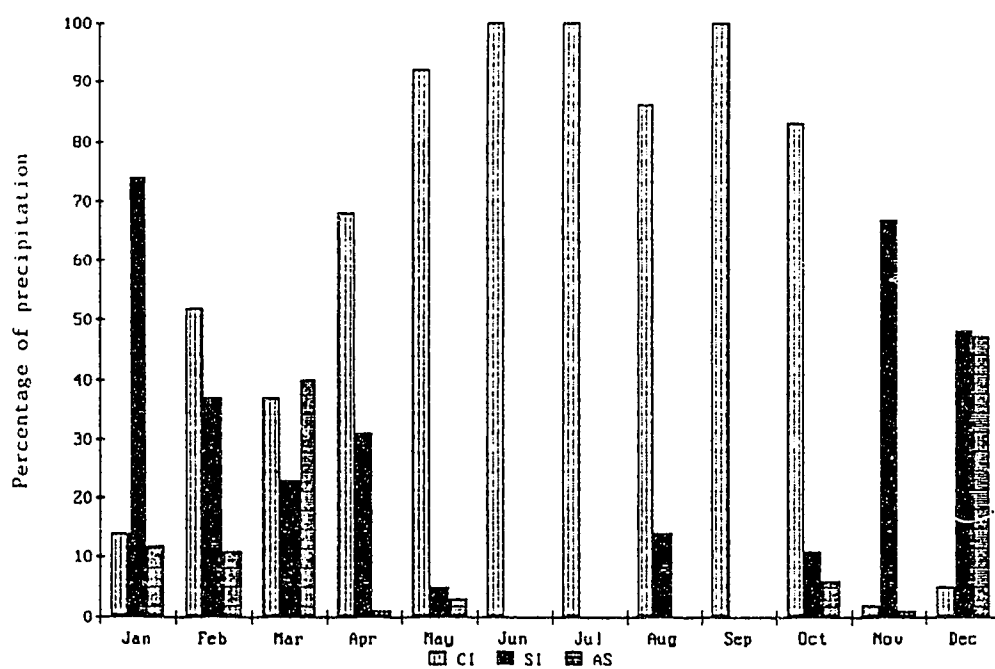


Fig. 3. Relative contribution, to the monthly precipitation amount, from soundings that were convectively unstable (CI), symmetrical unstable (SI) and absolutely stable (AS). The monthly percentage values constitute the average of the 1990 and 1991 values.

4.6 Discussion and conclusion

Twice-daily soundings were analyzed for two calendar years to determine the monthly frequencies of the potential for convective instability and slantwise instability. When the frequency values were averaged for the four seasons and expressed as a percentages, the results were:

| | <u>Mar-May</u> | <u>Jun-Aug</u> | <u>Sep-Nov</u> | <u>Dec-Feb</u> |
|-------------------------|----------------|----------------|----------------|----------------|
| Convective instability: | 75% | 98% | 65% | 27% |
| Slantwise instability: | 14% | 2% | 23% | 41% |
| Absolute stability: | 11% | 0% | 12% | 32% |

These percentages are also shown in Figure 4. Clearly, convective instability was frequently observed during spring and fall, while during summer almost every sounding indicated CI. Slantwise instability was common during the winter, less common during spring and fall and rare during the summer. The percentages shown in line 2 above represent cases of "pure" symmetrically unstable soundings only; when soundings that had convectively unstable layers and also symmetrically unstable layers were counted, the frequency of occurrence of slantwise instability was significantly larger. In most of these "mixed-instability" cases, however, the slantwise instability will likely be overshadowed by the convective instability because of their different time scales.

To study the link between CI and CSI with precipitation,

all the soundings associated with precipitation recorded at Stony Plain within 12 hours after the radiosonde release were identified. The monthly frequency values for cases with precipitation accumulation that were convectively unstable,

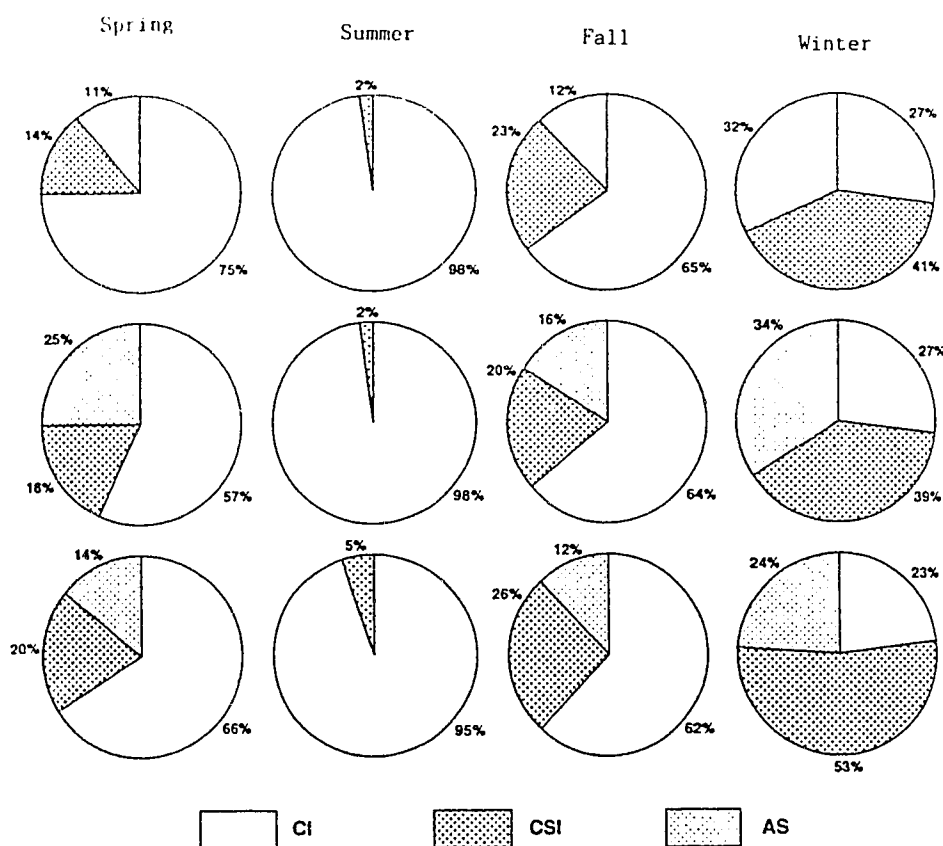


Fig. 4. Pie diagrams showing the seasonal variations of the importance of convective instability, slantwise instability and absolute stability. Shown are: the percentage of cases that had CI, CSI and AS (top); the percentage of "soundings with precipitation" that had CI, CSI and AS (middle); and the percentage of total precipitation, associated with CI, CSI and AS (bottom).

slantwise unstable or absolutely stable were estimated. When averaged over the seasons, and expressed in percentages, the frequency of occurrences were:

| | <u>Mar-May</u> | <u>Jun-Aug</u> | <u>Sep-Nov</u> | <u>Dec-Feb</u> |
|-------------------------|----------------|----------------|----------------|----------------|
| CI with precipitation: | 57% | 98% | 64% | 27% |
| CSI with precipitation: | 18% | 2% | 20% | 39% |
| AS with precipitation: | 25% | 0% | 16% | 34% |

The data indicated that during spring, summer, and fall most of the precipitation events were associated with soundings that were convectively unstable (see also Figure 4). This was particularly true during the summer months, where convective instability was observed in 98% of the total events. During the winter, precipitation events occurred most frequently in association with slantwise unstable soundings, but only by a very small margin.

For many hydrological applications, the primary interest lies in the monthly accumulation of precipitation, rather than in the frequency of precipitation events. Thus, the total precipitation amount that could be attributed to convectively unstable, slantwise unstable and absolutely stable soundings were calculated. The relative contribution of these three stability categories were as follows:

| | <u>Mar-May</u> | <u>Jun-Aug</u> | <u>Sep-Nov</u> | <u>Dec-Feb</u> |
|-----------------------------|----------------|----------------|----------------|----------------|
| % of precipitation for CI: | 66% | 95% | 62% | 23% |
| % of precipitation for CSI: | 20% | 5% | 26% | 53% |
| % of precipitation for AS: | 14% | 0% | 12% | 24% |

The percentages indicate (see also Figure 4) that about two thirds of the total precipitation comes from convectively unstable soundings during spring and fall. In the summer, almost the entire rain amount was associated with CI, while during winter CI may be responsible for about one quarter of the total snow. About half of the winter precipitation was associated with soundings which showed a potential for the release of CSI. It should be pointed out that these values constitute an upper limit, because the data available were insufficient to find out clearly whether conditional symmetric instability was actually released to form multiple rolls of slanted circulation.

The frequent build-up of convectively unstable layers over Alberta stands in sharp contrast with marine tropical conditions. Observations have indicated that the tropical atmosphere is always very close to neutral stability for reversible adiabatic parcel ascent from the subcloud layer (Xu and Emanuel 1989). The reason why a tropical atmosphere lacks the presence of convective instability is that, almost no external work is required to lift the moist air from the surface to its level of free convection. Therefore, whenever

a small amount of convective instability is generated, it is released almost immediately. Maybe the frequent occurrences of CI in the Alberta soundings are closely related to the presence of an inversion layer, which is a characteristic feature of this region, due to subsidence at the lee side of the Rocky Mountains. This low level subsidence inversion (also termed capping lid), allows the gradual build-up of convective instability in the mid-levels due to differential advection of temperature and moisture. It is speculated that the inversion layer is also instrumental for the build-up of symmetrically unstable layers that were indicated in the Alberta sounding data in the cooler months.

References

- Admirat, P., G. G. Goyer, L. Wojtiw, E. A. Carte, D. Roos and E. P. Lozowski, 1985: A comparative study of hailstorms in Switzerland, Canada and South Africa. *J. Climatology*, 5, 35-51.
- Aktary, N. and G. W. Reuter, 1993: Observations of a snow band in a symmetrically unstable flow over Alberta. *Beiträge zur Physik der Atmosphäre*, (submitted).
- Al-Jumily, K. J., R. B. Charlton and R. G. Humphries, 1991: Identification of rain and hail with circular polarization radar. *J. Appl. Meteor.*, 30, 1075-1087.
- Anderson, K., 1991: Model to predict lightning occurrence and frequency over Alberta. MSc. thesis, Department of Geography, University of Alberta, Edmonton, 91 pp.
- Bennetts, D. A. and B. J. Hoskins, 1979: Conditional symmetric instability a possible explanation for frontal rainbands. *Quart. J. Roy. Meteor. Soc.*, 105, 945-962.
- and P. Ryder, 1984: A study of mesoscale convective bands behind cold fronts. Part I: Mesoscale organization. *Quart. J. Roy. Meteor. Soc.*, 105, 121-145.
- Bolton, D., 1980: The computation of equivalent potential temperature. *Mon. Wea. Rev.*, 108, 1046-1053.
- Byrd, G. P., 1989: A composite analysis of winter season overrunning precipitation bands over the southern

- plains of the United States. J. Atmos. Sc., 46, 1119-1132.
- Chisholm, A. J., 1973: Alberta hailstorms. Part I: Radar case studies and airflow models. Meteor. Monogr., 36, Amer. Meteor. Soc., Boston, 1-36.
- Cheng, L. and D. C. Rogers, 1988: Hailfalls and hailstorm feeder cells - an Alberta Case Study. J. Atmos. Sci., 45, 3533-3545.
- Donaldson, N. R. and R. E. Stewart, 1989: On the precipitation regions within two storms in Atlantic Canada. Atmos. Ocean, 27, 108-129.
- Emanuel, K. A., 1979: Inertial instability and mesoscale convective systems. Part I: Linear theory of inertial instability in rotating viscous fluids. J. Atmos. Sci., 36, 2425-2449.
- _____, 1983a: The Lagrangian parcel dynamics of moist symmetric instability. J. Atmos. Sc., 40, 2368-2376.
- _____, 1983b: On assessing local conditional symmetric instability from atmospheric soundings. Mon. Wea. Rev., 111, 2016-2033.
- _____, 1988: Observational evidence of slantwise convective adjustment. Mon. Wea. Rev., 116, 1805-1816.
- Gyakum, J. R., 1987: Evolution of a surprise snowfall in the United States Midwest. Mon. Wea. Rev., 115, 2322-2345.
- Hedley, M. and M. K. Yau, 1991: Anelastic modeling of explosive cyclogenesis. J. Atmos. Sci., 48, 711-727.

- Hobbs, P. V., 1978: Organization and structure of clouds and precipitation on the mesoscale and microscale in cyclonic storms. *Rev. Geophys. Space Phys.*, 16, 741-755.
- Iribarne, J. V. and W. L. Godson, 1981: Atmospheric thermodynamics. Sec. Ed. D. Reidel Publishing Company, Dordrecht, Holland, 259 pp.
- Krauss, T. W. and J. D. Marwitz, 1984: Precipitation processes within an Alberta supercell hailstorm. *J. Atmos. Sci.*, 41, 1025-1034.
- Kuo, Y. -H. and S. Low-Nam, 1990: Prediction of nine explosive cyclones over the western Atlantic Ocean with a regional model. *Mon., Wea., Rev.*, 118, 3-25.
- Parsons, D. B. and P. V. Hobbs (1983): The mesoscale and microscale structure and organization of clouds and precipitation in midlatitude cyclones. VII: Formation, development, interaction and dissipation of rainbands. *J. atmos. Sci.*, 40, 559-579.
- Rogers, R. R. and M. K. Yau, 1989: A short course in cloud physics. Pergamon Press, Oxford, 293 pp.
- Reuter, G. W. and M. K. Yau, 1990: Observation of slantwise convective instability in winter cyclones. *Mon. Wea. Rev.*, 118, 447-458.
- ___ and ___, 1993: Assessment of slantwise convection in ERICA cyclones. *Mon., Wea. Rev.*, 121, 375-386.
- ___ and C. D. Nguyen, 1993: Organization of cloud and

- precipitation in a severe Alberta storm. Atmosph. Research, (in press).
- Sanders, P. and L. F. Bosart, 1985: Mesoscale structure in the megalopolitan snowstorm of 11-12 February 1983. Part I: Frontogenetical forcing and symmetric instability. J. Atmos. Sci., 42, 1050-1061.
- Seltzer, M. A. and R. E. Passarelli and K. A. Emanuel, 1985: The possible role of symmetric instability in the formation of precipitation bands. J. Atmos. Sci., 42, 2207-2219.
- Shutts, G. J., 1990: SCAPE charts from numerical prediction model fields. Mon. Wea. Rev., 118, 2745-2751.
- Smith, S. B. and M. K. Yau, 1987: The mesoscale effect of topography on the genesis of Alberta hailstorms. Beitr. Phys. Atmos. 60, 371-392.
- ___ and ___, 1993: The causes of severe convective outbreaks in Alberta. Part I: A comparison of a severe outbreak with two non-severe events. Mon. Wea. Rev., 121, 1099-1125.
- Snook, J. S., 1992: Current techniques for real-time evaluation of conditional symmetric instability. Wea. and Forecasting, 7, 430-439.
- Thorpe, A. J. and K. A. Emanuel, 1985: Frontogenesis in the presence of small stability to slantwise convection. J. Atmos. Sci., 42, 1809-1824.
- Tripoli, G. J. and W. R. Cotton, 1981: The use of ice-liquid

water potential temperature as a thermodynamic variable in deep atmospheric models. Mon. Wea. Rev., 109, 1094-1102.

Wolfsberg, D. G., K. A. Emanuel and R. E. Passarelli, 1986: Band formation of a New England winter storm. Mon. Wea. Rev., 114, 1552-1569.

Wojtiw, L., 1975: Climatic summaries of hailfall in Central Alberta (1957-73). Alberta Research Council, Edmonton, 102 pp.

Xu, K. M. and K. A. Emanuel, 1989: Is the tropical atmosphere conditionally unstable? Mon. Wea. Rev., 117, 1471-1479.

Zhang, D. L. and H. R. Cho, 1992: On the development of negative moist potential vorticity in the stratiform region of a simulated squall line. Mon. Wea. Rev., 120, 1322-1341.

Chapter 5

Relationship between slantwise instability,

vertical shear and precipitation:

Results for central Alberta

Remarks: This chapter (although containing important results on slantwise instability in central Alberta and its impact on regional precipitation) is not intended for submission to a technical journal in its present form. With the use of more years of data and under a more refined form, however, it may be submitted for publication in the future. Since the data set and the method of analysis are identical to those described in Chapter 4, they will not be repeated here. In addition, the introduction and the background material have been kept fairly brief, in order to concentrate on the major points.

5.1 Introduction

The "climatological" analysis, reported in Chapter 4, showed that between 80 to 100 mm of the yearly precipitation amounts in central Alberta are likely to be due to conditional symmetric instability. The assessment was based on the moist Richardson number, defined as the square of the ratio of the moist Brunt-Väisälä frequency to geostrophic windshear:

$$Ri_m = \frac{f + (\partial v / \partial x)}{f} \frac{\Gamma_m}{\Gamma_d} \frac{g}{\theta_e} \frac{(\partial \theta_e / \partial z)}{(\partial v / \partial z)^2}, \quad (1)$$

where the notations are identical to those in the chapter 4.

When the Ri_m value is less than zero convective instability is present. The flow will be absolutely stable when $Ri_m > 1$ and the potential for conditional symmetric instability (CSI) will be present whenever $0 < Ri_m < 1$.

Intuition suggests that a Ri_m value close to (but still larger than) zero should indicate a larger potential for CSI than a value close to (but still less than) one. In other words, the Ri_m magnitude calculated for a particular layer may be thought of as a type of "measure" for the intensity of slantwise instability stored in the layer in question. The CSI theory backs the relation between the Ri_m value and the amount of instability. Specifically, the value of Ri_m determines the instantaneous forcing which acts on a moving tube of air. The intensity of symmetric instability, however, depends also on the path length over which the tube of air is accelerated upwards; in other words the depth of the slantwise unstable layer is an important factor to determine the amount of latent energy which is available for conversion, during the release of symmetric instability.

From a forecasting point of view, it would be useful to know whether the relationship between Ri_m and the intensity of slantwise instability can be extended to some statistical relationship between the Ri_m numerical value and the amount of precipitation which falls on the ground. Furthermore, the vertical distribution of the symmetrically unstable layers should be examined more closely to see whether the depth of

the slantwise unstable layer is correlated with the observed precipitation. From (1) it follows that, for a fixed moist Brunt-Väisälä frequency, an increase in the geostrophic wind shear causes a decrease of Ri_m which weakens the symmetric stability or strengthens the symmetric instability, whatever the case may be. In a statistical sense, one would expect that, in a large sample of data, layers with CSI ($1 > Ri_m > 0$) should tend to have larger shear values and stable layers ($Ri_m > 1$) smaller shear values.

This chapter analyzes and documents the vertical profile of Ri_m values and their relationship to observed shear and precipitation. The data sets and the method of computing the Ri_m and thermal shear values (dv/dz) have been discussed in detail in the previous chapter.

5.2 Vertical shear and slantwise instability relationship

This section attempts to find out whether the expected correlation between Ri_m and shear values was indeed evident in the observed sounding data. To avoid complications arising from comparing results for different heights, it was decided to confine the analysis to the single layer from 90 to 80 kPa. The rationale for combining the layers 90-85 kPa and 85-80 kPa was based on the finding that slantwise convection is mostly occurring beneath 80 kPa (see Section 5.3). In order to have a large data set, all soundings that were convectively stable in the 90-80 kPa layer were considered, regardless of their

thermal structure aloft. For 1990, a total of 191 soundings had $\partial\theta_e/\partial z > 0$, and out of this total, 43 cases were unstable for CSI (i.e. $Ri_m < 1$), while the remaining 148 soundings were absolutely stable (i.e. $Ri_m < 1$). For 1991, the numbers were 214, 46, and 168, respectively.

For each of these cases, the vertical windshear between 90 and 80 kPa along the major thermal direction was computed as $(v_{80} - v_{90}) / (z_{80} - z_{90})$. Table 1 lists the results in histogram format, in which the windshear magnitude was divided in ten separate intervals, each having the range of $2 \text{ ms}^{-1}\text{km}^{-1}$.

For the period of analysis 73% of the absolutely stable layers were associated with windshear values smaller than $6 \text{ ms}^{-1}\text{km}^{-1}$. The percentage drops with increasing windshear, levelling off beyond shear values of about $14 \text{ ms}^{-1}\text{km}^{-1}$. The results for the individual years are similar. Concerning the symmetric instability close to 80% of the cases corresponded to (dv/dz) values larger than $6 \text{ ms}^{-1}\text{km}^{-1}$. The distribution of the percentages of slantwise unstable layers approximates a 'bell-shape' distribution, with 53% of the cases occurring in the of $6\text{-}12 \text{ ms}^{-1}\text{km}^{-1}$ range.

What is Table 1 showing? Throughout the period, from January 1990 to December 1991, symmetric instability was associated with intermediate wind shear values, whereas absolute stability was associated with rather smaller wind shear values. Based on the 1990 and 1991 Stony Plain upper air data, it is estimated that there is close to 80 % chance that

Table 1. Comparison of the number of absolutely stable (AS) and conditional symmetrically unstable (CSI) layers for different ranges of $\partial v/\partial z$ in the 90-80 kPa layer. Results are shown for the years 1990 and 1991 separately as well as their totals expressed as percentages.

| $\partial v/\partial z$ $\text{ms}^{-1}\text{km}^{-1}$ | Number of cases in 1990 | | Number of cases in 1991 | | Percentage of cases in 90+91 | |
|---|----------------------------|-------------------|----------------------------|-------------------|---------------------------------|-------------------|
| | AS | CSI | AS | CSI | AS | CSI |
| | $\text{Ri}_m > 1$ | $\text{Ri}_m < 1$ | $\text{Ri}_m > 1$ | $\text{Ri}_m < 1$ | $\text{Ri}_m > 1$ | $\text{Ri}_m < 1$ |
| 0-2 | 47 | 2 | 49 | 3 | 30% | 6% |
| 2-4 | 34 | 5 | 50 | 1 | 27% | 7% |
| 4-6 | 20 | 3 | 30 | 2 | 16% | 6% |
| 6-8 | 22 | 9 | 20 | 4 | 13% | 15% |
| 8-10 | 13 | 8 | 9 | 8 | 7% | 18% |
| 10-12 | 5 | 8 | 4 | 10 | 3% | 20% |
| 12-14 | 4 | 1 | 2 | 6 | 2% | 8% |
| 14-16 | 1 | 2 | 2 | 5 | 1% | 8% |
| 16-18 | 2 | 3 | 1 | 6 | 1% | 10% |
| 18-20 | 0 | 2 | 1 | 1 | 0% | 3% |
| Total: | 148 | 43 | 168 | 46 | 100% | 100% |

a convectively stable 90-80 kPa layer has the potential for slantwise instability, when its observed windshear exceeds $6 \text{ ms}^{-1}\text{km}^{-1}$. Clearly more years of data are needed to validate this estimate.

5.3 Vertical distribution of symmetrically unstable layers

The vertical distribution of slantwise unstable layers is analyzed and documented in this section. For each layer, it was determined how often the computed Ri_m had a value between zero and one. Since symmetric instability occurred more often

during January 1990 and January 1991 than in any other month (see chapter 4), it was decided to present the analysis for these two months in more detail and, after, briefly summarize the results for the other months. For each convectively stable sounding of January, all the layers that had CSI (i.e. $Ri_m < 1$) were identified. Table 2 indicates that symmetrically unstable layers occurred rather frequently (68 cases) below the 70 kPa (≈ 3 km ASL) level and seldom above it (10 cases). Thus, for the 2 months of January, slantwise instability tended to be a phenomenon of the low atmospheric levels. Table 2 also brings out information regarding the depth of slantwise unstable slabs. During the two months of January, only three cases had symmetrically unstable layers that "stretched" from 90 up to 70 kPa. Seven cases were identified with slantwise instability from 90 to 80 kPa and 7 additional cases with CSI from 85 to 70 kPa. In two cases, a stable layer was "sandwiched" between two slantwise unstable layers. Regarding the single-layer slantwise instability, it occurred 15 times in the 90-85 kPa layer, 7 in the 85-80 and 3 in the 80-70.

Similar tables were made for the other 22 months. For the sake of conciseness, the monthly tables were summarized in Table 3 which lists the monthly frequency of slantwise unstable conditions in each layer. Obviously, 58% of the soundings showed the potential for slantwise instability in the 90-85 kPa layer. The percentage of occurrences tend to decrease markedly with height, reaching about 10% between 50

Table 2. Vertical distribution of slantwise unstable layers for all soundings during January 1990 and January 1991 that had $Ri_m > 0$. The day (DD) and the hour (HH) of the soundings are specified. An asterisk indicates that a particular layer was slantwise unstable.

| January 1990 | | | | | | | January 1991 | | | | | | |
|--------------|----|----|----|----|----|----|---------------|----|----|----|----|----|----|
| Layers | | | | | | | Layers | | | | | | |
| DD/HH | 90 | 85 | 80 | 70 | 60 | 50 | DD/HH | 90 | 85 | 80 | 70 | 60 | 50 |
| | 85 | 80 | 70 | 60 | 50 | 40 | | 85 | 80 | 70 | 60 | 0 | 40 |
| 01/00 | * | | * | | * | | 05/12 | * | | | | | |
| 03/00 | | * | * | | | | 11/00 | | * | | | | |
| 05/12 | | * | * | | | | 13/12 | | * | * | | * | * |
| 06/00 | | * | * | | | | 14/00 | * | * | * | | | |
| 09/00 | * | | | | | | 14/12 | * | * | | | | |
| 10/00 | | * | | | | | 15/00 | | * | * | | | |
| 11/00 | | | * | | | | 15/12 | | * | | | | |
| 11/12 | * | * | | | | | 17/00 | * | * | * | | | |
| 12/12 | | * | | | | | 17/12 | * | | | | | |
| 14/00 | | | | * | | | 18/00 | * | | | | | |
| 14/12 | * | | | | | | 18/12 | | * | * | | | |
| 15/00 | | * | | | | | 19/12 | * | | | | | |
| 17/00 | * | | | | | | 20/00 | * | | | | | |
| 18/12 | * | | | | | | 24/00 | | * | | | | * |
| 19/00 | * | | | | | | 26/00 | * | * | | | | |
| 19/12 | * | * | | | | | 26/12 | * | | | | | |
| 20/12 | * | | | | | | 27/00 | * | | | | | |
| 21/00 | | | * | * | | | 28/00 | * | | | | | |
| 21/12 | * | | * | | | | 28/12 | * | | | | | |
| 22/12 | | | * | | | | 29/00 | * | * | | | | |
| 25/00 | * | * | | | * | | 30/12 | * | | | * | | |
| 25/12 | | * | * | | | * | 31/00 | * | * | * | | | |
| 26/12 | * | * | | | | | | | | | | | |
| 27/00 | | | * | | | | Total Jan 90: | 12 | 12 | 10 | 3 | 2 | 1 |
| 28/00 | | * | | | | | Total Jan 91: | 16 | 12 | 6 | 1 | 1 | 2 |
| 29/00 | | | * | | | | Total Period: | 28 | 24 | 16 | 4 | 3 | 3 |

Table 3. Vertical distribution of slantwise unstable layers for each month during 1990 and 1991. All soundings that were slantwise unstable ($0 < Ri_m < 1$) were included in the analysis. The total number of such soundings per month and the % of total in each layer are also listed.

| MM | YY | Total cases | Layers | | | | | |
|------------|----|-------------|----------|----------|----------|----------|----------|----------|
| | | | 90 85 | 85 80 | 80 70 | 70 60 | 60 50 | 50 40 |
| Jan | 90 | 26 | 12 | 12 | 10 | 3 | 2 | 1 |
| Feb | 90 | 23 | 17 | 7 | 5 | 4 | 5 | 5 |
| Mar | 90 | 20 | 13 | 6 | 4 | 2 | 4 | 1 |
| Apr | 90 | 9 | 4 | 7 | 2 | 0 | 1 | 0 |
| May | 90 | 2 | 1 | 0 | 0 | 1 | 1 | 0 |
| Jun | 90 | 1 | 0 | 1 | 1 | 0 | 0 | 0 |
| Jul | 90 | 1 | 1 | 1 | 0 | 0 | 0 | 0 |
| Aug | 90 | 3 | 1 | 1 | 1 | 0 | 0 | 0 |
| Sep | 90 | 4 | 0 | 1 | 3 | 1 | 1 | 0 |
| Oct | 90 | 22 | 15 | 11 | 5 | 5 | 4 | 3 |
| Nov | 90 | 20 | 9 | 6 | 4 | 8 | 4 | 3 |
| Dec | 90 | 26 | 15 | 10 | 3 | 4 | 5 | 3 |
| Jan | 91 | 22 | 16 | 12 | 6 | 1 | 1 | 2 |
| Feb | 91 | 19 | 9 | 12 | 9 | 2 | 3 | 2 |
| Mar | 91 | 13 | 7 | 5 | 3 | 3 | 1 | 1 |
| Apr | 91 | 8 | 3 | 4 | 0 | 0 | 2 | 1 |
| May | 91 | 4 | 2 | 3 | 2 | 1 | 2 | 0 |
| Jun | 91 | 0 | 0 | 0 | 0 | 0 | 0 | 0 |
| Jul | 91 | 1 | 1 | 0 | 0 | 1 | 0 | 0 |
| Aug | 91 | 0 | 0 | 0 | 0 | 0 | 0 | 0 |
| Sep | 91 | 2 | 2 | 1 | 0 | 0 | 0 | 0 |
| Oct | 91 | 13 | 10 | 6 | 5 | 0 | 1 | 0 |
| Nov | 91 | 17 | 11 | 5 | 0 | 2 | 1 | 1 |
| Dec | 91 | 25 | 15 | 11 | 4 | 2 | 5 | 3 |
| Total | | | 281 | 164 | 122 | 67 | 40 | 43 |
| % of Total | | | 100 | 58 | 43 | 24 | 14 | 15 |

and 40 kPa. Generally, the trend was similar for all months, without major seasonal variations.

Thus, in central Alberta symmetric instability is found primarily in the lower atmospheric layers, independent of a

particular season. A likely explanation for this finding is that the largest baroclinicity typically occurs close to the ground, causing the vertical wind shear to be larger in low levels, as compared to upper level shear values.

5.4 On the possible use of the moist Richardson number in predicting the amount of precipitation

The issue discussed in this section is whether the Ri_m magnitude, obtained from a single sounding data analysis, is related to the precipitation amount, accumulated within the next 12 hours, when a precipitation event is predicted. To address this problem, all soundings cases which satisfied the following three criteria were analyzed: (a) the sounding was convectively stable; (b) the sounding revealed at least one slantwise unstable layer; (c) at least 0.2 mm of precipitation was measured at the Stony Plain station for the 12 hours which followed the release of the sounding. Out of the total of 1399 soundings, only 65 satisfied these criteria and were included in the analysis (37 cases in 1990 and 28 cases in 1991). The actual release of instability requires a "triggering" mechanism in order to lift air parcels from the boundary layer up to its level of slantwise free convection. Usually these triggers occur only in the lower troposphere due to convergence associated with the mountain breeze or surface frontogenesis. Thus, the analysis was confined to the lowest symmetrically unstable slab, consisting of a single layer or

multiple layers, capped with a stable layer aloft. For each slab involved in the analysis, the average moist Richardson number, $\langle Ri_m \rangle$, was computed by

$$\langle Ri_m \rangle = \frac{\sum_{j=1}^{j_{\max}} (Ri_{mj} \Delta p_j)}{\sum_{j=1}^{j_{\max}} (\Delta p_j)}, \quad (2)$$

where $j=1,2,\dots,j_{\max}$ denotes the layer index with j_{\max} being the total number of layers in the slantwise unstable slab and Δp_j denotes the pressure difference between the bottom and top of the j th layer. Table 4 shows the results.

What are the conclusions to be drawn from this table? For some cases very small $\langle Ri_m \rangle$ values were indeed accompanied by relatively large precipitation amounts; for example, the $\langle Ri_m \rangle$ value of 0.1 yielded precipitation amounts of 7.4 mm and 19.5 mm at 12 UTC 3 October 1990 and at 12 UTC 26 January 1991, respectively. On the other hand, however, the similar small $\langle Ri_m \rangle$ magnitude of 0.1 was associated with less than 1 mm of precipitation on 27 April 1990 and 31 October 1991. A similar dichotomy was found for large $\langle Ri_m \rangle$ values. In some cases, large $\langle Ri_m \rangle$ values were matched with very small amounts of precipitation; for example $\langle Ri_m \rangle = 0.9$ was matched with 0.3 mm on 27 January 1990 and with 0.4 mm on 2 December 1991. On the contrary, in some other cases the same large $\langle Ri_m \rangle = 0.9$ was associated with 6.0 mm and 5.5 mm on 17 December 1990 and 3 December 1991, respectively. Similarly, mixed results were found concerning the depth of symmetrically unstable layers.

Table 4. The average moist Richardson number $\langle Ri_m \rangle$, the 12-hourly accumulated precipitation and the depth of the symmetrically unstable soundings.

| 1990 | | | | | | 1991 | | | | | |
|------|----|----|--------------------|--------------|----------------|------|----|----|--------------------|--------------|----------------|
| MM | DD | HH | <Ri _m > | Prec (mm) | Depth (kPa) | MM | DD | HH | <Ri _m > | Prec (mm) | Depth (kPa) |
| Jan | 1 | 00 | 0.2 | 0.3 | 90-85 | Jan | 26 | 00 | 0.1 | 0.3 | 90-80 |
| Jan | 3 | 00 | 0.4 | 0.5 | 85-70 | Jan | 26 | 12 | 0.1 | 19.5 | 90-85 |
| Jan | 9 | 00 | 0.1 | 2.0 | 90-85 | Jan | 27 | 00 | +0.0 | 2.2 | 90-85 |
| Jan | 20 | 12 | 0.5 | 0.6 | 90-85 | Jan | 28 | 12 | 0.5 | 1.5 | 90-85 |
| Jan | 27 | 00 | 0.9 | 0.3 | 80-70 | Jan | 29 | 00 | 0.5 | 1.5 | 90-80 |
| Jan | 28 | 00 | 0.7 | 1.6 | 85-80 | Jan | 30 | 12 | 0.5 | 0.8 | 90-85 |
| Jan | 29 | 00 | 0.8 | 2.0 | 70-60 | Feb | 12 | 12 | 0.4 | 0.3 | 85-70 |
| Feb | 8 | 00 | 0.3 | 0.2 | 90-85 | Feb | 15 | 12 | 0.8 | 1.8 | 85-70 |
| Feb | 9 | 00 | 0.8 | 0.2 | 90-80 | Feb | 22 | 00 | 0.5 | 5.4 | 90-85 |
| Feb | 10 | 12 | 0.5 | 8.0 | 90-85 | Mar | 3 | 12 | 0.5 | 4.2 | 70-50 |
| Feb | 15 | 00 | 0.6 | 1.0 | 85-80 | Mar | 4 | 00 | 0.5 | 1.2 | 90-85 |
| Feb | 20 | 12 | 0.7 | 0.2 | 90-80 | Mar | 10 | 00 | 0.4 | 0.2 | 90-85 |
| Feb | 24 | 12 | 0.8 | 0.2 | 70-60 | Mar | 23 | 12 | 0.2 | 0.2 | 90-85 |
| Mar | 19 | 12 | 0.7 | 1.6 | 85-80 | Apr | 5 | 12 | 0.7 | 16.0 | 60-50 |
| Apr | 07 | 00 | 0.6 | 10.2 | 85-80 | May | 24 | 12 | 0.5 | 7.9 | 90-80 |
| Apr | 07 | 12 | 0.7 | 1.5 | 85-70 | Jul | 7 | 12 | 0.6 | 1.0 | 90-85 |
| Apr | 14 | 12 | 0.3 | 1.6 | 90-80 | Oct | 30 | 00 | 0.1 | 2.5 | 90-85 |
| Apr | 27 | 00 | 0.1 | 0.8 | 85-80 | Oct | 31 | 00 | 0.1 | 0.2 | 80-70 |
| May | 13 | 12 | 0.5 | 0.6 | 90-85 | Nov | 4 | 12 | 0.6 | 1.0 | 50-40 |
| Aug | 29 | 12 | 0.2 | 22.6 | 80-70 | Nov | 16 | 12 | 0.8 | 0.2 | 50-50 |
| Oct | 01 | 12 | 0.2 | 0.2 | 80-70 | Nov | 20 | 00 | 0.9 | 1.4 | 90-85 |
| Oct | 03 | 12 | 0.1 | 7.4 | 90-85 | Nov | 30 | 12 | 0.8 | 0.5 | 90-85 |
| Oct | 08 | 00 | 0.7 | 0.4 | 90-85 | Dec | 2 | 00 | 0.9 | 0.4 | 90-85 |
| Oct | 09 | 00 | 0.3 | 0.4 | 85-80 | Dec | 3 | 00 | 0.9 | 5.5 | 80-70 |
| Oct | 25 | 12 | 0.4 | 0.4 | 85-80 | Dec | 4 | 00 | 0.3 | 1.4 | 70-60 |
| Nov | 10 | 00 | 0.2 | 4.0 | 80-60 | Dec | 4 | 12 | 0.6 | 0.2 | 80-70 |
| Nov | 11 | 00 | 0.8 | 0.4 | 70-50 | Dec | 12 | 00 | 0.2 | 0.4 | 90-80 |
| Nov | 20 | 00 | 0.1 | 1.6 | 85-80 | | | | | | |
| Nov | 22 | 12 | 0.6 | 14.0 | 80-60 | | | | | | |
| Nov | 23 | 00 | 0.9 | 2.3 | 90-85 | | | | | | |
| Dec | 17 | 00 | 0.9 | 6.0 | 85-80 | | | | | | |
| Dec | 17 | 12 | 0.5 | 1.2 | 85-80 | | | | | | |
| Dec | 23 | 00 | 0.2 | 1.0 | 90-85 | | | | | | |
| Dec | 23 | 12 | 0.9 | 1.0 | 90-85 | | | | | | |
| Dec | 24 | 12 | 0.9 | 2.6 | 90-85 | | | | | | |
| Dec | 25 | 12 | 0.7 | 0.7 | 90-85 | | | | | | |
| Dec | 27 | 00 | 0.8 | 0.5 | 90-85 | | | | | | |

Fairly deep layers caused significant precipitation in some cases, while in others little precipitation was observed.

It is evident that, the analyzed data do not suggest a statistical relationship between the 12-hourly precipitation amounts and the magnitude of the $\langle Ri_m \rangle$ or the depth of the slantwise unstable slab. Precipitation data shown on Table 4 are "point measurements"; i.e. precipitation readings at the Stony Plain raingauge. It is well known that precipitation can vary largely over relatively short distances, particularly in the case of heavy rain showers falling from convective storms. Therefore, a single point measurement of rainfall may not be representative of the actual rainfall of the area. The value obtained by averaging several surface rainfall measurements would be a better estimate of the mesoscale precipitation amount. However, this was not done in this study because 12-hourly resolution precipitation data could not be readily obtained for the stations in the vicinity of Stony Plain. It remains unclear to what extent the analysis may be affected by using "point" rather than "regionally averaged" measurements of precipitation amounts.

5.5 Conclusions and discussion

The Stony Plain soundings sampled between 1 January 1990 and 31 December 1991 were analyzed to characterize some features associated with symmetric instability. One of the points of this analysis was to test whether the presence of

symmetrically unstable layers was correlated with large vertical windshear values. Concentrating on the 90 to 80 kPa layer, the analysis indeed supported such a relationship. Specifically, about 75% of the absolutely stable cases were associated with $dv/dz < 6 \text{ ms}^{-1}\text{km}^{-1}$, while about 80% of slantwise unstable cases were associated with $dv/dz > 6 \text{ ms}^{-1}\text{km}^{-1}$. Thus, the observed data agreed well with the theory in stating that, the windshear in a particular atmospheric slab is a crucial factor for determining whether the layer is symmetrically stable or unstable. This finding was rather independent of the seasons and also independent of years. Operationally, the threshold of $6 \text{ ms}^{-1}\text{km}^{-1}$ may be used for classifying a convectively stable sounding as slantwise unstable in the low levels.

To characterize the vertical distribution of slantwise unstable layers, the soundings for January 1990 and January 1991 were examined in detail. The results for these months indicated that symmetric instability occurred more often below 70 kPa ($\approx 3 \text{ km}$) than above this level (68 cases below 70 kPa vs 10 cases above 70 kPa). For the entire 24 months of data, 58% of the cases showed a potential for symmetric instability in the 90-85 kPa slab. Higher up, however, this percentage decreased rapidly. Thus, it was concluded that in central Alberta slantwise instability was occurring mostly in the lower atmospheric levels.

The analysis tried to find out whether the 'amount' of precipitation was linked (in a statistical sense) to either

the depth of the lowest symmetrically unstable slab or the $\langle Ri_m \rangle$ value, defined as the Ri_m numerical value averaged over the lowest symmetrically unstable slab. The data used did not present any conclusive results and an explanation is required to clarify this apparent "disagreement" between observations and theory which clearly states that the Ri_m is a local measure for the degree of slantwise instability. One valid argument to put forward is that a much larger data set is needed for testing a statistical relationship between the accumulated precipitation amounts and $\langle Ri_m \rangle$ values, because the natural variability of precipitation is extremely large. A second explanation is that data from a single sounding only were used, without considering other factors. A statistical relationship between the mesoscale precipitation amounts and a parameter derived from single sounding data is meaningless because clearly precipitation amounts are largely determined by large scale forcing and available moisture amount, both of which are not evident from a single sounding. There is still a third reason involving the accuracy of the calculation of the moist Richardson number. Eq (1) clearly shows that Ri_m is quite sensitive to small changes in the observed quantities. For example, a small change in the temperature lapse rate can greatly affect Ri_m , particularly when thermal stratification is very close to convectively neutral. Similarly, a small difference in the observed windshear can significantly affect the Ri_m numerical value, particularly when there is little

thermal shear.

This analysis concludes that the moist Richardson number is not a reliable parameter for predicting the precipitation 'amount' at a given station. Since Ri_m is (vertically) a local measure of the degree of slantwise instability and is very sensitive to small inaccuracies in the observed data, it would serve to consider a global measure (along the vertical) to quantify the total amount of latent energy available for the entire sounding. Chapter 6 will indeed follow along this line and develop a global parameter based on slantwise instability and compare it with observed precipitation amounts.

Chapter 6

A slantwise Showalter index based on conditional symmetric instability: Results for central Alberta

6.1 Introduction

While the prediction of large-scale weather circulation systems has improved significantly during the past decades, reliable quantitative precipitation forecasts still remain a challenging problem. Most of the annual precipitation is produced by mesoscale weather systems that are too small to be resolved by conventional observation networks and handled satisfactorily by operational numerical weather prediction models.

Operational forecasters would gain if they had a simple tool providing them with a reliable check for the occurrence of mesoscale precipitation. This chapter proposes and tests the Slantwise Showalter Index ,SSI, as a parameter that may provide information regarding the likelihood of significant precipitation. This new index is based solely on observed temperature, humidity and wind data from 85 to 50 kPa, and the synoptic-scale absolute vorticity estimated from the 50 kPa upper air chart. The slantwise Showalter index can be thought of as a generalization of the classic Showalter Index ,SI, (Showalter 1953) but instead of approximating the convective instability, the SSI approximates the amount of conditional symmetric instability (or slantwise convective instability).

The rationale of using the SSI is based on the notion that significant steady rain is often associated with slanted circulation rolls driven by the release of the latent heat associated with conditional symmetric instability. There is ample evidence that long-lasting precipitation bands are closely related to conditional symmetric instability, based on observations and numerical simulations. A selection of the observed case studies is given below:

Oklahoma rain storm of 2-3 Dec 1982 (Emanuel 1983)

East coast snowstorm of 11-12 Feb 1983 (Sanders and Bosart 1985)

New England snowstorm of 11 Dec 1982 (Wolfsberg et al. 1986)

Illinois snowstorm of 9 Dec 1982 (Gyakum 1987)

Midwest snowstorm of 30-31 Jan 1982 (Moore and Blakeley 1988)

Nova Scotia snowstorm of 26 Feb 1986 (Donaldson and Stewart 1989)

Oklahoma snowstorm of 31 Jan 1985 (Byrd 1989)

Nova Scotia snowstorm of 30 Jan 1986 (Reuter and Yau 1990)

Alberta rainstorm of 16-17 Jul 1986 (Reuter and Nguyen 1993).

What these events had in common is that the precipitation bands were aligned in the direction of the thermal wind and conditional symmetric instability was diagnosed as a major forcing for the precipitation bands. It should be pointed out that all these events were characterized by a rather shallow slantwise unstable layer - usually a few hundred meters only. Studies were also made to investigate the "climatology" of

conditional symmetric instability for a specific geographical region. Seltzer et al. (1985) analyzed many precipitation events over New England. For the cases where the radar echoes indicated a banded formation the air flow was found to be slantwise unstable. Reuter and Yau (1990) identified seven cases which were either neutral or unstable for slantwise convection during the 2-month period of the Canadian Atlantic Storm Project (CASP). They concluded that slantwise convection seems to be ubiquitous for baroclinic zones such as Atlantic Canada in winter months. A detailed analysis of dropsonde data, collected during the Experiment of Rapidly Intensifying Cyclones over the Atlantic (ERICA) gave additional evidence that conditional symmetric instability produced areas of heavy precipitation ahead of the warm frontal zones associated with developing marine winter cyclones (Reuter and Yau 1993). Byrd (1989) showed that moist symmetric instability provided the major forcing for many over-running precipitation bands in the southern plains of the United States.

More evidences of the role symmetric instability in organizing precipitation comes from numerical simulations using high-resolution models. Mailhot and Chouinard (1989) and Hedley and Yau (1991) indicated that the air mass on the warm side of the warm front was symmetrically unstable. In all the cases, the unstable region had significant upward motion and rainfall. More recently Zhang and Cho (1992) analyzed three-dimensional simulation results for a mid-latitude squall line.

The trailing stratiform cloud was diagnosed to be convectively stable but slantwise unstable, resulting in strong stratiform rainfall. Shutts (1990) computed charts showing regions with conditional symmetric instability based on simulated fields by the United Kingdom operational weather prediction model. They recommended that these charts be tested in an operational setting. Early results from real-time use of SCAPE charts in operational weather forecasting over the Great Plains were very promising (Snook 1992).

The main purpose of this chapter is to introduce the SSI index based on a simplified assessment of the potential for conditional symmetric instability for a very deep layer which extends from 85 to 50 kPa. This study will also examine the usefulness of this new index in identifying deep slantwise overturning for central Alberta using sounding data from Stony Plain. Twelve consecutive months of data were analyzed to determine the seasonal variations of SSI and the associated precipitation events. This chapter is organized as follows. Section 2 deals with the definition of SSI, including the related theory of conditional symmetric instability. Section 3 provides an estimate of the error in the SSI index arising from inaccurate sounding measurements. The data base and the method of analysis are presented in Section 4. Results will be shown and interpreted in Section 5, whereas the last section summarizes the major findings.

6.2 Slantwise Showalter Index

Symmetric instability arises from an unstable balance or distribution of body forces acting on a two-dimensional tube of air in a baroclinic air flow. The combined effect of the gravity forces acting in the vertical and centrifugal forces acting in the horizontal (due to the earth's rotation) can sometimes accelerate the tube in a slantwise direction; this is referred to as symmetric instability. The dry atmosphere, with a few exceptions, is stable for symmetric instability. However, the latent heat effects during cloud condensation can greatly destabilize the flow, and occasionally can lead to conditional symmetric instability, CSI, (or moist symmetric instability or slantwise convective instability).

The theory of moist symmetric instability is now well established and documented in many papers (e.g. Stone 1966; Bennetts and Hoskins 1979; Emanuel 1979; 1983) and textbooks (e.g. Rogers and Yau 1989; Ray 1986; Cotton 1990). The key concept in the theory of symmetric instability is that of the absolute angular momentum M (ms^{-1}) defined by

$$M \equiv v + f x \quad (1)$$

where f is the local Coriolis parameter (s^{-1}), v is the wind component (ms^{-1}) in the direction of the thermal wind and x is the distance normal to the thermal shear direction with positive values pointing towards the warm air. M constitutes a conserved variable, provided the flow is two-dimensional,

friction is neglected and f remains locally uniform. It is also assume that the flow is in geostrophic balance, which leads to the geostrophic thermal wind relation

$$\frac{\partial v}{\partial z} = \frac{g}{fT} \frac{\partial T}{\partial x}, \quad (2)$$

where T is the virtual temperature ($^{\circ}\text{K}$), z is height and g is the gravitational acceleration. With these assumptions, the total potential energy of the flow called Slantwise Convective Available Potential Energy (SCAPE), is

$$SCAPE \equiv \int_M^{z_2} g \frac{T_t - T}{T^*} dz, \quad (3)$$

where T_t denotes the virtual temperature of the pseudo-adiabatically displaced tube at height z , T is the virtual temperature of the ambient air at height z and z_1 and z_2 denote the initial and final heights of the displaced tube of air, respectively. T^* is a reference temperature which can be set to $T^* = [T(z_1) + T(z_2)]/2$ and the subscript M indicates that the integration must be carried out along the surface of constant M value, which is given by $M_1 = v(z_1) + f x_1$. The importance of (3) is in the fact that the susceptibility of moist baroclinic flows to CSI can be assessed by lifting a tube of air along a surface of constant M and comparing its temperature to that of its environment. If the flow is barotropic (no thermal shear) then M surfaces are vertical and (3) represents the standard analysis of the Convective Available Potential Energy (CAPE);

i.e. the positive area on a tephigram. If the flow, however, is baroclinic, then (3) includes the centrifugal contribution to the total potential energy (Emanuel 1983).

Central to concepts of both CAPE and SCAPE are the usual assumptions of parcel theory, namely that there is no mixing between parcel and environment and that the net perturbation pressure gradient force on the parcel is negligible. The time scales associated with the release of cumulus and slantwise instabilities differ greatly. The time scale is equal to the moist Brunt-Väisälä period (10-20 min) for cumulus convection and equal to f^{-1} (2-4 hours) for slantwise convection. Since convective instability is released much faster than the moist symmetric instability the amount of SCAPE is really immaterial when a positive CAPE value is present. In other words, cumulus convection will always provide the overriding forcing for the cloud development and, slantwise roll circulations will only start after the CAPE has been totally depleted.

It is possible to use only one single vertical sounding to estimate the SCAPE, provided some information about the vertical component of the absolute vorticity is available. Emanuel (1983) showed that, by combining (1), (2) and (3) the integration along a constant M surface can be replaced by an integration in the vertical such that

$$SCAPE = \int_{z_1}^{z_2} \left[g \frac{T_t - T}{T^*} + \frac{1}{2} \frac{f}{\eta} \frac{d[(v - v_1)^2]}{dz} \right] dz, \quad (4)$$

where x is the direction normal to the geostrophic wind,

$v=v(z)$ is the ambient wind speed in the y direction, and v_1 is the parcel's v at z_1 . With the y axis aligned parallel to the flow, the vertical component of the absolute vorticity η becomes

$$\eta = f + \frac{1}{g} \frac{dv}{dz} \frac{dz}{dx}. \quad (5)$$

The first term in (4) represents the standard positive area on a tephigram showing the gravitational contribution to the potential energy, while the second term is the contribution from the centrifugal forces. To evaluate parcel stability one can simply add a "slantwise adjustment" term ΔT

$$\Delta T = \frac{1}{2} \frac{T^*}{g} \frac{f}{\eta} \frac{d[(v - v_1)^2]}{dz} \quad (6)$$

to the temperature of the lifted tube of air (T_t) at each level and evaluate the sounding in the usual way. ΔT can be approximated by

$$\Delta T \approx \frac{1}{2} \frac{T^*}{g} \frac{f}{\eta} \frac{(v - v_1)^2}{z - z_1}. \quad (7)$$

Evaluating the SCAPE using (4) is not without difficulty, because the levels z_1 and z_2 should agree with the tube's Level of Free Convection (LFC) and with the level of zero buoyancy, respectively. This, of course, is equally needed for computing the usual CAPE. The degree of convective instability is often expressed by easily calculated indices such as the Showalter Index, Lifted Index, Total Totals, George K Index, Rackcliff Index, Jefferson Index, Boyden Index and others. These indices

provide rough estimates of the CAPE based on thermodynamic data from only a few selected levels. Relevant to this study is Showalter's (1953) stability index defined as follows: A parcel from 85 kPa is lifted dry adiabatically to saturation and then pseudo-adiabatically to 50 kPa. Then, the lifted parcel 50 kPa temperature is subtracted from the observed 50 kPa air temperature: $SI_{85} = T_{50} - T_{lft85}$. This index has been found to be a significant forecast tool for predicting severe thunderstorms in central and western United States (Showalter 1953), in Alberta (Anderson and Charlton 1990), in Scandinavia (Andersson et al. 1990) and in South Africa (Reuter 1990). In analogy to the idea that SI provides a rough estimate for the CAPE, the SI evaluated along a surface of constant M gives a rough estimate of the amount of SCAPE. This study defines the Slantwise Showalter Index (SSI) to be exactly the SI along a constant M surface. The SSI_{85} (from 85 kPa) is given below,

$$SSI_{85} \equiv SI_{85}|_M = T_{50} - T_{lft85}|_M \approx T_{50} - (T_{lft85} + \Delta T_{85}) \quad (8)$$

provided $SI_{85} \geq 0$; and whenever $SI_{85} < 0$ the SSI is set equal to zero because of the different time scales of convective and slantwise instabilities. The lifted temperature along the slanted M surface is estimated by computing the temperature of a parcel lifted vertically from 85 to 50 kPa and adding to it the adjustment term ΔT_{85} . This term represents the effective contribution of the centrifugal effects which is determined by the amount of thermal shear and the absolute vorticity of the

large scale flow. Specifically, ΔT_{85} is given by

$$\Delta T_{85} = \frac{T^*}{2g} \frac{f}{\eta_{50}} \frac{(v_{50} - v_{85})^2}{(z_{50} - z_{85})} \quad (9)$$

where the subscripts indicate the pressure levels. For later use, the index SSI_{90} is also introduced which differs from SSI_{85} in that the lifted parcel originates from the 90 kPa level. This index is given by

$$SSI_{90} \equiv SI_{90}|_M = T_{50} - T_{lft90}|_M \approx T_{50} - (T_{lft90} + \Delta T_{90}), \quad (10)$$

where ΔT_{90} is given by (9) for the 90-50 kPa layer. Again, the SSI_{90} is set equal to zero when the SI_{90} is negative.

6.3 Error analysis

All observations are subject to some errors: sounding measurements are no exception. Nevertheless, it is common practice to ignore the uncertainty associated with balloon sounding data. Even the research literature remains rather silent about quantifying the sounding measurements errors and their effects on various stability parameters. This chapter will not follow this example, but instead, will attempt to quantify the inaccuracy in the SSI values, calculated with inaccurate sounding measurements. The distribution of the errors from in-situ sensors is usually close to a normal distribution (Brooks and Carruthers 1953, p. 86). Therefore, the precision of the measurements can be best quantified in terms of the root-mean-square (rms) errors. Golden et al.

(1986) documented the rms errors of typical operational sounding data: the temperature rms error is 0.6 °C, that of relative humidity is 10% and that of the wind speed is 3 ms⁻¹. These values are adopted in the present estimates.

Based on (8) and (9), the rms error of SSI₈₅ consists of three major terms: error in the thermodynamic data (inaccurate $T_{50}-T_{1ft85}$ value), error in the wind data (inaccurate $v_{50}-v_{85}$ value) and error involving the synoptic forcing (an inaccurate f/η_{50} value). Substituting (9) into (8) and calculating partial differentials results in

$$d(SSI_{85}) = d(T_{50} - T_{1ft85}) + \alpha \left[\frac{f}{\eta_{50}} \right] d(\Delta v) + \alpha \frac{\Delta v}{2} d \left[\frac{f}{\eta_{50}} \right] \quad (11)$$

where,

$$\Delta v = v_{50} - v_{85} , \quad \alpha = \frac{T^* \Delta v}{g(z_{50} - z_{85})} . \quad (12)$$

Since the quantities $T_{50}-T_{1ft85}$, $v_{50}-v_{85}$ and f/η_{50} are measured independently, their errors should not be correlated with each other. For such uncorrelated error terms, the rms error of the sum $\langle SSI_{85} \rangle$ can be computed by

$$\langle SSI_{85} \rangle = \sqrt{\langle T_{50} - T_{1ft85} \rangle^2 + \left[\frac{f\alpha}{\eta_{50}} \right]^2 \langle \Delta v \rangle^2 + \left[\frac{\alpha \Delta v}{2} \right]^2 \left\langle \frac{f}{\eta_{50}} \right\rangle^2} \quad (13)$$

where $\langle x \rangle$ denotes the rms error in the variable x (Brooks and Carruthers 1953, p. 226). The wind speed error at 85 kPa is well correlated with the wind speed error at 50 kPa, provided both measurements were made using the same radio theodolite

(Golden et al. 1986). As a result, here it can be assumed that $\langle v_{50} - v_{85} \rangle \approx \langle v_{50} \rangle \approx 3 \text{ ms}^{-1}$. Similarly, the error margins of T_{50} and T_{lift85} are usually well correlated, implying that the error in the difference between the observed and lifted temperatures at 50 kPa is similar to that in T_{50} : $\langle T_{50} - T_{\text{lift85}} \rangle \approx \langle T_{50} \rangle \approx 0.6 \text{ }^{\circ}\text{C}$.

For estimating the error $\langle \text{SSI}_{85} \rangle$ in (13), typical values of $T^* = 270 \text{ }^{\circ}\text{K}$, $g = 9.8 \text{ ms}^{-2}$, $v_{50} - v_{85} = 20 \text{ ms}^{-1}$, $z_{50} - z_{85} = 4000 \text{ m}$, and $(f/\eta) = 1$ were used here. A rather generous margin of error was assigned to the large-scale absolute vorticity value at 50 kPa by letting $\langle f/\eta_{50} \rangle = 0.4$. Substitution into (13) gives

$$\langle \text{SSI}_{85} \rangle = \sqrt{(0.6)^2 + (0.138 \times 3)^2 + (1.38 \times 0.4)^2} = 0.9 \quad (14)$$

The rms error of SI_{85} contains only the first term, involving the thermodynamic data. Thus $\langle \text{SI}_{85} \rangle = 0.6 \text{ }^{\circ}\text{C}$. A similar analysis for the 90-50 kPa layer indicated that $\langle \text{SSI}_{90} \rangle \approx \langle \text{SSI}_{85} \rangle = 0.9$ and $\langle \text{SI}_{90} \rangle \approx \langle \text{SI}_{85} \rangle = 0.6 \text{ }^{\circ}\text{C}$.

6.4 Database and method of analysis

Stony Plain was selected for testing the SSI usefulness, because its northern location (53.5° N , 114.1° W) assured a large Coriolis parameter ($f = 1.17 \times 10^{-5} \text{ s}^{-1}$) that helps maintain the thermal wind balance (2). More than one-half of the mean annual precipitation of 529 mm falls during the summer months in convective showers. The analysis is based on the data collected from 1 January to 31 December 1990. This particular year represented a rather "normal" year as far as seasonal

precipitation was concerned (Table 1). Individual monthly values showed some variability. For example, June 1990 was rather dry whereas July was rather wet, compared to the climatology. Radiosondes were launched daily at 0000 and 1200 UTC from Stony Plain. This work required data for mandatory pressure levels only and data was obtained from the Alberta Weather Centre archive for upper air observations. Out of a total of 730 cases, 704 soundings were analyzed for convective and slantwise instability, while the remaining 26 soundings had to be discarded because of missing data. Accumulated precipitation amounts were recorded every 12 hours at about 0000 and 1200 UTC. Being interested in mesoscale precipitation events, the 0000 UTC sounding was matched with the amount of precipitation accumulating between 0000 and 1200 UTC, while

TABLE 1. Monthly precipitation accumulation and the number of days with precipitation for the "normal" year and 1990. The normal year values are the 30 year climatology.

| Month | Precipitation (mm) | | Days with precipitation | |
|-------|--------------------|-------|-------------------------|------|
| | Normal | 1990 | Normal | 1990 |
| Jan | 26.8 | 14.4 | 12 | 15 |
| Feb | 21.0 | 16.3 | 10 | 12 |
| Mar | 21.2 | 16.2 | 11 | 6 |
| Apr | 26.3 | 60.3 | 8 | 12 |
| May | 48.4 | 50.6 | 10 | 13 |
| Jun | 98.9 | 52.7 | 15 | 15 |
| Jul | 96.0 | 159.6 | 14 | 16 |
| Aug | 73.6 | 85.6 | 13 | 12 |
| Sep | 45.3 | 14.6 | 11 | 7 |
| Oct | 20.0 | 32.6 | 7 | 12 |
| Nov | 22.6 | 32.3 | 8 | 7 |
| Dec | 28.7 | 31.9 | 11 | 14 |
| Total | 528.8 | 567.1 | 130 | 141 |

the 1200 UTC sounding data were correlated with 1200-2400 UTC precipitation.

Some details about computing the SI_{85} and SSI_{85} indices are given next. The 85 kPa parcel was lifted dry adiabatically to its lifting condensation level, LCL. To ensure condensation occurred below 50 kPa, the LCL pressure (P_{LCL}) was found by the potential temperature relationship using T_{LCL} , the temperature at the lifting condensation level; this latter was calculated by Bolton's (1980) expression

$$T_{LCL} = \left[\frac{1}{T_d - 56} + \frac{\ln(T/T_d)}{800} \right]^{-1} + 56 \quad (15)$$

where T and T_d denote the air and dewpoint temperatures ($^{\circ}K$) at 85 kPa, respectively. Then, after reaching LCL the parcel continues to rise pseudo-adiabatically up to 50 kPa level. The lifted temperature at 50 kPa, T_{lft85} was computed by regression equations using the parcel wet-bulb temperature at 85 kPa; the latter was found by Newton's successive approximation method, using T and T_d . The thermal wind was found by subtracting the observed wind vector at 85 kPa from the 50 kPa wind vector. The thickness $z_{50} - z_{85}$ was computed using the height values obtained from integrating the hydrostatic balance using the observed pressure and temperature values.

The η_{50} values for Stony Plain ($53.5^{\circ}N$, $114.1^{\circ}W$) were read off the 50 kPa height/vorticity charts produced twice daily by the Canadian Meteorological Centre (CMC). These charts were available from the University of Alberta microfiche archive.

6.5 Results

To explore the usefulness of SSI, the analysis focused mainly on events, where the sounding data yielded a negative value for SSI, indicating the potential for moist symmetric instability. Table 2 shows the monthly frequencies of negative SSI values for parcels originating from the 85 kPa and 90 kPa levels, respectively. To allow comparison with the likelihood of convective activity, the monthly frequencies of negative values for SI_{85} and SI_{90} are also listed. The data show a large seasonal variability in the convective and moist symmetric stability properties. During the seven cold months (October-April) of 1990, the air mass did not indicate deep layers of convective or slantwise instabilities, with few exceptions. For example, only two cases of negative SSI_{85} were encountered out of a total of 426 soundings sampled in the seven cold

TABLE 2. Monthly frequency of soundings (0000 and 1200 UTC) for each of $SI_{85} < 0$, $SI_{90} < 0$, $SSI_{85} < 0$ and $SSI_{90} < 0$ in 1990.

| Month | SI_{85} | SI_{90} | SSI_{85} | SSI_{90} |
|-------|-----------|-----------|------------|------------|
| Jan | 1 | 0 | 0 | 1 |
| Feb | 1 | 0 | 0 | 0 |
| Mar | 0 | 0 | 0 | 0 |
| Apr | 0 | 1 | 1 | 0 |
| May | 5 | 7 | 2 | 1 |
| Jun | 10 | 14 | 5 | 5 |
| Jul | 8 | 15 | 4 | 6 |
| Aug | 10 | 19 | 6 | 4 |
| Sep | 1 | 3 | 2 | 2 |
| Oct | 1 | 0 | 0 | 2 |
| Nov | 0 | 0 | 1 | 0 |
| Dec | 0 | 0 | 0 | 1 |
| Total | 37 | 59 | 21 | 22 |

months. In the summer, however, there were 2 to 6 soundings per month that had negative SSI values. In terms of percentage this amounted to about 5-10% of the total soundings released. Negative SI_{90} values occurred more frequently than negative SI_{85} values. For the winter, however, the number of negative SI_{85} exceeded those of SI_{90} , indicating that the layer 90-85 kPa was quite stable during this season. The precise numbers listed in Table 2 could be debatable, due to inaccuracies in these stability parameters (see Section 6.3). However, the primary conclusion that deep layers of convectively or moist-symmetrically unstable air occur mainly during the summer months remains valid.

Theory states that negative SI and SSI values constitute only necessary but not sufficient conditions for the potential release of the instabilities on the microscale and mesoscale, respectively. One of the important sufficiency conditions is the presence of enough water vapour to assure saturation of the lifted air, allowing for moist pseudo-adiabatic processes rather than dry adiabatic processes. Moist conditions below the cloud base also are needed to avoid depletion of rain due to evaporation. A second condition to be met for the actual release of the potential instability is the presence of a triggering mechanism that can lift the air mass to reach its level of free (slantwise) convection. During the spring and summer, surface heating due to solar radiation is usually sufficient to trigger convection. However, in the cold season

surface heating is minimal and often the needed low-level lifting is missing to get the process started.

The first criterion of having "sufficient" humidity can be conveniently quantified in terms of the relative humidity at either 85 or 90 kPa. Based on the results of the 1990 Stony Plain data, a relative humidity value less than about 35% was usually insufficient to produce surface rainfall, even when the SSI values are negative. Therefore, the remainder of this chapter concentrates on those soundings, for which the low level relative humidity values were $\geq 60\%$. It must be stressed that the precise magnitude of this 60% "cut-off" value is not very important. The data was re-analyzed using the threshold values of 50% and 70% and in both cases the findings were very similar to those presented here, based on relative humidity values larger than 60%. Table 3 lists all the cases which had $RH_{85} \geq 60\%$ and either $SI_{85} \leq 0$ or $SSI_{85} \leq 0.9$ for the entire 1990. Table 3 also shows the thermal wind ($\Delta v_{85} = v_{50} - v_{85}$), the absolute vorticity (η_{50}) and the observed 12-hourly accumulated amounts of precipitation (PREC) at Stony Plain.

There were 15 soundings with negative SI_{85} values and they occurred during the period late May to early September. Thus, thunderstorm outbreaks, as diagnosed with a negative value of SI_{85} , were strictly summer-time events during 1990. Cases 8 to 15 were events which had a potential for thunderstorm activity (as indicated by negative SI_{85} values) but no surface rain fall was recorded at Stony Plain site. Convective cells generally

TABLE 3. List of soundings with $RH_{85} \geq 60\%$ and either $SI_{85} < 0$ or $SSI_{85} < 0.9$.

| | Case | RH_{85} | Δv_{85} | η_{50} | SI_{85} | SSI_{85} | PREC |
|----|----------|-----------|-----------------|-------------|-----------|------------|------------------|
| 1 | 05/20/12 | 92 | 4.8 | 9 | -0.3 | 0.0 | 5.1 |
| 2 | 06/07/00 | 87 | 9.3 | 12 | -1.2 | 0.0 | 0.9 |
| 3 | 07/01/00 | 61 | 15.6 | 14 | -2.3 | 0.0 | 1.4 |
| 4 | 07/06/00 | 75 | 16.2 | 10 | -1.2 | 0.0 | 0.6 |
| 5 | 07/16/12 | 91 | 2.6 | 13 | -1.6 | 0.0 | 0.6 |
| 6 | 07/25/00 | 85 | 6.6 | 11 | -1.2 | 0.0 | 6.8 |
| 7 | 08/22/00 | 67 | 3.1 | 14 | -5.3 | 0.0 | 0.2 |
| 8 | 06/28/12 | 64 | 1.3 | 10 | -1.6 | 0.0 | 0.0 |
| 9 | 06/29/00 | 63 | 6.9 | 14 | -0.2 | 0.0 | 0.0 |
| 10 | 07/26/00 | 87 | 7.4 | 9 | -4.5 | 0.0 | 0.0 |
| 11 | 08/06/00 | 60 | 12.6 | 13 | -3.4 | 0.0 | 0.0 |
| 12 | 08/18/00 | 93 | 6.9 | 10 | -0.1 | 0.0 | 0.0 |
| 13 | 08/18/12 | 99 | 2.1 | 14 | -0.3 | 0.0 | 0.0 |
| 14 | 08/27/00 | 100 | 6.0 | 12 | -0.6 | 0.0 | 0.0 |
| 15 | 09/06/00 | 64 | 25.0 | 10 | -1.1 | 0.0 | 0.0 |
| 16 | 06/06/12 | 76 | 11.9 | 10 | 0.1 | -0.5 | 0.1 |
| 17 | 06/11/00 | 88 | 13.9 | 10 | 0.5 | -0.3 | 1.8 |
| 18 | 07/02/12 | 91 | 42.3 | 16 | 1.4 | -3.5 | 28.8 |
| 19 | 07/03/00 | 97 | 21.3 | 10 | 1.2 | -0.6 | 0.6 |
| 20 | 08/15/00 | 81 | 24.6 | 10 | 0.1 | -2.5 | 17.5 |
| 21 | 08/16/00 | 67 | 21.3 | 11 | 0.1 | -1.6 | 0.1 |
| 22 | 09/17/00 | 75 | 20.2 | 20 | 0.2 | -0.7 | 0.0 ¹ |
| 23 | 06/11/12 | 98 | 18.5 | 18 | 1.1 | 0.3 | 0.8 |
| 24 | 03/20/00 | 63 | 17.5 | 13 | 1.5 | 0.5 | 1.4 |
| 25 | 02/11/00 | 72 | 36.6 | 14 | 4.7 | 0.5 | 0.0 |
| 26 | 02/11/12 | 92 | 41.5 | 14 | 5.9 | 0.6 | 0.0 |
| 27 | 12/05/12 | 64 | 14.0 | 14 | 0.6 | 0.1 | 0.0 |

¹ 3.2 mm at Edmonton

RH_{85} : Relative humidity at 85 kPa (%)
 Δv_{85} : Difference in wind vector at 50 and 85 kPa (ms^{-1})
 η_{50} : Absolute vorticity at 50 kPa (10^{-5} s^{-1})
 SI_{85} : Showalter Index based on 85 and 50 kPa data
 SSI_{85} : Slantwise Showalter Index based on 85 and 50 kPa data
 PREC : Stony Plain 12-hourly accumulated precipitation, mm

occur at a spatial scale that is too small to be resolved by operational surface observations; cases 8 to 15 (Table 3) are probably examples of this small-scale phenomenon. It should be pointed out that cases 9, 12, 13 and 14 had negative SI_{85} values that are within the ± 0.6 rms error margin for SI and thus they may actually not be indicative for conditionally unstable conditions.

Now the focus shifts to cases 16 to 22 that had deep moist layers of symmetrically unstable air (i.e. $SSI_{85} < 0$ and $RH_{85} \geq 60\%$). Cases 16 to 21 had precipitation during the next 12 hours. In case 22, the sounding of 0000 UTC 17 September did not produce precipitation at Stony Plain, yet rainfall was recorded 40 km downwind at Edmonton municipal airport (3.2 mm) and other neighbouring stations. The rms error margin of SSI_{85} had been estimated as 0.9. The most relaxed requirement (i.e. $SSI_{85} < 0.9$) adds five more soundings (cases 23 to 27) that were likely to have a deep layer of moist-symmetrically unstable air. On the other hand, the most stringent requirement (i.e. $SSI_{85} < -0.9$) reduces the number of slantwise unstable cases to only three soundings (cases 18, 20 and 21). Two of these three soundings produced significant rainfalls of 28.8 mm (case 18) and 17.5 mm (Case 20).

Table 4 summarizes the results for cases showing negative stability indices based on computations for parcels lifted from the 90 kPa level, which is about 200 m above the surface. All the convectively unstable conditions occurred during the

summer. There were 9 cases (1 to 9) with negative SSI_{90} values and associated with rainfall at Stony Plain, while in 13 cases (10 to 22) no surface rain was recorded at Stony Plain. This finding emphasize the small-scale nature of the summertime cumulus convection.

A total of 11 cases (23 to 33) had $RH \geq 60\%$ and $SSI_{90} < 0$ suggesting the potential for moist symmetric instability (Table 4). Only two soundings (cases 32 and 33) occurred during the winter, both of which did not produce precipitation at Stony Plain. Based on these two cases, during the winter season slantwise convective instability over central Alberta merely remained a potential without actual release, since triggering was lacking. For the summer, however, 5 of the 9 cases (23 to 27) with negative SSI_{90} values had indeed rainfall at Stony Plain. Cases 28, 29, 30 and 31 had no rain at Stony Plain but showers were recorded at downwind sites. It should be pointed out that the SSI_{90} index identified three cases of strong rainfall (71.6 mm for 0000 UTC and 28.8 mm for 1200 UTC both on 2 July 1990, and 17.5 mm for 0000 UTC 15 August 1990). The 71.6 mm flooding event ($SSI_{90} = -1.4$) was not evident from the SSI_{85} , suggesting that one should compute both SSI_{85} and SSI_{90} . Again, the inaccuracy in the SSI_{90} values should be considered. Allowing for an error margin of -0.9 would add case 34 to the potentially unstable soundings. For the most stringent criterion $SSI_{90} < -0.9$, however, the slantwise unstable

TABLE 4. List of soundings with $RH_{90} \geq 60\%$ and either $SI_{90} < 0$ or $SSI_{90} < 0.9$.

| Case | RH_{90} | Δv_{90} | η_{50} | SI_{90} | SSI_{90} | PREC |
|-------------|-----------|-----------------|-------------|-----------|------------|------------------|
| 1 05/24/00 | 63 | 14.9 | 8 | -0.4 | 0.0 | 5.8 |
| 2 06/07/00 | 71 | 12.9 | 12 | -1.6 | 0.0 | 0.9 |
| 3 06/07/12 | 73 | 0.3 | 10 | -0.2 | 0.0 | 0.3 |
| 4 07/06/00 | 60 | 17.9 | 10 | -2.0 | 0.0 | 0.6 |
| 5 07/16/12 | 89 | 2.3 | 13 | -0.2 | 0.0 | 0.6 |
| 6 07/25/00 | 86 | 6.0 | 11 | -3.2 | 0.0 | 6.8 |
| 7 07/25/12 | 80 | 8.5 | 11 | -2.4 | 0.0 | 0.2 |
| 8 08/20/12 | 100 | 6.0 | 12 | -4.1 | 0.0 | 0.1 |
| 9 08/22/12 | 89 | 5.7 | 17 | -2.2 | 0.0 | 0.8 |
| 10 05/19/12 | 83 | 6.6 | 12 | -0.2 | 0.0 | 0.0 |
| 11 05/21/12 | 83 | 3.8 | 12 | -0.9 | 0.0 | 0.0 |
| 12 06/16/12 | 67 | 3.3 | 9 | -0.3 | 0.0 | 0.0 |
| 13 06/28/12 | 72 | 2.1 | 10 | -2.9 | 0.0 | 0.0 |
| 14 06/29/00 | 69 | 5.8 | 14 | -4.5 | 0.0 | 0.0 |
| 15 07/26/00 | 67 | 7.6 | 9 | -4.9 | 0.0 | 0.0 |
| 16 07/27/00 | 74 | 6.9 | 14 | -1.9 | 0.0 | 0.0 |
| 17 08/09/12 | 70 | 9.3 | 11 | -0.6 | 0.0 | 0.0 |
| 18 08/12/12 | 64 | 18.8 | 10 | -2.2 | 0.0 | 0.0 |
| 19 08/19/00 | 89 | 7.8 | 11 | -0.7 | 0.0 | 0.0 |
| 20 08/27/00 | 91 | 9.0 | 12 | -2.4 | 0.0 | 0.0 |
| 21 09/01/12 | 100 | 9.5 | 14 | -2.1 | 0.0 | 0.0 |
| 22 09/17/00 | 88 | 20.0 | 20 | -2.1 | 0.0 | 0.0 |
| 23 07/02/00 | 61 | 31.9 | 14 | 1.4 | -1.4 | 71.6 |
| 24 07/02/12 | 95 | 43.7 | 16 | 2.6 | -2.1 | 28.8 |
| 25 07/03/00 | 97 | 22.4 | 10 | 0.7 | -1.2 | 0.6 |
| 26 07/17/00 | 82 | 14.5 | 16 | 0.1 | -0.4 | 0.1 |
| 27 08/15/00 | 63 | 25.5 | 10 | 0.3 | -2.0 | 17.5 |
| 28 05/24/12 | 96 | 16.3 | 10 | 0.4 | -0.6 | 0.0 ¹ |
| 29 08/18/00 | 91 | 11.2 | 10 | 0.3 | -0.3 | 0.0 ² |
| 30 08/26/12 | 87 | 8.0 | 14 | 0.0 | -0.1 | 0.0 ³ |
| 31 09/06/12 | 75 | 20.9 | 10 | 0.7 | -0.9 | 0.0 ⁴ |
| 32 01/06/12 | 78 | 18.1 | 12 | 0.8 | -0.3 | 0.0 |
| 33 12/05/12 | 64 | 19.2 | 14 | 0.3 | -1.0 | 0.0 |
| 34 02/11/00 | 60 | 38.5 | 14 | 4.8 | 0.7 | 0.0 |

¹ 6.7 mm at Edmonton ² 1.6 mm at Edmonton³ 6.4 mm at Edmonton ⁴ 4.4 mm at Edmonton RH_{90} : Relative humidity at 90 kPa (%) Δv_{90} : Difference in wind vector at 50 and 90 kPa (ms^{-1}) η_{50} : Absolute vorticity at 50 kPa (10^{-5} s^{-1}) SI_{90} : Showalter index based on 90 and 50 kPa data SSI_{90} : Slantwise Showalter Index based on 90 and 50 kPa data

PREC : 12-hourly accumulated precipitation (mm) at Stony Plain

soundings number will be reduced to only five (cases 23, 24, 25, 27, and 33).

It is not certain that the precipitation events included in Tables 3 and 4 were actually forced by the release of moist symmetric instability. Observations of multiple precipitation bands aligned parallel to the thermal windshear vector would much strengthen the likelihood of the occurrence of slantwise convection. However, there was no unambiguous information about the spatial organization of the instantaneous rainfall as this can not be deduced from accumulated rainfall amounts. For example, a single precipitating cell moving in an easterly direction would generate a narrow west-east band of rainfall over the 12-hour period. The only data that can indicate the presence of an existing precipitation band come from radar reflectivity observations. However, data from the Carvel radar (located close to Stony Plain) were not archived during 1990.

Despite the lack of information regarding the spatial distribution of rainfall, it seems worthwhile to examine the relationship between a negative SSI value and the rainfall as measured at Stony Plain. Thus, precipitation events were split into 7 different classes, based on the 12-hourly accumulated amounts recorded at Stony Plain. Table 5 lists the number of events for each precipitation class together with the number of cases associated with negative SSI_{85} and SSI_{70} values. The cases that had 12-hourly accumulation amounts more than 15 mm were "correlated" quite well with the SSI values. For the few

heavy rain events, where the SSI values were positive, the precipitation was associated with strongly-developed surface lows.

The magnitude of SSI is related to the amount of latent heat stored in the environment. During the release of moist symmetric instability, this latent energy is converted to kinetic energy which results in enhanced upward motions. For identical large-scale forcing, a larger value of $(-SSI)$ will indicate a larger amount of latent energy available, which should produce a stronger updraft causing more condensation and precipitation. Based on this link of events, one would expect that soundings with larger values of $(-SSI)$ should be correlated with larger precipitation amounts, provided that

TABLE 5. Number of observed events and number of cases correctly predicted by the conditions $\{SSI_{85} < 0 \text{ and } RH_{85} \geq 60\%$ and $\{SSI_{90} < 0 \text{ and } RH_{90} \geq 60\%$ for different ranges of 12-hourly accumulated precipitation.

| Precipitation Range (mm) | Number of cases | Number of cases with $SSI_{85} < 0$ | Number of cases with $SSI_{90} < 0$ |
|-----------------------------|--------------------|--|--|
| 30-80 | 1 | 0 | 1 |
| 20-30 | 3 | 1 | 1 |
| 15-20 | 2 | 1 | 1 |
| 10-15 | 3 | 0 | 0 |
| 5-10 | 11 | 0 | 0 |
| 0.1-5 | 78 | 5 | 2 |
| 0 | 200 | 4 | 7 |
| Total cases | 298 | 11 | 12 |

the large-scale forcing remains the same for all cases. The data presented in Table 5 is consistent with this notion: Large ($-SSI_{85}$) values were indeed associated with large rainfall, while small ($-SSI_{85}$) values usually had small rain amounts. However, the data points are too few and have too large error margin to provide any firm conclusion. There is clearly a tremendous variability in the amount of mesoscale precipitation which depends on the larger scale forcing and moisture availability, which are not evident from a single sounding.

6.6 Discussion and conclusion

The Slantwise Showalter Index (SSI) is defined as the generalized Showalter Index for a parcel lifted from the 85 kPa (or 90 kPa) level along a surface of constant absolute angular momentum. Emanuel's (1983) technique was adapted to approximate the SSI value, using observed data from a single vertical sounding and the 50 kPa vorticity chart. Based on the magnitudes of the thermal wind shear and absolute vorticity, a "temperature adjustment term" was added to the temperature of the vertically lifted air parcel. This "adjustment" in parcel temperature constitutes the energy change associated with the centrifugal effects. An air mass with a negative SSI value shows the potential for slantwise convection. In the presence of convective instability, slantwise overturning will not occur, since the time scale of cumulus convection is much

smaller than the time scale of moist symmetric instability. Accordingly, the SSI was set to zero, whenever a sounding was diagnosed to be unstable for cumulus convection as indicated by a negative SI value.

An important feature of the SSI is that it quantifies the stability properties of a deep layer of the flow, extending from 85 kPa to 50 kPa pressure levels. It is here that the SSI index differs from the (classical) SCAPE, which was tested by Shutts (1990) and more recently by Snook (1992). A large value of SCAPE indicates either a deep layer of moderate instability or a shallow layer of strong instability.

The usefulness of the SSI index to identify precipitation in central Alberta was also examined. Twice-daily accumulated precipitation measurements and twice-daily soundings for the entire year of 1990 provided an extensive data set. The major findings are given below:

(1) It serves to compute SSI index for air parcels lifted from the 90 kPa level as well as the 85 kPa level. For soundings with strong low-level windshear the SSI_{90} index provides more information about the slantwise stability properties, while for soundings with a surface inversion the SSI_{85} index seems more appropriate.

(2) During the warm season (May-September 1990), about one quarter of all the observed soundings had negative SI values suggesting the potential of deep cumulus convection. About 5% of warm season soundings had negative SSI values, associated

with the potential for deep slantwise convection.

(3) Despite its scarce occurrences, a negative SSI value is probably useful in helping to forecast precipitation. During 1990, negative SSI values "predicted" two of the four events, when the rain accumulation exceeded 20 mm in 12 hours. During the summer, whenever the sounding data indicated a deep layer of moist-symmetrically unstable air (i.e. $SSI_{\text{ss}} < 0$) and moist low-level conditions (i.e. $RH \geq 60\%$), rain was observed at Stony Plain or a nearby downwind station within the next 12 hours. Many rainfall days, however, were not associated with moist symmetric instability but were due to frontal lifting, surface cyclogenesis or upright convection.

(4) During the spring, fall or winter, soundings associated with negative SSI values were very scarce indicating that the airmass over central Alberta did not contain deep layers of moist-symmetrically unstable air.

(5) Typical measurement inaccuracy, in balloon sounding data, does impact on the computed SI and SSI values. The present analysis suggests that the root-mean-square errors of SI and SSI are 0.6 and 0.9, respectively. Making allowance for errors of this size will change the frequency values presented here.

These findings require additional investigations. The observed flow patterns for the cases with negative SSI values should be examined to assure that the flow was indeed quasi-two-dimensional. In addition, the validity of the thermal wind balance has to be confirmed. The spatial distribution of the

precipitation should also be examined to determine whether the observed precipitation was indeed organized in bands aligned in the direction of the thermal shear. To make these findings more significant one must also consider the temporal evolution of the precipitation events, as monitored by weather radars. Further evidence of the usefulness of the SSI requires testing at other geographical locations. If a consistent picture emerges about the skilfulness of SSI, an experimental testing in operational setting is warranted. This thesis proposes the SSI index, or some refined version of it, as a useful tool for operational forecasting to identify some of the significant rain events in the Canadian Prairies. However, SSI should not be used independent of other guidance, because it is derived from a single sounding data and, thus, contains no information about the larger scale forcing and moisture availability.

References

- Anderson, K. and R. B. Charlton, 1990: Predicting lightning occurrence and frequency from upper air soundings over Stony Plain, Alberta. Preprints, 16th Conf. Severe Local Storms/Conf. Atmos. Elec., Kananaskis Park, Amer. Meteor. Soc., Boston, J40-J45.
- Andersson, T., M. Andersson, C. Jacobson and S. Nilsson, 1989: Thermodynamic indices for forecasting thunderstorms in southern Sweden. Meteorological Magazine, 116, 141-146.
- Bennetts, D. A., and B. J. Hoskins, 1979: Conditional symmetric instability a possible explanation for frontal rainbands. Quart J. Roy. Meteor. Soc., 105, 945-962.
- Bolton, D., 1980: The computation of equivalent potential temperature. Mon. Wea. Rev., 108, 1046-1053.
- Brooks, C. E. P. and N. Carruthers, 1953: Handbook of statistical methods in meteorology. York House, London. 412 pp.
- Byrd, G. P., 1989: A composite analysis of winter season overrunning precipitation bands over the southern plains of the United States. J. Atmos. Sc., 46, 1119-1132.
- Cotton, W. R., 1990: Storms. 1st Edition, ASTeR Press, Fort Collins, Colorado, 158 pp.
- Donaldson, N. R. and R. E. Stewart, 1989: On the precipitation regions within two storms affecting

- Atlantic Canada. Atmos. Ocean. 27, 108-129.
- Emanuel, K. A., 1979: Inertial instability and mesoscale convective systems. Part I: Linear theory of inertial instability in rotating viscous fluids. J. Atmos. Sci., 36, 2425-2449.
- _____, 1983: On assessing local conditional symmetric instability from atmospheric soundings. Mon. Wea. Rev., 111, 2016-2033.
- Galway, J. G., 1956: The lifted index as a predictor of latent instability. Bull. Amer. Meteor. Soc., 37, 528-529.
- Golden, J. H., R. Serafin, V. Lally and J. Facundo, 1986: Atmospheric Sounding Systems. In: Mesoscale Meteorology and Forecasting, (P. S. Ray ed.), Amer. Meteor. Soc., Boston, 50-70.
- Gyakum, J. R., 1987: Evolution of a surprise snowfall in the United States Midwest. Mon. Wea. Rev., 115, 2322-2345.
- Hedley, M. and M. K. Yau, 1991: Anelastic modelling of explosive cyclogenesis. J. Atmos. Sci., 48, 711-727.
- Kuo, Y. -H. and R. J. Reed, 1988: Numerical simulation of an explosively deepening cyclone in the eastern Pacific. Mon. Wea. Rev., 116, 2081-2105.
- Mailhot, J. and C. Chouinard, 1989: Numerical forecasts of explosive winter storms: Sensitivity experiments with a meso- α scale model. Mon. Wea. Rev., 117, 1311-1341.
- Moore, J. T. and P. D. Blakley, 1988: The role of

- frontogenetical forcing and conditional symmetric instability in the Midwest snowstorm of 30-31 January 1982. Mon. Wea. Rev., 116, 2151-2171.
- Ray, P. S. (Editor), 1986: Mesoscale meteorology and forecasting. Amer. Meteor. Soc., Boston, 793 pp.
- Reuter, G. W., 1990: Radar observations of precipitation production in thunderstorms. Atmos.-Ocean, 28, 216-229.
- ____ and M. K. Yau, 1990: Observation of slantwise convective instability in winter cyclones. Mon. Wea. Rev., 118, 447-458.
- ____ and____, 1993: Assessment of slantwise convection in ERICA cyclones, Mon. Wea. Rev., 121, 375-386.
- ____ and C. D. Nguyen, 1993: Organization of cloud and precipitation in a severe Alberta storm. Atmospheric Research. (in press).
- Rogers, R. R. and M. K. Yau, 1989: A short course in cloud physics. 3rd Edition. Pergamon Press, Oxford, 293 pp.
- Sanders, F. and L. F. Bosart, 1985: Mesoscale structure in the megalopolitan snowstorm of 11-12 February 1983. Part I: Frontogenetical forcing and symmetric instability. J. Atmos. Sc., 42, 1050-1061.
- Seltzer, M. A., R. E. Passarelli and K. A. Emanuel, 1985: The possible role of symmetric instability in the formation of precipitation bands. J. Atmos. Sci., 42, 2207-2219.
- Showalter, A. K., 1953: A stability index for thunderstorm

- forecasting. Bull. Amer. Meteor. Soc., 34, 250-252.
- Shutts, G. J., 1990: SCAPE charts from numerical prediction model fields. Mon. Wea. Rev., 118, 2745-2751.
- Snook, J. S. 1992: Current techniques for real-time evaluation of conditional symmetric instability. Wea. Forecasting, 7, 430- 439.
- Stone, P. H., 1966: On non-geostrophic baroclinic stability. J. Atmos. Sci., 23, 390-400.
- Wolfsberg, D. G., K. A. Emanuel and R. E. Passarelli, 1986: Band formation of a New England winter storm. Mon. Wea. Rev., 114, 1552-1569.
- Zhang, D.-L. and H.-R. Cho, 1992: On the development of negative moist potential vorticity in the stratiform region of a simulated squall line. Mon. Wea. Rev., 120, 1322-1341.

Chapter 7

Summary, conclusions and recommendations

7.1 Summary and conclusions

This thesis is one the few studies of the occurrences of Conditional Symmetric Instability (CSI) in continental weather systems and the first study that deals with CSI over Alberta. The observational data used in this thesis included 1460 upper air soundings sampled above Stony Plain, Alberta, in 1990 and 1991. The twice-daily Stony Plain precipitation data were also analyzed.

The snowstorm of 4-5 October 1990 which produced heavy snowfall in central Alberta was examined in detail. Weather maps indicated that synoptic forcing for ascending motion (due to PVA and warm air advection) was rather insignificant. The Penhold radar reflectivity data indicated that the heavy snow fell mainly from a precipitation band that was aligned in the direction of the strong thermal shear. Using the method of single sounding, the flow was found to be moist-symmetrically unstable during the twelve hours period when heavy snow was recorded. The study also included the effects of the absolute vorticity, an improvement on previous studies which neglected these effects.

Using two years (1990 and 1991) of sounding data, the seasonal variation of the frequency of the occurrence of CSI

was examined. The analysis indicated that 20% of the total soundings contained layers that were potentially unstable for slantwise convection. Only 2% of the summer soundings had the potential for slantwise instability, whereas during the three months of winter, the observed frequency of slantwise unstable soundings was 40%. The frequency values of the spring and fall were about 20%. For the purpose of comparison, the frequency of convective instability was also examined. 98% of the summer soundings were convectively unstable, but only 27% of winter soundings. Clearly, convective instability is mainly a warm season phenomenon, whereas slantwise convection occurs mainly in the cool seasons.

The importance of convective and slantwise instabilities in producing the observed precipitation was also investigated. The results suggested that almost all of the observed summer time rainfall fell on days when the soundings indicated the potential for convective instability. During the winter time, slightly more than half of the observed snow fell on days when the soundings showed the potential for slantwise instability. On an annual basis, as much as 75% of the precipitation may be attributed to conditions that had the potential for convective instability, whereas slantwise instability would account for about 15-20% of the total precipitation accumulation.

As CSI can contribute significantly to the precipitation during the cold seasons, this analysis examined in detail the vertical distribution of the slantwise stability properties of

the atmosphere and how this might affect precipitation. The result was, that CSI occurred predominantly in the 90-85 kPa slab and its presence decreased rapidly with height. The trend was similar in individual months. The correlation between the observed precipitation amount and the moist Richardson number, which provides a local estimate of the CSI intensity, was also investigated. No clear results were evident.

The last part of this research is concerned with the possible application of conditional symmetric instability to predict the precipitation potential. The potential for severe convection is often indicated by the classical Showalter Index (SI). In this thesis, the SI index has been extended to obtain the Slantwise Showalter Index (SSI). The new index is meant to detect the potential for long-lasting precipitation associated with slantwise overturning.

The SSI index is defined as follows: an air parcel from 85 kPa is lifted along a surface of constant angular momentum M dry adiabatically until saturation occurs, and then pseudo-adiabatically up to 50 kPa. At the 50 kPa level, the slantwise lifted parcel temperature is subtracted from the observed air temperature. A negative SSI value indicates the potential for deep slantwise convection in the layer. This study examined also a modified version of SSI and in this case the lifted air parcel originates from 90 kPa rather than from 85 kPa.

Radiosonde data are usually subject to inaccuracies in thermodynamic and wind measurements and inaccurate sounding

data will impact on computed stability indices. For this study the root-mean-square error for SSI was 0.9 °C, compared to 0.6 °C for the standard Showalter Index.

In this work, a data analysis was carried out to test the usefulness of this new SSI index (with base level 85 kPa and 90 kPa) for the period from 1 January to 31 December 1990. The computed SSI values were then compared with the precipitation amounts that accumulated at the station within the next twelve hours. Very few cases of negative SSI values were found. This indicates that deep layers of slantwise unstable air are not common in central Alberta. However, the few cases of negative SSI values, combined with humid conditions in the low levels, were indeed useful for identifying some of the rain events of central Alberta.

7.2 Recommendations for further research

The research reported in this thesis was motivated by the need for a better understanding and knowledge of the formation and organization of mesoscale precipitations in the weather systems of Alberta. Since little was known about the CSI role in these weather systems, this thesis focused on assessing the climatological variability of the occurrence of CSI in central Alberta. A logical extension of this work would be to analyze a much larger data sample (5 years or more) and to enlarge the area of rainfall measurements in order to include the adjacent stations' precipitation data. In this manner a more accurate

"climatology" of slantwise convection for this region will be obtained. Moreover, a study of the occurrence of CSI, with a view to the spatial distribution of precipitation as revealed by weather radar CAPPI images is necessary. In addition, area averaged radar data could improve the estimate of the regional precipitation. The data collected by C-band radar at Carvel, Alberta, are suitable for such studies because this radar is operated by the Atmospheric Environment Service throughout the entire year. Unfortunately, the Alberta Research Council's extensive radar data archive is not appropriate for studying the seasonal variability of slantwise convection, because the radar located at Penhold was operated only during the summer months.

A normal extension of the present analysis would be to study the dynamics of the mesoscale flows during the build-up and release of moist symmetric instability. The best approach for clarifying the dynamics of the flow would be to make a few detailed case studies. For these cases the data should include upper air sounding data from a network of radiosonde stations and also Doppler radar measurements of the radial component of the wind vector. By combining information from the soundings and Doppler radar measurements, the dynamics of the slantwise convection could become evident. Once a suitable data set for a case study is available, it could be used to simulate the event using a numerical cloud scale model. In the past, high resolution simulation of slantwise convective instability was

always based on an idealized initial environment. With a good data set of an observed case, however, it would be possible to use the observed values for model initialization and this will allow one to check the model performance by comparing its results with the observed data fields. A synthesis of numerical model results and remote-sensing observations should provide a more complete picture of the dynamics which give rise to slantwise convective overturning.

Despite many past attempts to investigate conditional symmetric instability, it can be expected that active research will continue during this decade to provide a complete picture of slantwise convection and its interaction with large scale atmospheric flows.